UiT The Arctic University of Norway

Faculty of Biosciences, Fisheries and Economics, Department of Arctic and Marine Biology

Novel methanotrophic community assemblages in a terrestrial methane seep in Svalbard

Pernille Maria Skaset Fåne

Master's thesis in Molecular Environmental Biology – BIO-3950 – August 2020

Table of Contents

List of Tables

Main text

Appendix

List of Figures

Main text

Appendix

Acknowledgement

I would like to thank my supervisors Dimitri Kalenitchenko and Alexander Tøsdal Tveit for all the help they have provided me with in the shape of guidance, discussions, explanations and insightful comments. I feel very grateful for having worked on such an interesting project and for having gotten the opportunity to go to Svalbard and get hands-on experience in the field, as well as a lot of lab experience at UiT. Thank you, Dimitri for having taught be the basics of bioinformatics, which I know will be a valuable skill in the future. Thank you both for always taking the time to talk to be in person or online whenever I have had questions. You have made the process much easier with your positive attitudes and good humors.

A special thank you to Franziska who was a cheerful field companion, lab partner and foremost good friend and supporter in fun and in stressful periods. Thank you for optimizing the extraction protocol with me and for extracting with me.

A big thank you to the methane research group that I have been a part of for the past one and a half years. I feel very lucky to have been part of a group with so many knowledgeable, kind and fun people. Thank you for all useful advice, help and discussions. I have had a lot of fun with all of you and I appreciate all the activities that have been organized.

Moreover, I would like to thank the other master students for sharing this experience with me and for all the interesting and weird conversations we have had in our breaks.

Lastly, I would like to thank my flat mates, friends and family for supporting me, keeping me grounded and for helping me to stay relatively stress-free.

Abbreviations I: General

AOM	anaerobic oxidation of methane
ANME	ANaerobic MEthanotrophic archaea
BLAST	basic local alignment search tool
CH_4	methane gas
CO_2	carbon dioxide gas
DNA	deoxyribonucleic acid
dw	dry weight
EMP	Environmental Microbial Project
FISH	fluorescence *in situ* hybridization
GHSZ	gas hydrate stability zone
H_2O	water
LGM	last glacial maximum
mcrA	gene encoding methyl-coenzyme M reductase
MMO	methane monooxygenase
MOB	methane oxidizing bacteria
NA	nucleic acids
O_2	oxygen gas
PCI	phenol chloroform isoamylalcohol
PCR	polymerase chain reaction
Pg	petagram (1 Pg = 1 billion tons)
pMMO	particulate methane monooxygenase
RNA	ribonucleic acid
rRNA	ribosomal ribonucleic acid
SMTZ	sulfate-methane transition zone
SOC	soil organic carbon

SR sulfate reduction

SRB sulfate reducing bacteria

Tg terragram (1 Tg = 1 million tons)

TNA total nucleic acids

Abbreviations II: Sediment types

DS dry sediment

MS mini source sediment

PF pond flow sediment

SP still pond sediment

SS source sediment

StS stream sediment

WS wet sediment

Abstract

Recent studies have concluded that groundwater driven methane escape through open system pingos is an important greenhouse gas source in the vulnerable high Arctic. In wetlands and marine sediments, large quantities of methane are consumed by methane oxidizing bacteria (MOB) and ANaerobic MEthanotrophic (ANME) archaea, preventing its release to the atmosphere. The methanotrophic capacity of open system pingos is understudied, and microbial community profiling is of key interest, to infer the magnitude of the methane filter and for high resolution prediction of methane evasion. In this thesis, we mapped the microbial community assemblages across hydrological transitions at the open system pingo Lagoon pingo (N78°14’22 E015°45’16). In summer, methane-saturated and oxygen limited groundwater discharges continuously through a main source, forming crater-like ponds, providing potential habitats for methanotrophy. We sampled sediments in August 2019 and coordinated these with methane flux measurements and oxidation rate assays. Environmental parameters and 16S rRNA gene diversity revealed a radial mosaic of habitat patches, made by the seep water. We found distinct and unusual microbial communities inhabiting these habitat patches, suggesting high levels of specialization and adaptation to an unusual terrestrial system with marine influences. Phylogenetic analyses of 16S amplicons unveiled MOB and ANME communities in the crater pond. The MOB sequences were dominated by the type I genus *Methylobacter*, which was >97% affiliated to the arctic wetland strain *Methylobacter tundripaludum* SV97. The highest relative abundances of *Methylobacter* coincided with methane oxidation rates in waterlogged habitats. The distribution of the MOB could not be explained by any environmental parameters measured in this study alone, however it is likely that the MOB are largely controlled by water and/or the dissolved methane, oxygen and nutrients. Surprisingly, *Methylobacter* was prevalent in sediments continuously flushed with anoxic groundwater, indicating adaptations to oxygen limitation. The archaeal 16S library was dominated by ANME-3 and 2a/b, with lesser representation of ANME-1a. ANME OTU affiliation to sulfate dependent marine clades coincided with sulphur cycling taxa in the source sediments, suggesting a potential for anaerobic oxidation of methane coupled with sulfate reduction, making this an intriguing terrestrial equivalent of cold marine methane seeps. The microbial community we present in this thesis depicts a system contrasting fundamentally from previously reported ecosystems in the Arctic and elsewhere. We confirm that methane is one of the primary energy sources at the seep site and that the atmospheric transfer of methane is mitigated by MOB and possibly ANME.

Keywords:

Lagoon pingo, open system pingo, methane, methane oxidizing bacteria, *Methylobacter* ANME, Arctic, Svalbard.

1 Introduction

1.1 Methane as a climate gas

Methane (CH_4) is the most abundant organic gas in the atmosphere. Following industrialization, atmospheric levels of methane have risen by 150% (Reay et al., 2018), and its accumulation is responsible for 20% of the global temperature rises in this period (Kirschke et al., 2013). In 2016 the atmospheric concentration of methane amounted to 1,853 ppb (Figure 1), surpassing concentrations seen the past 650,000 years (Spahni et al., 2005). Although the atmospheric levels of methane are but a fraction of the atmospheric concentrations of carbon dioxide (CO_2), its global warming potential over a 100 year period is 28-34 times higher than CO_2 (IPCC, 2014). The continued increase of atmospheric methane is predicted to attribute to further increases in global temperatures and altered precipitation cycles, subsequently interfering with the global methane cycle (Kirschke et al., 2013). Natural ecosystems consist of methane sources and sinks emitting and mitigating atmospheric methane transfer, respectively (Conrad, 2009). Alterations of the balance between sources and sinks caused by global climate change can lead to positive feedback responses that further accelerate releases of methane from wetlands, soils, freshwater and marine habitats (Reay et al., 2018).

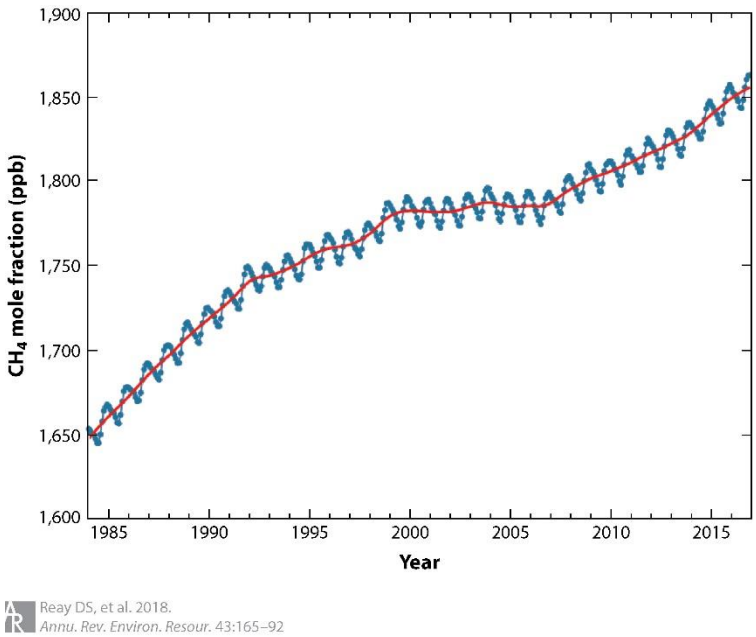

Figure 1: Global average atmospheric methane concentrations displayed in mole fraction in the period 1984-2016. The average mole fraction is shown by the red line, while the monthly averages are displayed by the blue dots and line. The observations are retrieved from 125 weather stations. Figure retrieved from (Reay et al., 2018).

1.2 Carbon storages in the Arctic

The Arctic is one of the most significant carbon reservoirs on Earth, as perennially frozen ground (permafrost), glaciers and ice act as greenhouse gas lids, interlocking carbon in the shape of dead organic matter and natural gas reserves. Approximately 1,700 Pg (1 Pg = 1 billion tons) of carbon is predicted to be found in northern circumpolar permafrost (Schuur et al., 2008; Tarnocai et al., 2009). An additional 10^3-10^6 Pg of hydrocarbon gas is stored in crystalline structures called clathrate hydrates found in submarine permafrost and continental shelf sediments (Kvenvolden, 1988; Buffett and Archer, 2004; Milkov, 2004; Archer et al., 2009). Together, these reservoirs surpass atmospheric concentrations of carbon, and the atmosphere is thus sensitive to even small methane emissions. The Arctic is among the regions that have been affected most severely by increasing temperatures due to climate change over the past 40 years, and future permafrost loss is predicted in the future (IPCC, 2014).

1.2.1 Arctic methane sinks and sources in nature

Northern permafrost wetlands contain 1/3 of the world's soil organic carbon (SOC) (Tarnocai et al., 2009). The SOC is primarily exposed to microbial degradation during the summer months in a seasonally thawed active layer resting on top of the permafrost table. Due to its high water content and oxygen (O_2) depletion, the active layer is particularly suited for the anaerobic process called methanogenesis, executed by archaea (Joabsson and Christensen, 2001). Methanogenesis is responsible for ~70% of the global emissions of methane annually (Conrad, 2009). Climate projections suggest elevated temperatures and increased precipitation in the Arctic towards the end of the 21st century (Førland et al., 2011; Thomas et al., 2018). These trends coincide with increased vertical deepening of the active layer, making previously unavailable SOC accessible to degradation processes such as methanogenesis (Vaughan et al., 2014). Upon thawing permafrost wetland-peat in laboratory incubations, Mackelprang et al. (2011) measured elevated methane release, coinciding with increased fractions of methanogens, and a metagenomic shift in gene expression toward carbon and nitrogen cycling genes, indicative of SOC degradation. However, the release of methane from wetlands is largely mitigated by the oxidation of methane (Conrad, 2009). This process is performed by methanotrophs that act as filters, removing methane in these ecosystems. Methane can be oxidized aerobically and anaerobically. Most methane oxidizing bacteria (MOB) oxidize methane aerobically and are found in overlying, aerated soil layers, in water beds and in association with mosses (Bodelier et al., 2019). Aerobic methanotrophs (MOB

filter) consume ~30 Tg CH_4 $year^{-1}$ (1 Tg = 1 million tons), accounting for 5 – 6% of the annual atmospheric oxidation, thus making it one of the major biological sinks of methane in the world (Reay et al., 2018). Anaerobic oxidation of methane (AOM) is an important sink in marine environments (Reeburgh, 2007). However, in recent years, AOM have gained increasing attention as a potential methane sink also in terrestrial systems (Gupta et al., 2013; Valenzuela et al., 2017; Miller et al., 2019), suggesting that the modelled filter capacity of terrestrial environments have been incomplete. In fact, high AOM levels were detected in peat soil retrieved from a 1,500 km latitudinal transect across North America, independent of peat characteristics (Gupta et al., 2013). Based on experimental tracing of ^{13}C biomass assimilation in microcosms Gupta et al. (2013) estimated anaerobic mitigation of methane in northern peatlands to range between 1.6 – 49 Tg $year^{-1}$. Evidence of potential AOM rates from arctic peat samples also indicate that these soils are more efficient methane filters than previously perceived, where AOM potentially reduce 25 – 34% of the methane produced in these soils (Miller et al., 2019). However, these studies did not include *in situ* rates of AOM, thus the efficiency of the AOM filter under natural conditions remains unknown.

Methane is the dominant gas found in marine clathrates hydrates (Archer, 2007) and its origin can be both biological (methanogenesis) and/or thermogenic (geological formation) (Stolper et al., 2014). Clathrates remain stable under specific pressure- and temperature conditions, defined as the gas hydrate stability zone (GHSZ) (Kvenvolden, 1988). At 0°C, the integrity of these methane clathrates are sustained at minimum 300 m depth, however due to cooler water currents in the Arctic, clathrates can be found in shallower sediments (Archer et al., 2009; O'Connor et al., 2010). Clathrates found today in the Arctic have remained stable since the retreat of the last glacial maximum (LGM)-ice sheet 15,000 years ago (Clark et al., 2009; Crémière et al., 2016). Crater-like structures called pockmarks, mark the sea floor on the Barents Sea-, West Spitsbergen Shelf and in several fjords on Svalbard (Forwich et al., 2009; Crémière et al., 2016; Portnov et al., 2016; Panieri et al., 2017; Roy et al., 2019), marking disassociated clathrates formed by rapid methane expulsion. The dissociation was triggered by the retreat of the LGM ice sheet, which changed temperature and pressure conditions, consequently shifting the GHSZ (Crémière et al., 2016; Portnov et al., 2016) (Figure 2). Today the destabilization of arctic clathrates located on shallow banks is vulnerable to increasing bottom water temperatures (Archer et al., 2009). Although hydrate estimates are speculative, its magnitude is so large that if merely 10% of these storages were released from marine sediments, the climatic effect would be equivalent to scenarios where the atmospheric

concentrations of CO_2 were elevated by a factor of ten (Archer, 2007). Further destabilization of arctic hydrates can thus cause rapid methane release through existing escape paths such as pockmarks as observed in the past.

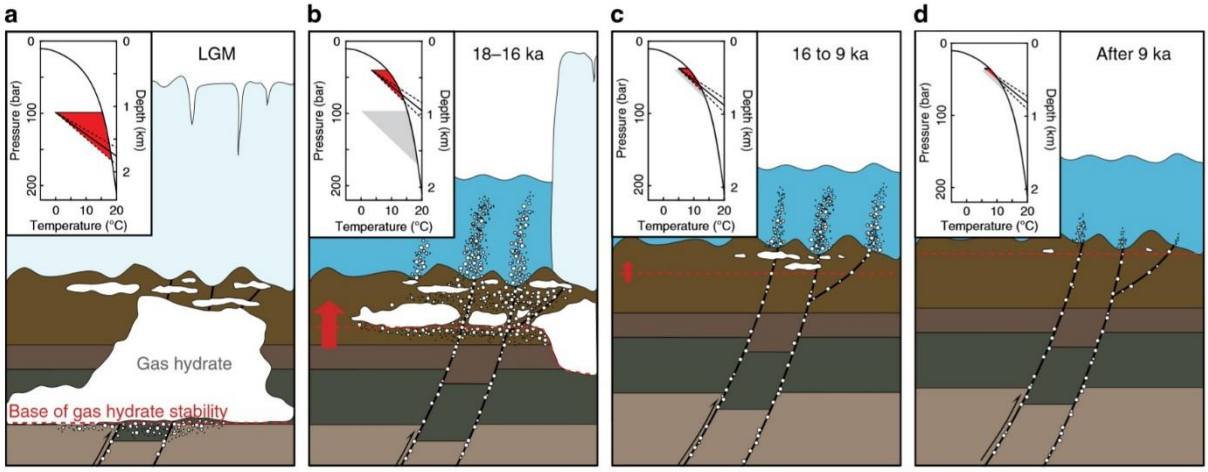

Figure 2: Glacier retreat followed by gas hydrate destabilization and evasion of methane through pockmarks in the Barents Sea shelf. (a) The gas hydrate stability zone (top left) penetrated 600 m below the sediment surface during the last glacial maximum (LGM). (b) Glacial retreat caused a lateral shift in the stability zone, enhancing the destabilization of methane clathrates, causing methane evasion and the subsequent formation of pockmarks. (c and d) Further disassociation of methane clathrates in combination with benthic sediment heave. The lower boundary of the GHSZ is indicated by the dashed red line. Figure retrieved from (Crémière et al., 2016).

The escape of methane from geological sources through marine vents, such as cold seeps, hydrothermal vents, black smoker chimneys and mud volcanos is estimated to reach between 60 – 80 Tg annually (Etiope, 2012). The methane source potential of the ocean is further elevated through methanogenesis, accounting for 85 – 300 Tg $year^{-1}$, which is up to 25% of the global methane production (Knittel and Boetius, 2009). However, the ocean is only attributed ~2% of the annual methane budget (Reeburgh, 2007), as approximately 90% of all methane emitted from benthic sources is mitigated through AOM in sediments and by aerobic MOB in the overlaying water column (Knittel and Boetius, 2009; Reay et al., 2018). The pinnacle role of AOM in the methane cycle has increased research pressure focusing on ANaerobic MEthanotrophic (ANME) archaea (Reeburgh, 2007). However, the response of the anaerobic filter to elevated water temperatures and methane emissions due to climate change remains uncertain.

1.3 The biological methane filter: the methanotrophs

1.3.1 Aerobic methane oxidation

MOB use the single-carbon compound methane as their sole energy source (Bowman, 2006). Methane is oxidized into methanol, and further into formaldehyde, which can be assimilated by the cell, or further oxidized to formate and CO_2 for energy conservation (Hanson and

Hanson, 1996). The initial oxidative attack on methane is catalysed by the enzyme methane monooxygenase (MMO), mainly appearing as membrane bound particulate enzyme (pMMO) (Hanson and Hanson, 1996). MOB have a ubiquitous distribution and can be found in a variety of habitats where methane is available (Kalyuzhnaya et al., 2019). The wide diversity of methanotrophs reflects adaptation to a large spectrum of temperatures, pH-values and salinity gradients (Bodelier et al., 2019). MOB thrive in oxic-anoxic transition zones but also live under micro-aerobic and anoxic conditions (Kojima et al., 2009a; Wrede et al., 2012; Katsuyama et al., 2013; Danilova et al., 2016).

The most studied MOB are members of the phylum Proteobacteria and are divided into type I and type II, based on phylogenetic and morphological studies. Type I are found within the Gammaproteobacterial order *Methylcoccales*, consisting of genera such as *Methylomonas*, *Methylobacter*, *Methylococcus*, while the type II are Alphaproteobacteria and include the genera *Methylocystis* and *Methylosinus* (Hanson and Hanson, 1996). Up until recently it was widely conceived that the ability to oxidize methane among bacteria was restricted to the phylum Proteobacteria. However, Pol et al. (2007) found that certain Verrucomicrobia have methane oxidizing abilities, and more recently Ettwig et al. (2010) also observed that methanotrophy was not restricted to obligate aerobes and Archaea, as *Candidatus* Methylomirabilis oxyfera, from the candidate Phyla NC10, can oxidize methane under anoxic conditions by synthesizing O_2 via nitrite reduction (Ettwig et al., 2010). This year De Anda et al. (submitted 2020) reported potential methanotrophic Archaea found outside the known taxonomical groups, potentially expanding our knowledge of methanotrophic microorganisms.

1.3.2 Anaerobic methane oxidation

ANME encompass archaea that can oxidize methane under anoxic conditions. These are evolutionarily related to methanogenic Archaea and use methyl-coenzyme M reductase (encoded by the gene *mrcA*), a key enzyme in methanogenesis, in reverse to oxidize methane (Heller et al., 2008).

The full enzymatic processes of AOM in different ANME remains unknown (Krüger et al., 2003; Hallam et al., 2004; Scheller et al., 2010). Biochemical evidence is lacking as the enrichment of ANME presents challenges (Bhattarai et al., 2019). In marine AOM, sulphate is the most common terminal electron acceptor and methane oxidation to reduce sulphate is mediated by consortia of ANME and sulfate reducing bacteria (SRB) (Figure 3) (Bhattarai et

al., 2019). The AOM-sulfate reduction (SR) net-reaction has a low energy yield (-34 kJ mol^{-1} CH_4), and the growth rates of ANME-SRB are thus slow (Nauhaus et al., 2007). Moreover, the accumulation of sulphide from sulfate reduction can become toxic over time and/or inhibit AOM activity. Furthermore, the dissolved methane concentrations observed *in situ* is challenging to obtain in laboratory enrichments. As gas-tight serum bottles introduce pressure limitations, the dissolved methane concentration in incubations are inherently lower than in natural systems (Bhattarai et al., 2019). Phylogenetic investigations of ANME using 16S rRNA gene and *mcrA* as genetic markers display a phylogenetically diverse group inhabiting three lineages (ANME-1, -2 and -3) with further subdivisions within ANME-1 and ANME-2 (Knittel and Boetius, 2009). ANME-2 and 3 are distantly related to the methanogenic Methanosarcinales, while ANME-1 had showed to cluster with Methanosarcinales and Methanomicrobiales (Knittel and Boetius, 2009; Bhattarai et al., 2019).

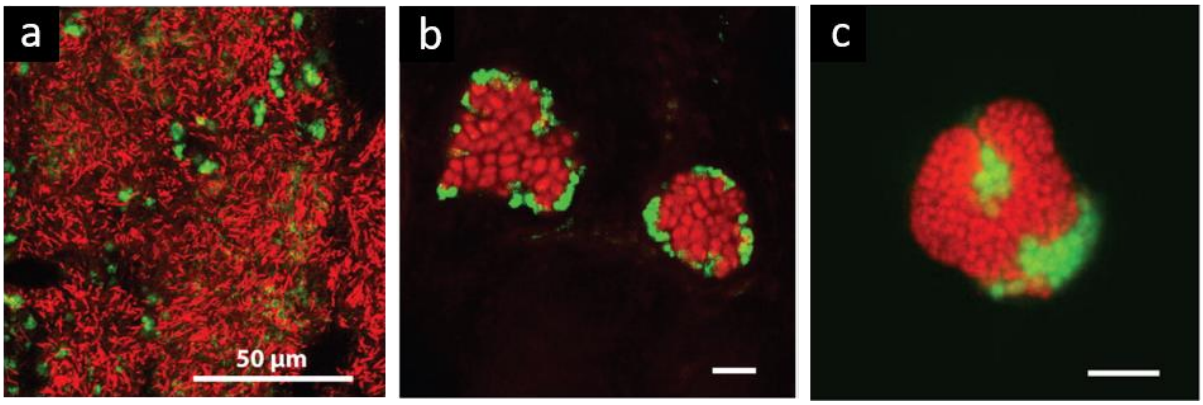

Figure 3: ANME and SRB consortia visualized through fluorescence in situ hybridization (FISH) or catalysed reporter disposition (CARD-FISH). ANME and the SRB are dyed with red and green, respectively. (a) ANME-1 and SRB in a loose, mat formation with Desulfosarcina. (b) ANME-2 in shell-like consortia with Desulfosarcina. (c) ANME-3 in shell-like consortia with Desulfobulbus. Figure retrieved from (Knittel and Boetius, 2009) and modified.

AOM activity in ANME is restricted to anaerobic environments where methane co-occurs with terminal electron acceptors such as sulfate (Boetius et al., 2000), nitrate (Haroon et al., 2013), manganese, iron (Beal et al., 2009) and humic substances (Valenzuela et al., 2017). So far, a few lineages of ANME; ANME 2d and *Candidatus* Methanoperedens nitroreducens, are known to couple AOM with denitrification, using nitrate as the final electron acceptor (Haroon et al., 2013). In marine sediments, ANME-1 and -2 commonly form consortia with SRB from the Deltaproteobacteria branch *Desulfosarcina/Desulfococcus*, while ANME-3 forms consortia with Desulfobulbaceae (Knittel and Boetius, 2009). The mechanisms linking AOM to sulfate reduction is under debate (Stams and Plugge, 2009). Several studies have proposed a linkage of methane oxidation to sulfate reduction indirectly via intermediates, such as acetate and formate (Meyerdierks et al., 2010), or directly via nanowires and surface

cytochromes that transfer electrons directly to SRB (Meyerdierks et al., 2010; McGlynn et al., 2015; Wegener et al., 2015; Vigneron et al., 2019). However, scientific evidence claim that the syntrophic relationship of ANME and SRB is not obligate, as all clades have been observed in solitary states (Orphan et al., 2002; Knittel et al., 2005; Vigneron et al., 2013). The biochemical pathways enabling solitary AOM activity are not fully understood. Metagenomic and metatranscriptomic evidence suggest that ANME-1 can reduce elemental sulphur to hydrogen sulphide using a sulphide-oxidoreductase complex interacting with quinones (Vigneron et al., 2019). Evidence collected by Milucka et al. (2012) also indicated that ANME-2 can execute the AOM-SR reaction by itself, converting sulfate to disulphide, which can further be converted into sulfate and sulphide by SRB.

As AOM is commonly SRB mediated, ANME frequently occur in sulfate-methane transition zones (SMTZ) where methane discharges from the subsurface and sulphate diffusion from the overlying water column meet (Bhattarai et al., 2019). These zones frequently occur in marine sediments overlying hydrocarbon reservoirs, such as cold seeps (Orphan et al., 2004) hydrothermal vents (Teske et al., 2002; Biddle et al., 2012) and marine mud volcanos (Niemann et al., 2006; Lösekann et al., 2007). ANME are mostly known from marine environments, possibly due to substantial research efforts directed toward these organisms in marine habitats. Recently, they have also been observed in freshwater (Timmers et al., 2016) and terrestrial habitats (Chang et al., 2012; Wrede et al., 2012; Gupta et al., 2013; Miller et al., 2019). ANME composition is shaped by environmental stressors (Rossel et al., 2011) and their distribution is controlled by variables such as temperature, salinity, methane and sulfate. ANME-1 has a broad distribution and thrive within a wide range of temperatures, salinities and sulfate concentrations and some strains exhibit AOM activity from 5 to 70°C (Holler et al., 2011; Vigneron et al., 2013). ANME-2 and 3 have demonstrated narrower temperature ranges of growth optimum (Bhattarai et al., 2019), from <0 to ~12°C (Nauhaus et al., 2005) and thus often appear in colder environments. ANME-3 were predominantly reported from marine environments, especially in connection to mud volcanos (Niemann et al., 2006; Lösekann et al., 2007) and subterrestrial environments (Dutta et al., 2019).

1.4 Terrestrial methane seeps

In natural systems methane sources are often balanced by methane sinks (Conrad, 2009). However, systems where methane can largely bypass microbial oxidation exist. Terrestrial methane seeps are channels, that enable methane to escape directly into the atmosphere from

subsurface hydrocarbon pools (Dimitrov, 2002). In contrast to wetlands and the ocean, the methane does not have to travel through overlying soil, sediment and/or water column with high oxidation potential. Terrestrial seeps are divided into macro- and micro-seeps, where macro-seeps contain three groups: mud volcanos, water- and dry seeps. In water seeps hydrocarbons are transported to the surface with groundwater, while dry seeps only emit gas (Etiope et al., 2009). Mud volcanos expel a mix of gas, water, and fine-grained sediments, and deposits from the mud volcano can form mounds with characteristic crater-like ponds (Figure 4) (Kopf, 2002; Etiope et al., 2009). Oxidation of methane is possible within these discharge ponds; however, the amount of methane available for microbial oxidation in the ponds is not well known. There are 926 terrestrial mud volcanos globally (Dimitrov, 2002), from which 20 – 40 Tg CH_4 is emitted annually (Etiope et al., 2009). These systems thus have an important role in the global methane budget.

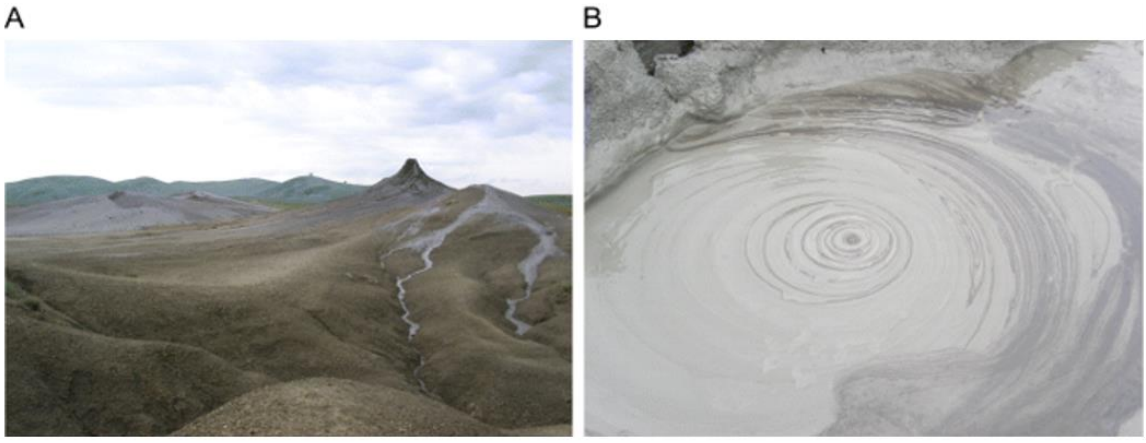

Figure 4: (A-B) Mud volcanos in Romania. (B) Vent expelling sediment rich water and hydrocarbon gas. Figure retrieved from (Alain et al., 2006).

Multiple lines of evidence have revealed methanotrophic bacteria and archaea in terrestrial mud volcanos (Alain et al., 2006; Chang et al., 2012; Cheng et al., 2012; Wrede et al., 2012; Wang et al., 2014; Tu et al., 2017). These environments, though strictly terrestrial, have shown a high influence of marine associated ANME. The 16S clone- and amplicon libraries were dominated by ANME-2, with lesser representation of ANME-1 (Alain et al., 2006; Chang et al., 2012; Wrede et al., 2012; Wang et al., 2014). In a Taiwanese mud volcano ANME-1 was the only ANME lineage that could be identified (Cheng et al., 2012). ANME-3 was not detected in any of the studies. The AOM filter efficiency of two mud volcanos was inquired by measuring the conversion of isotope labelled CH_4 to CO_2 and by SR in anoxic incubations (Alain et al., 2006; Cheng et al., 2012). In both studies SR was detected, but consumption of CH_4 was only detected in Alain et al. (2006). Due to high SR rates and very

low AOM rates (~2 nmol g^{-1} day^{-1}), Alain et al. (2006) concluded that AOM was SRB mediated, although not an important process at the site, compared to marine seep sites (Treude et al., 2003). The accumulation of sulphide in anaerobic enrichments of ANME rich mud also support AOM-SR, however no such association could be confirmed through fluorescence *in situ* hybridization (FISH) and microscopy (Wrede et al., 2012). In the sulfate depleted Lei-Gong-Hu mud volcano in Taiwan, Tu et al. (2017) showed that the ANME active mud could use a variety of electron acceptors, including sulfate, fumarate, ferrihydrite and nitrate. However, based on geochemical profiles at the site and genomic data collected, it was proposed that AOM was coupled with iron and manganese reduction, mediated by partnering bacteria. Similar evidence was collected in two previous studies done at the same study location (Chang et al., 2012; Wang et al., 2014).

Aerobic methane consumption was only assessed in Alain et al. (2006) and Cheng et al. (2012). Methane oxidation in aerobic incubations was observed in both studies, however the data collected could not be used for rate quantification. Type I MOB were detected at the Lei-Gong-Hu mud volcano (Wang et al., 2014; Tu et al., 2017) and in the Appenines (Wrede et al., 2012). Tu et al. (2017) reported that the *mmoXYZBC* gene (encoding for MMO) abundances were highest in the surface sediments and vent fluids where oxygen was likely available. However, prior to this study, Wang et al. (2014) observed 16S rRNA and *pmoA* genes (encoding pMMO) affiliated to type I methanotrophs in anoxic mud layers at the same site. The type I MOB genus *Methylobacter* was also observed in both aerobic and anaerobic mud samples in the Appenines (Wrede et al., 2012). The study concluded that the aerobic methanotrophs likely replaced the anaerobic communities under favourable oxygen and redox conditions, as many members from aerobic type I methanotrophs could be enriched from both oxic and anoxic mud layers.

These studies were conducted in temperate regions, however, terrestrial mud volcanos are found at all latitudes (Dimitrov, 2002), and many systems remains unexplored. In Arctic regions, mud volcanos appear in the shape of permafrost structures called open system pingos (Kristiansen et al., 1995; Kopf, 2002). Recent studies have identified significant groundwater driven methane evasion through open system pingos on Svalbard (Hodson et al., 2019; Hodson et al., 2020). By measuring subaerial methane fluxes from four pingo seeps in Adventdalen (Svalbard), Hodson et al. (2020) could conclude that these systems attribute to 16% of the total annual methane emissions in Adventdalen valley. These systems are understudied, and the microbial community and its oxidation capacity is unknown.

1.5 Pingos

Pingos are perennial ice-cored permafrost hills with a pan-Arctic distribution. Global estimates report >11,000 pingos (Grosse and Jones, 2010) and their distribution density is highly correlated with permafrost landmass. The majority of pingos are located in Canada (Mackay, 1978), Alaska (Jones et al., 2012) and Northern Asia (Lomborinchen, 2000; Fukui et al., 2007). Fewer pingos are found in Svalbard (Liestøl, 1977), Greenland (Müller, 1959; Worsley and Gurney, 1996), Scandinavia (Lagerbäck and Rodhe, 1985) and China (Wang and French, 1995).

All pingos form through (i) the accumulation of sub-surface groundwater in permanently thawed ground within the permafrost (taliks), (ii) the incorporation of a pressure system, forcing the water upwards, and (iii) the freeze expansion of this water subsequently leading to land heave. The ice core grows until an equilibrium is reached between the groundwater pressure and the pressure from the overlaying strata (Gurney, 1998). The morphology of a pingo system is highly dependent on its genesis and are therefore systematized accordingly into "closed-" and "open systems", based on the origin of the water (Müller, 1959). Closed system pingos form in lake basins where water has drained through taliks, following surface freezing. Hydrostatic pressure from within closed system result in land heaving (Jones et al., 2012). Open system pingos are products of sub-permafrost pooling of water, resulting in artesian aquifers. In reaching its hydrostatic equilibrium, artesian pressure causes upwelling and subsequent freezing. As the water forges, it finds a way through the weakest points of the permafrost layer (Gurney, 1998).

1.5.1 Open system pingos: the arctic mud volcano

There are about 80 pingos in Svalbard (Hjelle, 1993), of which the majority are located in west Spitsbergen. These periglacial structures are open systems, appearing most commonly at sea level along shorelines and river deltas, where the thickness of the permafrost is reduced (Yoshikawa and Nakamura, 1996). The open system pingos are characterized by groundwater outlets, emerging from one or various points of the ice-cored mounds. In these systems the artesian pressure often acts over large areas (Liestøl, 1977), making the open system pingo very dynamic in nature. Consequently, these systems are frequently found in clusters with multiple groundwater discharges, in contrast to closed system pingos (Gurney, 1998).

1.5.2 Pingo formation in Adventdalen, Svalbard

The last deglaciation cycle of Arctic ice sheets started ~20,000 years ago (Clark et al., 2009), with Adventfjorden emerging ~11,000 years ago (Svendsen and Mangerud, 1997). The post glacial release of methane from gas hydrates, depicted in Figure 2, is evident in Adventfjorden, where pockmarks are found (Forwich et al., 2009). Upon the regression of the LGM ice sheet, the removal of subglacial pressure caused fjord floor elevation (through a process called isostatic rebound) in Adventdalen (Figure 5). The vertical land heave, outpaced the sea-level rise (Gilbert et al., 2018), and relict submarine sediment deposits (~10,000 years old) are found up to 70 m above sea level in Adventdalen today (Lønne, 2005). In combination with isostatic rebound, pingo formation was supported by hydraulic pressure from sub-permafrost groundwater pools due to vertical permafrost migration (Hornum et al., 2020). Ice core formation and subsequent expansion of pockmarks was estimated to have started 8-3,000 years ago (Yoshikawa and Nakamura, 1996), providing escape pathways for subsurface methane through open system pingos. Little is known about the origin and distribution of the subsurface groundwater and the methane, however, carbon isotope composition indicate that thermogenic methane mixes with microbial biogenic methane below the permafrost (Hodson et al., 2020).

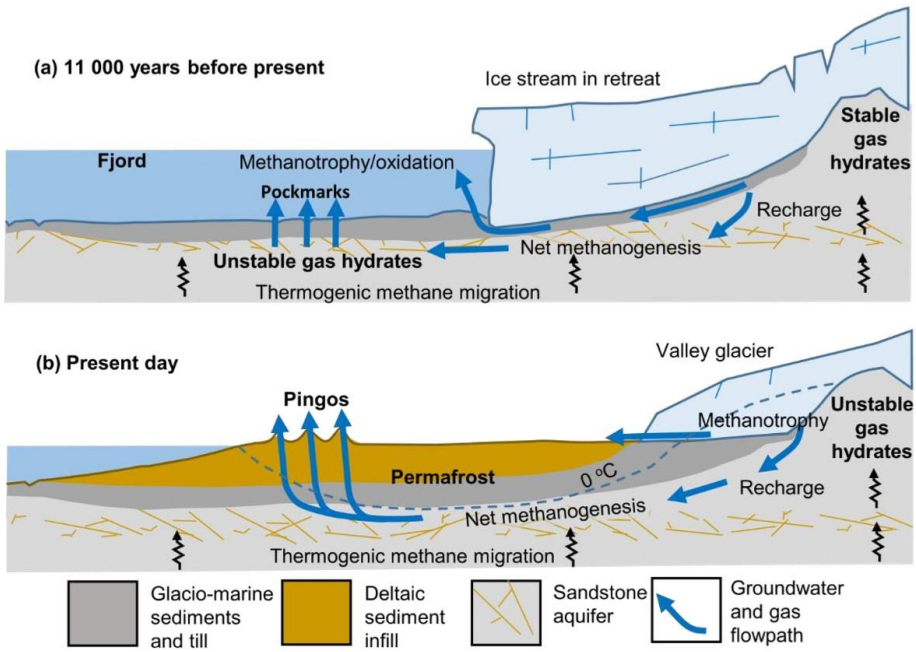

Figure 5: Schematic of the formation of open system pingos in Adventdalen. (a) Arctic ice sheets retreat under post LGM conditions 11,000 years prior in Adventfjorden. Methane evading from destabilized gas hydrates through pockmarks is subject to methane oxidation. (b) Isostatic rebound of fjord sediments with pockmarks have outpaced eustatic sea-level rise. The relic channels, through pockmarks, connecting the subsurface to the sediment surface are still intact. Groundwater driven methane from unstable gas hydrates and from methanogenesis escape through open system pingos. Figure retrieved from (Hodson et al., 2020).

1.5.3 Lagoon pingo

Six pingo structures have so far been discovered in Adventdalen (Hodson et al., 2020). Four of these are characterized by uninterrupted annual groundwater discharge, feeding ca. 1040 kg CH_4 into the atmosphere annually (Hodson et al., 2020). Of these, Lagoon pingo is one of the most studied in Adventdalen (Orvin, 1944; Svensson, 1970; Liestøl, 1977; Yoshikawa, 1993; Yoshikawa and Harada, 1995; Yoshikawa and Nakamura, 1996). It is the outermost of the pingos in the valley, sheltered from the tidal influences of Adventfjorden by Moskuslagunen (Figure 7). The system is the youngest in Adventdalen, estimated to be about 160±20 years old (Yoshikawa and Nakamura, 1996) and is still a growing system. Methane enriched, oxygen limited groundwater is discharged continuously from three documented sources (Hodson et al., 2019), forming crater ponds, where algal biofilms are found during the growth season. The pingo system consists of finely grained, mud-like marine sediments lacking vegetation cover, making it sensitive to seasonal weathering (Svensson, 1970). The annual estimates of methane emissions from Lagoon pingo is 76.5 kg CH_4 $year^{-1}$, amounting to 7% of the annual atmospheric methane emitted from the four open system pingos in Adventdalen (Hodson et al., 2020). In winter, sub-zero degrees causes the pond to freeze and form 1-2 m thick ice-caps (Figure 6). The expulsion of methane saturated groundwater remains uninterrupted throughout the winter months (Hodson et al., 2019). Visible cracks in the ice-caps suggest that water escape and subsequent freezing occurs throughout the winter season (Hodson et al., 2019). With positive temperatures in spring and summer, the ice-cap melts, causing flooding, erosion, and collapse of surrounding pingo sediments, rearranging the structure of the pingo. Alterations in the ice-cap cover and water levels in the pond cause fluctuations in methane emissions (Hodson et al., 2019). Due to ice melt and the subsequent dilution of the methane saturated groundwater, emissions drop early on in the melt season. An increase of gas expulsion coincide with erosions, as meltwater exits the pond and the pond is filled

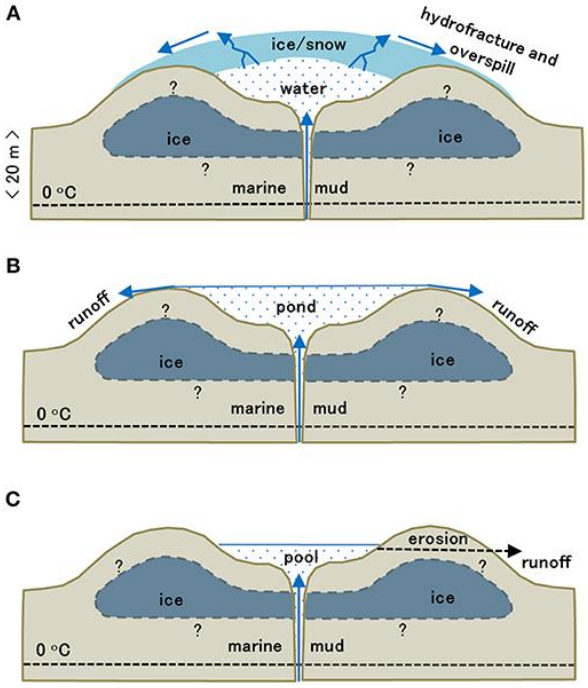

Figure 6: Chronologic schematic of annual hydrologic dynamicity of Lagoon pingo in spring and summer season. (A) Ice-cap melt and pressurized fluids cause ice rupture and water spill. (B) Flooding of pond due to ice melt. (C) Erosion and collapse of surrounding pond sediments. Question marks indicate the uncertainty of the groundwater distribution below the pingo. Figure retrieved from (Hodson et al., 2019).

with methane enriched groundwater (Hodson et al., 2019). The groundwater continues to exit the pond throughout the summer months via a ~60 m long stream reaching surrounding wetlands.

The extreme seasonal alterations in physical conditions, such as freeze-thaw and drought-flooding cycles, in combination with fluctuating methane- and oxygen availability suggest that Lagoon pingo is a challenging habitat for microbial life. Until this point, no microbial profiling has been executed at the four open system pingos in Adventdalen, and the methanotrophic filter potential of these sites is unknown. Due to the high influence of pingo emissions on the local estimates from Adventdalen, Hodson et al. (2019) called for the inclusion of these systems into global methane budgets. Mapping of the overall microbial community with a specific focus on methanotrophic organisms is of key interest and will allow an understanding of the microbial ability to exploit these subsurface methane sources. Furthermore, it is of considerable importance to infer the magnitude of the methane filter and provide high resolution predictions of methane evasion from these systems.

1.6 Objective

The main goal of this master thesis was to investigate and characterize the microbial community in an overlooked arctic system, the open system pingo. To explore the spatial distribution and variation of the microbial community across the Lagoon pingo, 42 sediment samples (in duplicates) were sequenced using primers targeting the 16S rRNA gene. The variation of the community structure was explored along gradients from the methane enriched groundwater source of the pingo to the outskirts of the waterlogged crater. Secondly, key OTUs linked to the methane cycle at Lagoon pingo were investigated, and their potential relationship to environmental parameters were examined.

1.7 Hypotheses

1. Lagoon pingo was originally a part of the marine ecosystem, made terrestrial by isostatic rebound (Gilbert et al., 2018). The surface strata found on site is thus uplifted sediment deposits from the fjord prior to vertical land heave, and fundamentally different from terrestrial soil. Following exposure of atmospheric air and weathering, the system is also expected to differ from seafloor sediments. In addition, the site is subject to continuous subsurface pressure of methane, caused by groundwater discharge evading from the main source and several mini sources on site (Hodson et al., 2019). *H1: The microbial*

ecosystem investigated at Lagoon pingo is inhabited by microorganisms from both terrestrial and marine methane rich environments.

2. Lagoon pingo is a dynamic system that is subject to annual freeze-, thaw-, erosion- and collapse cycles (Hodson et al., 2019). The system is lacking vegetation to keep the sediments united, making it sensitive to seasonal weathering (Svensson, 1970). Also, the methane supply is patchy. *H2: The pingo system consists of multiple microbial habitats with different community composition and structure.*
    a. Low levels of oxygen have been found in the groundwater discharge at Lagoon pingo (Hodson et al., 2019). As the water flows across the pingo crater, dissolved oxygen might be introduced to the water by photosynthesis or wind. *H2A: Aerobic methane oxidizers will not be found in sediments submerged in methane saturated water located close to the source, but rather further away from the source.*
3. The system at Lagoon pingo is subject to a constant, groundwater discharge carrying methane gas from sub surface reservoirs (Hodson et al., 2019; Hodson et al., 2020). The methane saturated water emerges from the spring, filling the pingo crater and flowing across and down the pingo. In addition to the main seep, several smaller seeps have been observed on site. Methane rich water emerges from several sources, suggesting that it is the main energy source for microorganisms in this system.
    a. *H3A: Methane oxidizing organisms make up a large fraction of the microbial community.*
    b. *H3B: The relative abundance of methanotrophs correlates with the availability of methane.*

2 Materials and methods

In the current project we focused our attention on an open system pingo situated in the valley mouth of Adventdalen, Svalbard. This project is part of the CLIMAGAS project that aims to gather geochemical, hydrological and microbiological data to develop predictive models for methane evasion from terrestrial seeps in Adventdalen.

2.1 Site description

Lagoon pingo (N78°14'22 E015°45'16) is an open system pingo located in Adventdalen, Svalbard, on the Northern side of Adventdalen river (Figure 7). The pingo lies by the coast, separated from the tidal water by the Moskuslagoon. The system consists of several elevated mounds with craters, approximately 500 m in length, 150 m in width and <10 m in height (Yoshikawa and Nakamura, 1996). The first groundwater spring was described in the 1920's (Orvin, 1944), while several were described in later years (Yoshikawa, 1993; Yoshikawa and Nakamura, 1996). Lagoon pingo has currently three active springs (Hodson et al., 2020). The spring studied here has a diameter of 0.5 m and is located on the northernmost pingo mound (Figure 8) and has an average groundwater discharge of 0.26 L s^{-1}. The groundwater has been characterized as brackish, with low levels of oxygen for cold water. The redox-potential of the ground water is low, favouring hydrogen sulphide (H_2S) formation, biological phosphorus release, acid formation and methane production (Hodson et al., 2019). The low redox-potential is possibly caused by the microbial removal of nitrate and sulphate (Hodson et al., 2020).

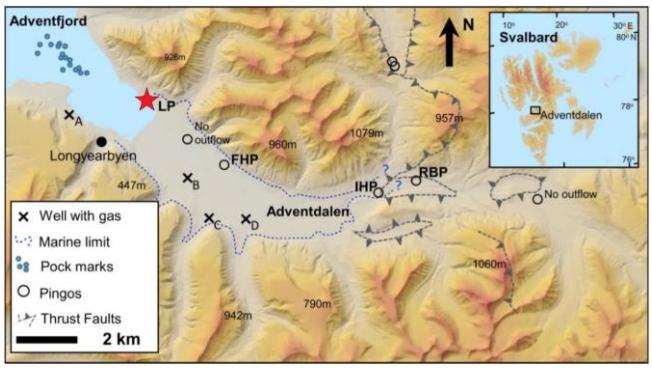

Figure 7: Map over Adventdalen and its respective pingos. Lagoon pingo is marked with a red star. Figure is modified from Hodson et al. (2020).

Figure 8: The main crater at Lagoon pingo.

The stream created by the discharge flows from South to North East where it exits the crater. The pond has a characteristic hydrogen sulphide odour, reported as early as the 1920's (Orvin, 1944). Wet sediment surfaces and areas with dry elevated sediment surrounds the dry crater. The dry sediments are covered by ~1 cm layer of precipitated salts, possibly originating from evaporated water (Svensson, 1970; Yoshikawa and Nakamura, 1996). Surrounding the pond, small discharges (2 – 5 cm diameter) of sub-surface water were observed. These discharges sometimes appeared and shut down within a single day, suggesting a constant water pressure throughout the crater sub-surface.

2.2 Field campaign

A field campaign was launched in early August 2019. In order to profile the microbial community within the various sediment features of the pingo habitat, we sampled sediments from six transects (Figure 9A). Transect 1-5 (T1-5), called the core transects, started at the main source or within the pond, and moved to the outer edges of the crater. Each or these transects consisted of six sampling points, called chamber 1-6 (C1-6). The sixth transect, called the stream transect (TS), followed the moving groundwater discharging from the main source, flowing across the crater pond and exited the pingo crater in the stream. TS was the longest transect, comprising of 12 sampling points (C1-12). C1 was always placed at the main source in all transects, apart from T3 (Figure 9A), and the chamber number (sampling point) increased radially from the main source to the outskirts of the crater. The second and third chamber (sampling point) in transect 1 were thus called T1C2, T1C3 and so on.

2.2.1 Sediment characterization

Due to the marine origin of the study site, we refer to the terrestrial pingo "soil" samples as sediment samples. We distinguished the different sediment samples based on the presence of water and later corroborated these with sediment pH and water content (%), measured for all sampling points. The sediments were divided into seven categories (Figure 9). The waterlogged part of the crater was divided into areas with moving water (pond flow sediment: PF) and static water (still pond sediment: SP). Humid sediments without an overlying water column were classified as wet sediments (WS). Sediments sampled from the stream were grouped into stream sediments (StS) and the dry sediments, mainly observed outside the crater pond, were classified as dry sediment (DS). Small discharges were called mini sources (MS). Sediments form the main spring were called source sediments (SS). The five first sampling points of TS (C2-6) were in the pond, and were thus considered PF. The remaining six sampling points (TSC7-12) were located in the stream and were considered StS.

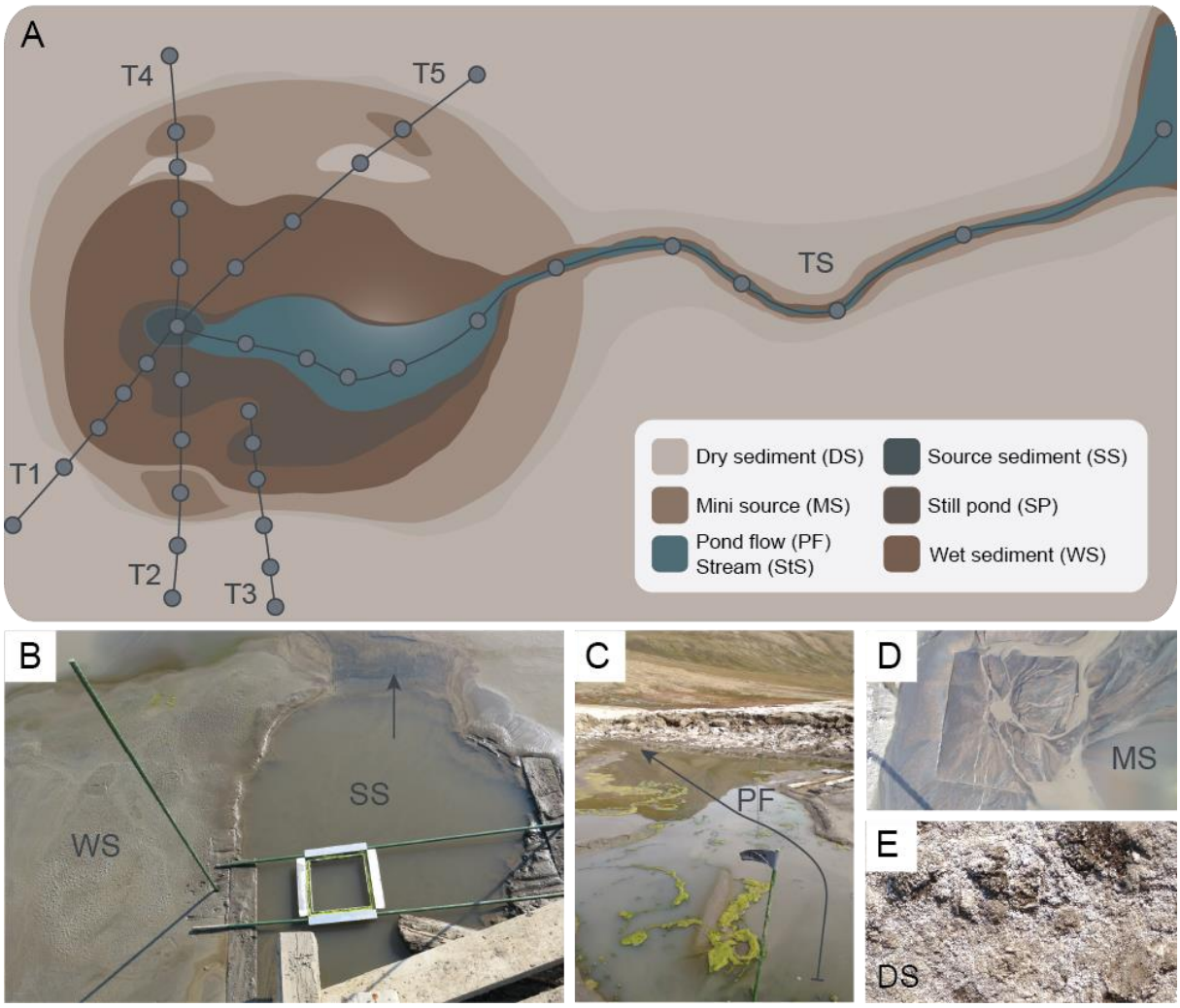

Figure 9: Overview of Lagoon pingo and the sediment types found therein. (A) Schematic of the pingo crater and the exiting stream. Transects 1-5 (T1-5) and the stream transect (TS) with sampling points are depicted as lines and dots, respectively. Each transect started at the source (SS) with sampling point chamber 1 (C1), except for in T3, and traversed the inundated and the wet sediment to the outer edges of the crater. (B) The main source (SS) seeping methane enriched groundwater. A metal frame for methane flux measurements is positioned at the base of the source hole. The arrow demonstrates the direction of water moving into the pond. Clay-like wet sediment (WS) was found surrounding the source (SS) and the pond. (C) Green algal biofilms were observed in clusters throughout the pond. The arrow demonstrated the movement of the flowing pond water (PF) toward the stream (StS). (D) A mini source (MS) emitting groundwater. The square from where the methane flux measurement was taken is visible in the sediment. (E) Dry sediment (DS) with white salt precipitates coating the surface. All sediments at the pingo was finely grained, as visible in B, D and E.

2.2.2 Sediment sampling

Sediments were collected from the upper 1 cm from all sampling points for nucleic acids extraction, pH measurements, methane concentration measurements and oxidation rate experiments. At each sampling point, the sediment sampling was coordinated with methane flux measurements. To tie all measurements together, sediments were collected from inside the flux chamber or directly next to the chamber. However, this was not possible at the source where fluxes were carried out at the water surface, while sediments were collected from the rim of the discharge. Sediments collected from TS, was collected from the pond and stream

bed, located below the methane flux chamber. Sediment samples for nucleic acid extraction were immediately frozen in a portable dry shipper (Air Liquide, Paris, France) on site (<-150°C). pH measurements were performed at UNIS, in 1:5 sediment:MilliQ. Remaining sediment analyses were performed at in Tromsø, at UiT.

2.3 Methane measurements

2.3.1 Methane flux measurements

Continuous measurements of methane fluxes, emitted from the pingo sediments, were recorded in a gas-tight, acrylic glass chamber, specially designed for this purpose. To inhibit the effect of solar heating, the chambers were covered in aluminium foil. Gas fluxes were carried through gas-tight perfluoroalkoxy tubes to a recirculating multiplexer (eosMX-P,Eosense, Dartmouth, Canada) and further detected by a laser spectrometer GHG analyser (U-GGA-915, Los Gatos Research, San José, USA). Prior to each measurement, the chambers and tubes were flushed with ambient air. In core transects (T1-T5) methane fluxes were recorded over five minutes, except for the source where measurements were shortened to one minute due to high methane concentrations. Similarly, measurements at the water surface in TS were recorded for three minutes. All methane flux measurements were conducted and analysed by Franziska Nagel and Tilman Schmider.

2.3.2 Methane oxidation rate

Approximately 10 g of sediment and 10 mL of spring water was placed in 120 mL serum bottles and closed with sterile butyl-rubber stoppers a crimp-caps. Methane was injected into the serum bottles via a gas-tight syringe. Methane concentrations in the headspace depended on expected methane level emitted from the system (see master thesis of Franziska Nagel (Nagel, 2020)). Oxidation rates were measured at t = 0 minutes and minimum once at an interval of 24 hours over three days. Flasks were incubated on site for 8 hours (6-17°C), followed by incubation in the laboratory for the reminder of the experiment (10°C). Methane concentrations were measured with GHG analyser. Methane oxidation rate measurements and calculations were performed by Franziska Nagel and Tilman Schmider.

2.3.3 Methane concentration

Methane concentration was measured in pingo sediments and in the water from the spring. Sediment (~1 mL) and water (~3 mL) was collected in glass exetainers. The lid was mounted and 1 mL/25 µL of the headspace (in sediment samples)/water (in spring samples) was

exchanged with the equivalent volume of NaOH (1 M), using an air-tight 1 mL NORM-JECT® syringe (Henke-Sass Wolf GmbH, Tuttlingen, Germany). Methane content measurements were performed in Tromsø, under the supervision of Dimitri Kalenitchenko. All calculations were done by Tilman Schmider in cooperation with Dimitri Kalenitchenko.

For in depth information on methodology of methane flux measurements, methane oxidation rate assays and the subsequent calculations of oxidation rate estimates and methane concentrations see Nagel (2020).

2.4 O_2 measurements

Oxygen profiles were recorded in the first 15 mm in TS, using a miniaturized 100 µm width Clarks type electrode (OX-100, Unisense, Aarhus, Denmark) and a microsensor multimeter (Unisense, Aarhus, Denmark). Vertical oxygen concentrations were measured perpendicular to the sediment surface, using a motorized micromanipulator (Unisense, Aarhus, Denmark) with a resolution of 100-250 µm. Hourly, two-point calibrations were done using saturated water and a mix of sodium ascorbate (0.1 M) and NaOH (0.1 M) as saturation- and zero oxygen standard, respectively. Up to four oxygen concentration profiles were done on sediment cores of 5 cm from each chamber in TS. The measurements were performed field tent on site. All oxygen measurements were executed by Dimitri Kalenitchenko.

2.5 Total nucleic acid (TNA) extraction

We optimized extraction procedures for optimal extraction of DNA and RNA from sediments from Lagoon pingo. The method was based on Angel et al. (2012) aiming to isolate total nucleic acids (TNA) from soil using a phenol/chloroform protocol. Samples for TNA extraction were kept at -80°C, prior to further processing. Introducing steel jars (Qiagen, Hilden, Germany) to crush and homogenize frozen sediment samples, we were able to increase the efficiency and make the protocol more replicable. We ground the sediment 3×30 s at frequency 30 Hz using a TissueLyser II (Qiagen, Hilden, Germany). The jars were frequently cooled in liquid nitrogen to keep the integrity of the samples. The equipment that was in direct contact with the sampled sediments was cleaned with ethanol and treated in a UV cabinet (UVC 500, UV Crosslinker, Hoefer) for 20 min at 9000 µJ/cm^2 prior to use. Approximately 0.2 g sediment was loaded into Lysis Matrix E 2 mL tubes (MP Biomedicals, California, USA) and further extracted in duplicates. The sediments were extracted three times with equal amounts of phenol chloroform isoamylalcohol (PCI) solution (ratio 25:24:1, pH 6.6-7.9) and TNS extraction buffer (10% SDS/500 mM TRIZMA/100 mM NaCl, pH 8),

volumes being 500 µL, 300 µL and 200 µL. Bead beating of samples was executed using an MP Biomedicals™ FastPrep-24™ (California, USA) at 5,0 m/s for 30 seconds. Between each extraction- and bead beating step the supernatant was transferred to new reaction tubes. All extracts were extracted with chloroform isoamylalcohol (CI) solution (ratio 24:1) and the TNA was precipitated with PEG-6000 (37.4 g of NaCl and 120 g polyethylene glycol; dissolved in 400 mL water and treated with 0.1% DEPC) and glycogen (Invitrogen by Thermo Fischer, 1 ml, 5 mg/mL). The pelleted nucleic acids (NA) were washed with ice cold 70% ethanol. The purified pellet was eluted with 50 µL nuclease free H_2O and 0.5 µL RNase inhibitor. For the full protocol see Appendix IA. The purity of the DNA isolates was measured by NanoDrop 1000 Spectrophotometer (Thermo Scientific, Wilmington, DE, USA). The quality of the TNA extracts was visually determined on a 1% TAE agarose gel, using Gel Documentation Systems (Bio-Rad, Hercules, CA), following gel electrophoresis. For details about chemicals see Appendix IB. The yield of DNA and RNA in all duplicates was assessed using Qubit® 2.0 Fluorometer (ThermoScientific, Massachusetts, USA). A substantial part of the extractions and quality checking of the extracts was conducted with Franziska Nagel.

2.6 Dry weight

In collaboration with Tilman Schmider, the water content in samples was identified and normalized to DNA concentrations per gram dry sediment. We assessed the moisture content of all samples according to the American Society for Testing and Materials standard procedure (ASTM D2974-20e1, 2020). The sediment from completed methane oxidation experiments were used to determine dry weight (dw). The sediment samples were sealed in 120 mL serum bottles and had been stored at ~4°C for approximately 6 months after sampling. The samples were dried at 105°C for 20 h in a drying oven (Memmert GmbH + Co. KG, Germany). We dried all samples in duplicates, apart from T1, T5C1, T5C4 and TSC2+C9, as one replicate of each of these had already been processed for other purposes. The weight of the bottles was determined before and after drying.

2.6.1 Calculation of sediment moisture

The calculation of moisture in sediment samples from Lagoon pingo were determined using equation 1, where A and B are sample weights before and after drying, respectively.

$$\text{Moisture content (\%)} = \frac{(\text{A} - \text{B}) \text{ x } 100}{\text{A}} \qquad 1$$

2.6.2 Normalized NA concentrations in extracted samples:

We calculated the DNA concentration (ng) per gram dw using equation 2, where a is the DNA concentration (ng) measured by Qubit®, and b is the elution factor of the samples. This part of the equation makes up the total DNA mass. The product was further divided by the dry weight of each extract (c) and multiplied by the water content in percentage (d).

$$\text{DNA}\left(\frac{\text{ng}}{\text{g}}\right)\text{dw} = \frac{\text{a} \times \text{b}}{\text{c} \times (1 - (\text{d} \div 100))} \qquad 2$$

3 Sequencing

3.1.1 Preparation

The suitability of the DNA for PCR amplification was evaluated in a set of tests. The full length of the 16S rRNA gene was targeted using primer pair Bac 27F/1492R (Table 1), using the PCR program (96°C×1 min;(96°C×1 min;54°C×1½ min;72°C×1 min) ×30;72°C×15 min;4°C×10 min;12°C×∞). We ran the setup on samples from T2, T3, T4 and TS, testing all sediment categories, except for StS. We obtained the most successful amplification at 100× dilution with PCR water. A PCR was launched targeting the *pmoA* gene, using two primer pairs 189F/661R and 189F/682R. However, we could not detect any products after 30 cycles. Regents used for the 16S and *pmoA* PCRs were from Invitrogen and Qiagen, respectively. The concentrations and volumes used were chosen according to the manufacturer's manual, and primer concentration in all runs was 10 µM.

Table 1: Primer pairs used for amplification of the 16S region in sediment samples from Lagoon pingo. Primer pair used for PCR amplification (27F/1492R) was executed at UiT, while the primer pairs 515F-Y/926R and 519F/1041R were used for Illumina Miseq sequencing, targeting the universal bacterial 16S rRNA gene and the archaeal 16S rRNA gene, respectively.[a,b]

Primer	Sequence (5'-3')	Target	Reference
27F	5'-AGAGTTTGATCCTGGCTCAG-3'	Bacteria and Archaea, entire 16S	(Weisburg et al., 1991)
1492R	5'-GGTTACCTTGTTACGACTT-3'		
515F-Y	5'-GTGYCAGCMGCCGCGGTAA-3'	Universal V4-V5 region	(Quince et al., 2011)
926R	5'-CCGYCAATTYMTTTRAGTTT-3'		(Parada et al., 2016)
519F	5'-CAGCMGCCGCGGTAA-3'	Archaea V4-V6 region	(Øvreås et al., 1997)
1041R	5'-GGCCATGCACCWCCTCTC-3'		(Kolganova et al., 2002)

[a] M = A or C; R = A or G; Y = C or T; W = A or T

[b] F = forward primer, R = reverse primer

3.1.2 Sequencing primers

To obtain sequences of the microbial community at Lagoon pingo, we applied primers targeting the hypervariable region V4-V5 of the universal biomarker gene 16S small subunit (SSU) rRNA gene. As sequencing technology limits read lengths, partial sequencing of the 16S rRNA gene is common practice, however a consensus of hypervariable region does not exist. Studies have shown that the choice of 16S region does affect the reliability of community structure- and diversity results (Teng et al., 2018), and a growing support of the V4-V5 region is emerging (Yang et al., 2016; Teng et al., 2018). Global initiatives to unify field-, experimental methods for microbial communities, such as the Environmental Microbial Project (EMP) (Gilbert et al., 2010), supports this notion, applying the universal primer pair 515F-Y/926R (Quince et al., 2011; Parada et al., 2016) targeting the V4-V5 region for 16S amplicon sequencing. This primer pair has been widely applied in HiSeq and MiSeq Illumina sequencing of 16S amplicon constructs and is recommended by the EMP. The results generated from the current sequencing, is therefore comparable to other studies. The primer pair 515F-Y/926R is considered a microbial "universal primer" as it targets both Bacteria and Archaea.

To profile the archaeal communities in depth, we applied the specific archaeal primer set 519F/1041R (Øvreås et al., 1997; Kolganova et al., 2002). This primer pair covers the hypervariable region V4-V6 and has been tested *in silico* (Klindworth et al., 2013) and experimentally on a variety of samples including surface seawater (Lambert et al., 2019),

wastewater (Gonzalez-Martínez et al., 2018) the human microbiome (Pausan et al., 2019) and faecal samples from ruminants (Goux et al., 2016).

3.1.3 Illumina MiSeq

Duplicate sediments from all 42 samples collected at Lagoon pingo were sequenced using two primer pairs, resulting in a total of 84 Bacteria and 84 Archaea libraries generated and sequenced through the Illumina MiSeq platform at IMGM Laboratories GmbH (Martinsried, Germany). Library preparation and sequencing was performed with V3 chemistry for a desired sequence depth of 25,000 read pairs. A set of sequencing runs, 13 bacterial and 25 archaeal, failed due to low DNA concentrations. These samples were successfully re-sequenced and the new sequence data was merged with the sequence data from the first run by IMGM.

3.2 Processing of sequence data

FASTA files containing raw pair end sequences and quality information received from IMGM were processed according to a script developed by Dimitri Kalenitchenko (Appendix IC). The script mainly applies the QIIME2 next-generation bioinformatics platform (Bolyen et al., 2019). Due to the magnitude of the raw data and the desire to parallelize the processing effort, the script was run on ABEL (UNINETT/SIGMA2) applying 16 central processing units. Prior to running the script, certain parameters were set. The minimum and maximum length of the sequences were set to 410 and 430 nucleotides for the primers 515F-Y/926R and 530 and 550 nucleotides for the primers 519F/1041R, respectively, to remove incorrect sequences.

3.2.1 Generating OTUs

The sequences received had already been demultiplexed based on barcodes by IMGM, and the data could be denoised. The Divisive Amplicon Denoising Algorithm 2, DADA2 (Callahan et al., 2016) was used for denoising the sequences to identify which reads were correct biological sequences. Here, all forward and reverse reads were truncated (at the 5’ end) from nucleotide position 294, respectively. Both forward and reverse reads were trimmed (at the 3’ end) by 3 nucleotides. By cleaving off bases from either side of the reads, the nucleotides that were incorporated in the first and the last sequencing cycles were removed. These nucleotides are often of low quality, making read identity difficult to establish. This way, the overlapping nucleotides between the forward and reverse reads would be more reliable and the final, merged product more correct. Forward and reverse reads

having a value of expected errors surpassing 1 were eliminated from the dataset using the DADA2 parameter *max--ee*.

Forward and reverse reads were merged into sequences of approximately 400 nucleotides using BBMerge v38.44 (Bushnell et al., 2017). The program uses the overlapping sequence between the forward and reverse reads to merge them. The merged reads in FASTQ files were further filtered using VSEARCH v2.13.3 (Rognes et al., 2016), and the threshold of expected number of errors were set to 1. Samples were labelled, concatenated and the quality of the sequences was inferred using mothur; *summary.seq*. Full length dereplication was executed using VSEARCH, creating an empty hash table into which sequences are computed. Non-identical sequences are entered into the table separately. Sequences that are identical to existing sequences in the hash table are clustered with their respective match (Rognes et al., 2016). Further, the sequences were sorted by decreasing abundance using *sortbysize*, the desired format for further processing by VSEARCH (Rognes et al., 2016). The dereplicated FASTA files where further denoised using UNOISE3 (Edgar, 2016), correcting sequencing errors in reads and deleting chimeras, then they were sorted by decreasing length using VSEARCH. Archaeal and prokaryote OTUs were clustered using USEARCH, applying the SILVA database v. 132. Applying the USEARCH function *cluster_smallmem*, a centroid clustering method using the UCLUST algorithm (Edgar, 2010) was selected, clustering sequences at 97% minimum sequence identity. Centroid clustering is based on allocating centroid sequences for clustering. Here, all sequences with 97% similarity to the centroid sequence were clustered together. From the generated clusters OTU tables were produced and taxonomy was assigned to the OTUs, using the *classify.seq* function from the mothur v1.43.0 software package (Schloss et al., 2009) with the SILVA v132 database (Yilmaz et al., 2013). The *classify.seq* function applies the Wang method investigating all kmers, and a bootstrap value was assigned to all queries. To have a relatively high confidence in the taxonomic assignment, all queries with a bootstrap value below 75 were removed. To infer the origin of the OTUs, OTU tables were computed by mapping the processed reads to the “raw” reference OTUs. These were generated based on a 97% minimum sequence identity and further converted into BIOM format (McDonald et al., 2012).

3.3 Rarefication of OTU tables

The universal- and Archaea specific primer pairs targeted the 16S rRNA gene in all prokaryotes and in Archaea, respectively. The 16S rRNA gene is found in genomic material

in chloroplasts and the mitochondria, and a large part of the OTUs were associated accordingly. Hence, all OTUs associated to chloroplasts and mitochondrial DNA, in addition to unknown taxa were removed from the dataset. The OTUs that were not related to the domain targeted by the primer set were also excluded from the tables. The end result left the universal OTU table containing OTUs associated with Bacteria and Archaea, while the archaeal OTU table consisted of solely OTUs related to Archaea.

Using QIIME2 the *core-metrics-phylogenetic* method was applied to rarefy the filtered OTU tables and execute alpha and beta diversity analyses. Here, a random subset of sequences within each sample is selected without replacement, thus normalizing the sequence data. The samples with sequence numbers below the set rarefication depth are removed from the dataset. Using the *--p-sampling-depth* argument the rarefaction depth was set to 5,821 and 1,000 sequences for the universal- and archaeal OTU table, respectively. The rarefication depth for the archaeal OTU table was almost six times lower than the universal OTU table, due to very low sequence numbers in archaeal samples after the removal of Bacteria associated OTUs. As the number of sequences per sample was relatively high in the universal OTU table, compared to the archaeal OTU table, the rarefication depth for the former was set to the lowest number of sequences within a sample. The rarefied OTU tables were referenced back to the reference OTU table and taxonomy was added to each OTU.

3.4 Cluster analyses

To explore local variability in microbial community structure a dendrogram was made to emphasise sample clustering based on likeness. OTU based clustering was assessed by running various hierarchical cluster analyses on the rarefied OTU tables using RStudio 1.1.463 (RStudio Team, 2016) with R 3.6.3 (R Core Team, 2020). The function *hclust* in the *vegan* (v2.5-6; Oksanen et al., 2019) package was applied, using the Bray Curtis diversity distance matrix, while testing for the optimal clustering method (single linkage, complete linkage, average linkage, central clustering and Ward's minimum variance clustering) according to (Borcard et al., 2011).

Quality control of the suitability of the clustering method to the datasets were executed by comparing the original dissimilarity matrices and the cophenetic distance matrix, making shepard-like plots and calculating the Gower distance (distance in sum of squares between the original and the cophenetic distances). In both cases, the average linkage, also called Unweighted Pair-Group Method applying arithmetic Averages (UPGMA) proved to be the

best fit. Here, a sample is grouped based on its mean dissimilarity with all other samples. All replicates were removed from both datasets and the desired cluster analysis (UPGMA) was executed once more. The final dendrogram was created using the *dendextend* (v1.13.4; Galili, 2015) package. Clustering trends were highlighted by colouring sample clusters (four and three groups for the universal- and the archaeal OTU table dendrogram, respectively), and coordinated with bar charts for displaying the relative abundance within each sample.

3.5 Circle packaging

Based on clusters defined by the dendrograms, the relative abundance of methane cycling OTUs (>50 sequences) were visualized using the R packages *packcircles* (v0.3.3; Bedward et al., 2018) and *ggplot2* (Wickham, 2016).

3.6 Phylogenetic assignment of target OTUs

To convey relatedness between selected methane cycling OTUs and known taxonomic groups, we used the basic local alignment search tool (BLAST). Specific OTUs were aligned to the online NCBI database. The identity between our OTUs were inferred through pairwise sequence alignment, using the global alignment tool EMBOSS Needle (EMBL-EBI).

3.7 Statistical testing

3.7.1 Alpha diversity

Alpha diversity analyses were done using RStudio. The function *diversity* in the *vegan* (v2.5-6; Oksanen et al., 2019) package was used to calculate the Shannon and Simpson indexes for the bacterial and archaeal rarefied OTU tables (Table A 1), using the equations $H = \sum_{i=1}^{R} p_i \ln \rho_i$ and $\lambda = \sum_{i=1}^{R} \rho i^2$, respectively. The total diversity for each index was acquired taking the exponential of the Shannon index and the inverse Simpson index. By dividing the total diversity on the OTU richness, evenness values for each index was obtained.

3.7.2 Correlation analyses

The association between variables such as OTU abundance and environmental parameters (methane flux, oxidation rate and methane concentration) was tested using *cor* function in R. The analyses were conducted using the option *pairwise.complete.obs* and the Spearman's rank correlation coefficient. A threshold of +/-0.6 was set as an indication of a relationship. Prior to analyses, the sequence data was row normalized. Correlations were visualized using the *corrplot* package (v0.84; Wei and Simko, 2017).

4 Results

4.1 Environmental parameters

4.1.1 Water content and pH

Water content and pH were measured for all sampling points at Lagoon pingo. These parameters are shown as averages for each sediment category (Table 2). Sediments in the middle of the crater (SS, SP, PF) and the stream (StS) were waterlogged. The mean water content of the sediments appeared to decrease with increasing distance from the source (see Appendix II: Figure A 1), however the relationship was not statistically significant. WS samples were generally found closer to the source than the MS and DS, however the water content of WS locations (17 – 50%) had a higher standard error than in the MS and DS locations, which implies that in some cases the water content in MS sediments exceeded that of WS sediments.

The pH of Lagoon pingo's sediments were alkalic, ranging from 8.4 – 10.6. The pH measured in the SS sediments were the least alkaline. Overall, pH measurements appeared to increase with decreasing water content in the core transects (T1-5) (Figure A 2). The most alkaline sediments were found in DS locations.

Table 2: The seven sediment categories established based on field observations. Distance to the source is shown as sampling points minimum and maximum distance (m). The average percentage of water in sediments was calculated for sampling points without an overlying water column. pH was measured for sediments at all sampling points. The standard error is presented in parentheses.

Sediment category	Min - Max distance to source (m)	Mean water content in sediment (%)	Mean pH
Source sed. (SS)	0	Waterlogged	8.67 (±0.05)
Still pond sed. (SP)	1 – 8	Waterlogged	9.40 (±0.04)
Wet sed. (WS)	2 – 10	33.36 (±5.21)	9.51 (±0.14)
Mini source sed. (MS)	7 – 14	28.33 (±2.44)	9.21 (±0.58)
Dry sed. (DS)	6 – 16	16.64 (±1.57)	10.05 (±0.19)
Pond flow sed. (PF)	2 – 20	Waterlogged	8.94 (±0.15)
Stream sediment (StS)	29 – 81	Waterlogged	9.12 (±0.04)

4.1.2 Methane fluxes

A spatial variation of the methane fluxes was observed at Lagoon pingo (Figure 10). Measurements made at DS, SP and WS locations never exceeded 4 nmol m^{-2} s^{-1}, while measurements from locations with running water ranged from 65 – 1,644 nmol m^{-2} s^{-1}. The highest methane fluxes were measured at the source with an average value of 1,260 ± 107 nmol m^{-2} s^{-1}. Based on Spearman's rank correlation coefficient we observed a decline in methane fluxes with increasing distance from the source in TS (rho = -0.88, $p < 0.01$) (Figure A 3). Methane fluxes decreased evenly from TSC1 (~990 nmol m^{-2} s^{-1}) to TSC12 (~1 nmol m^{-2} s^{-1}), with the exception of TSC4 where measurements exceeded that of the previous chambers, and TSC6 where measurements were equally low to that of TSC10 (~220 nmol m^{-2} s^{-1}). The average methane flux of PF sediments was 750 ± 140 nmol m^{-2} s^{-1}, while StS sediments emitted 320 ± 105 nmol m^{-2} s^{-1}. All measurements from TS exceeded 100 nmol m^{-2} s^{-1}, apart from C11 and 12 where the values dropped to 65 and below one, respectively. On average the MS locations (T2C4, T4C5 and T5C5) emitted more methane than StS on average with a value of 368 ± 186 nmol m^{-2} s^{-1}. However, the lowest measurement found in MS T5C5 was lower than in all StS locations (45 nmol m^{-2} s^{-1}), except for TSC12.

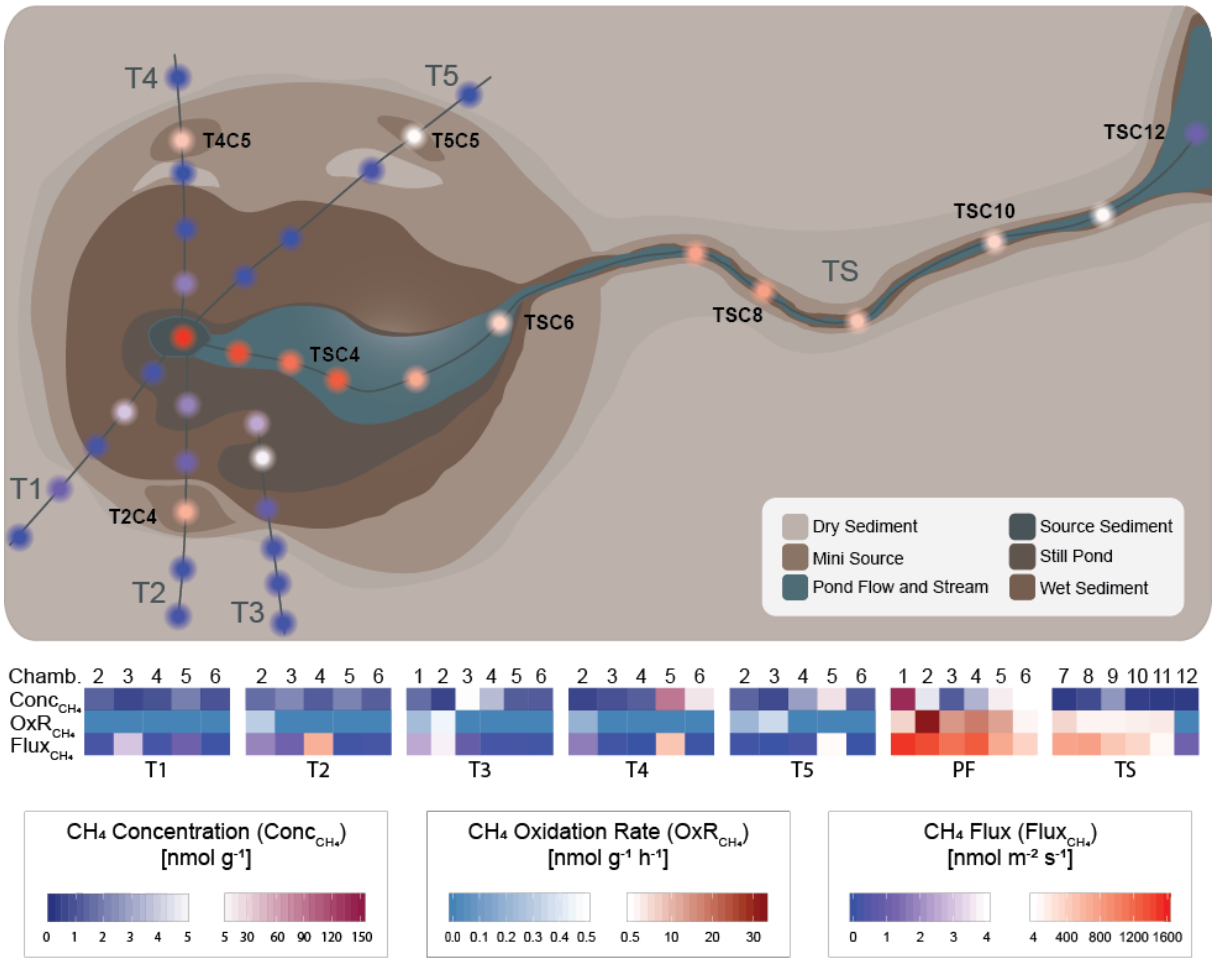

Figure 10: Schematic map of the pingo site displaying the measurements of methane concentration, methane fluxes and methane oxidation rate experiments for each sampling point (chamber). The methane flux measurements are displayed as circles conveying flux data between 0-1,600 nmol m^{-2} s^{-1}. Methane concentration, oxidation rate and flux are shown in bars, representing each sampling point in the transects (T1-5 and TS). Chamber numbers (Chamb.) are displayed over the bars. The source sampling point is only shown in the PF transect. Methane concentration and oxidation rates were measured in sediment samples, while methane fluxes were measured from the surfacing sediment and from the water surface in SS, SP, PF and StS. The sampling points that are mentioned in the main text are marked in the schematic. Data points conveying methane fluxes, oxidation rates and their respective scales were made by Tilman Schmider.

4.1.3 Methane oxidation rates

Similar to the methane flux trend, the methane oxidation rate waned with distance to the source in TS (rho = -0.75, $p < 0.01$) (Figure A 3). However, the average oxidation rate measured at the source was equal to the average of the StS sediments (TSC7-12), where rates never exceeded 6 nmol g^{-1} h^{-1}. In PF locations the methane oxidation rates registered were 12 – 30 nmol g^{-1} h^{-1}. No methane oxidation rates were detected in T1-5, except in certain SP and WS locations, though never exceeded 1 nmol g^{-1} h^{-1} in T1-5. A positive correlation was observed between methane flux and methane oxidation rates (rho = 0.85, $p < 0.01$) in TS (Figure A 3).

4.1.4 Methane concentration

No clear trend in sediment methane concentrations was observed (Figure 10), yet correlation analyses uncovered a negative relationship between methane concentrations and distance to the source (Figure A 3), as observed for methane flux- and methane oxidation rate data. The highest concentrations were measured in SS, however with large variation, ranging from 22 – 287 nmol g^{-1} sediment. A large variation in methane concentrations was also observed in MS locations (1 – 88 nmol g^{-1}). Unlike methane flux and oxidation rate measurements, no trend was observed in TS, ranging from 0 – 33.56 nmol g^{-1}. In WS, DS and SP, concentrations rarely exceeded 5 nmol g^{-1}, with exception of T4C6 (DS) where the concentration was 16 nmol g^{-1}. Of the three MS locations, the methane concentration was the lowest in the site where the methane flux was the highest.

4.1.5 Oxygen content

O_2 concentrations were measured for sediments and overlying water at all twelve sampling points in TS. Measurements confirmed that the groundwater from the spring was depleted in O_2. O_2 was also not detected in sediments lining the seep hole (SS). Concentrations in the water varied from ~300 – 550 µmol L^{-1} throughout the transect, with measurements peaking in the middle of the pond and beginning of the stream (C4-7, >450 µmol L^{-1}). The penetration depth and the concentration of O_2 in sediments varied between samples (4.8 – 12.8 mm and ~300 – 850 µmol L^{-1}, respectively) (Figure A 4). The maximum concentrations of O_2 in sediments were mostly found in the upper 3 mm, except for C10 where the O_2 concentration peaked at ~5 mm.

4.2 Microbial community structure

4.2.1 Environmental DNA sequencing

4.2.1.1 The concentration of DNA extractions

Total DNA concentrations from sediment samples varied from ~60.0 – 60,000 ng/g dw, with an average of ~5,500 ng/g dw (Figure 11). The highest concentrations of DNA were found in StS (average 19,306 ± 16,594 ng/g dw), PF (9,737 ± 8,723 ng/g dw) and SP (6,984 ± 3,072 ng/g dw). Sample TSC12 (both duplicates) from the StS category, contrasted from the remaining StS samples with a concentration of 40,000 – 60,000 ng/g dw. The lowest average concentrations were observed in the WS (2,132 ± 3,670 ng/g dw), SS (~935 ± 301 ng/g dw), DS (478 ± 435 ng/g dw) and MS (283 ± 264 ng/g dw) samples.

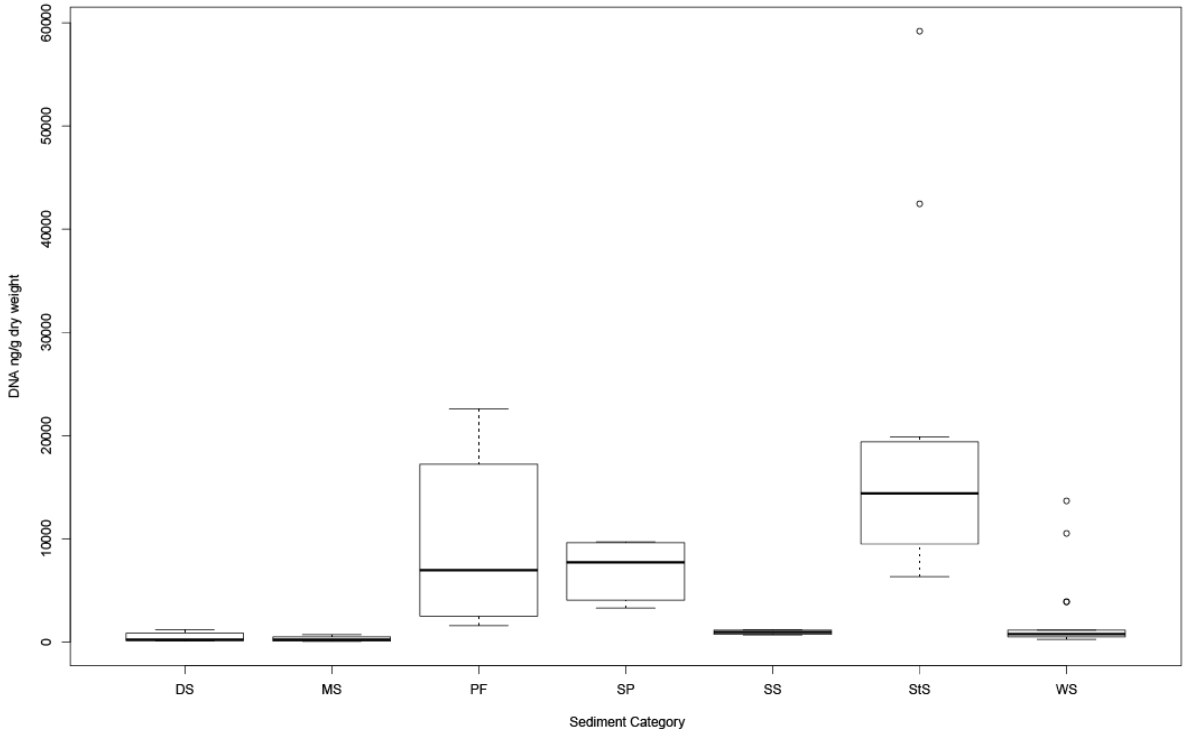

Figure 11: Extracted DNA (ng/g dw) in sediment samples according to sediment categories; dry sediment (DS), mini source (MS), pond flow sediment (PF), still pond sediment (SP), source sediment (SS), stream sediment (StS) and wet sediment (WS).

4.2.1.2 Archaeal and bacterial read numbers

Library yields obtained by Illumina MiSeq sequencing varied between the two 16S SSU rRNA gene primer pairs (515F-Y/926R and 519F/1041R) and between sampling points. Libraries obtained with universal and archaeal primer pairs contained in total ~2,475,000 and ~1,380,131 reads, respectively.

Of the sequences generated with the universal prokaryote primer pair, reads associated with bacterial OTUs (bOTUs) represented 98% of all sequences. Archaeal sequences represented 0.1%, and the remaining ~2% were assigned to Eukaryote and unknown taxa. Of the 98% bacterial sequences, 16.4% belonged to OTUs associated with rDNA in chloroplast and 0.1% in mitochondria, leaving 1,927,345 reads (~78% of total) after filtration. After this filtration step, the average sequence depth per sample was 22,944.58 ± 24,867. Three sub-samples (T3C3 B, T3C4 B and T4C2 B) had read numbers exceeding 95,000 sequences, disproportionally influencing the average sequence depth. After excluding these sub-samples, the average was reduced to 18,853 ± 11,792.9 sequences.

Sequence yields from the archaeal libraries were predominantly assigned to bacterial taxa (83% of total read number), of which half was identified as chloroplast 16S rDNA. Of the remaining sequences (17%), <0.05% were assigned as eukaryotic and unknown OTUs. Sum of archaeal sequences was 236,498, with a mean final sequence number of 16,430 ± 6,094.9 per sample, prior to rarefication.

Bacterial sequences obtained with the universal prokaryote primer pair was ubiquitous at Lagoon pingo (Figure 12). Bacterial sequences dominated the archaeal libraries obtained from the outskirts of the pingo crater, but at the source, T4C3, T5C2 and T5C3, archaeal reads made up the majority.

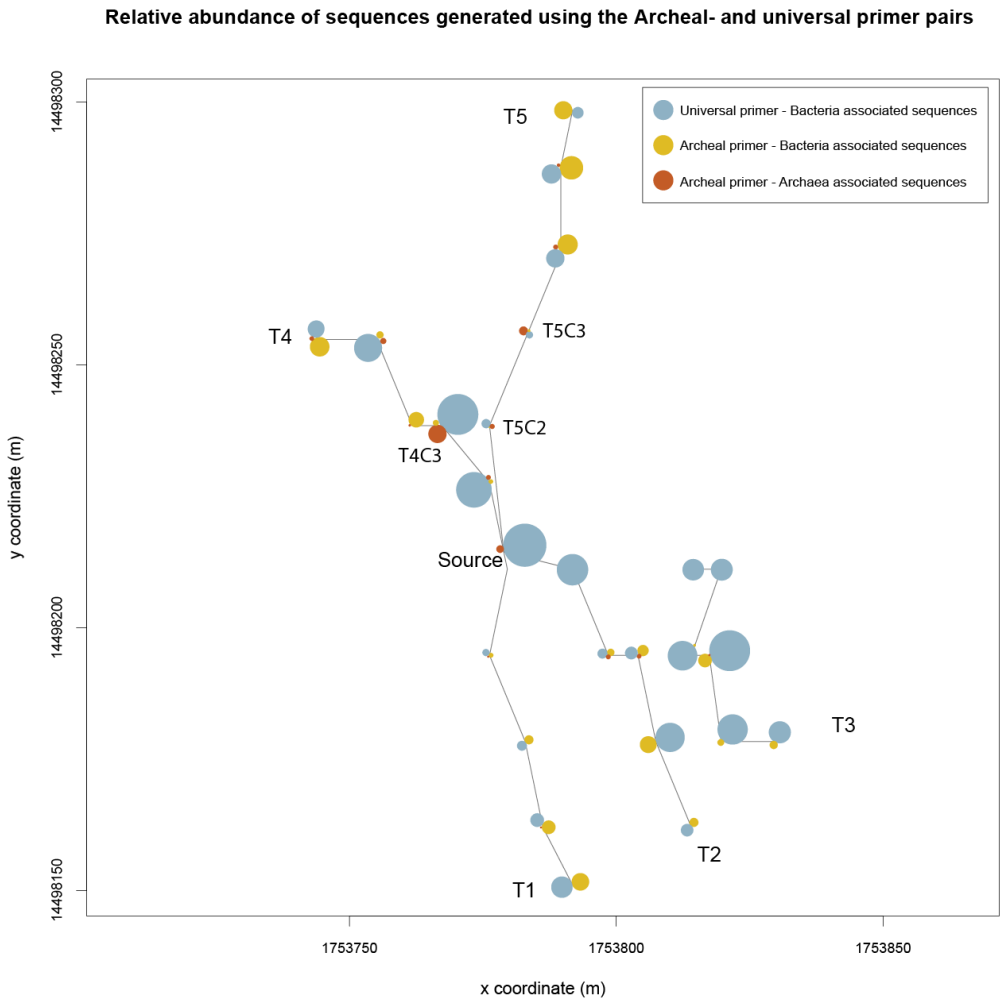

Figure 12: Relative abundance of SSU 16S rRNA gene amplicons generated by primers targeting A) all prokaryotes and B) Archaea. All bubbles sizes are relative to the sample with the highest read number in replicates. The relative abundance of archaeal sequences obtained in archaeal libraries is marked in brown, while the relative abundance of bacterial sequences generated by the universal- and archaeal primer pairs are marked in blue and yellow, respectively. The map is generated using non-rarefied data from filtered OTU tables. Rectangular coordinates are displayed in meters.

4.2.2 Bacterial community structure

Clustering of the bacterial communities were carried out using hierarchical clustering with average linkage (UPGMA) and the Bray Curtis distance. Four main clusters formed at 75% dissimilarity (Figure 13), where 76% of all samples were clustered with their respective sediment category. The clusters were thus named according to the dominating sediment type within each cluster: the pond flow/stream sediment (PF/StS), source sediment (SS), wet sediment (WS) and dry sediment (DS). Of the four major sediment categories (PF/StS, SS, WS and DS), 4 samples did not fall into the cluster assigned by their sediment category. In addition, the mini source (MS) and still pond (SP) sediments did not form separate clusters. MS sediments clustered with samples from static sediments (WS and DS) and the SP sediments clustered with samples from waterlogged locations (SS, PF and StS).

Two phyla, Bacteroidetes and Protobacteria, dominated the microbial communities in all clusters. The remaining phyla were less abundant, each accounting for 0.02 – 8% in all samples. The PF/StS cluster grouped separately at >80% dissimilarity, containing on average a higher abundance of Bacteroidetes (39 ± 7.81%) than Proteobacteria (33 ± 13.29%). In SS, WS and DS clusters, where Proteobacteria was the most abundant phyla, with 48.21 ± 6.25%, 45.94 ± 8.98% and 47.67 ± 7.91%, respectively. Bacteroidetes represented 29.83 ± 11.07%, 37.71 ± 11.81% and 32.57 ± 6.72% in SS, WS and DS, respectively. Verrucomicrobia represented 20 ± 9.94% of the microbial community in cluster PF/StS, while only <3% in the remaining clusters. The SS, WS and DS communities were placed in one cluster at 80% dissimilarity, with the SS and WS samples being slightly more alike.

The SS cluster differed from other clusters in its relatively high abundance of Epsilonbacteraeota (mean 9.6 ± 8.94%) and Firmicutes (mean 5.1 ± 5.6%), while in the StS, WS and DS clusters these phyla accounted for <2%, of the communities, respectively. Actinobacteria were found mainly in DS and WS. Cyanobacteria were found in the DS cluster.

The community variation within DS was lower than in the WS, PF/StS and SS cluster. The MS and SP samples were not clustered together; however, the majority of the MS and SP samples were grouped with sediment categories of water content exceeding 30% (Table 2). This was not the case for MS sample T5C5, that fell into the DS cluster along with WS samples T1C4 and T3C4. The three SP samples were more similar to the samples in clusters

defined by flowing water, while the MS samples appeared in the WS and the DS clusters where the sediment category was less influenced by running water.

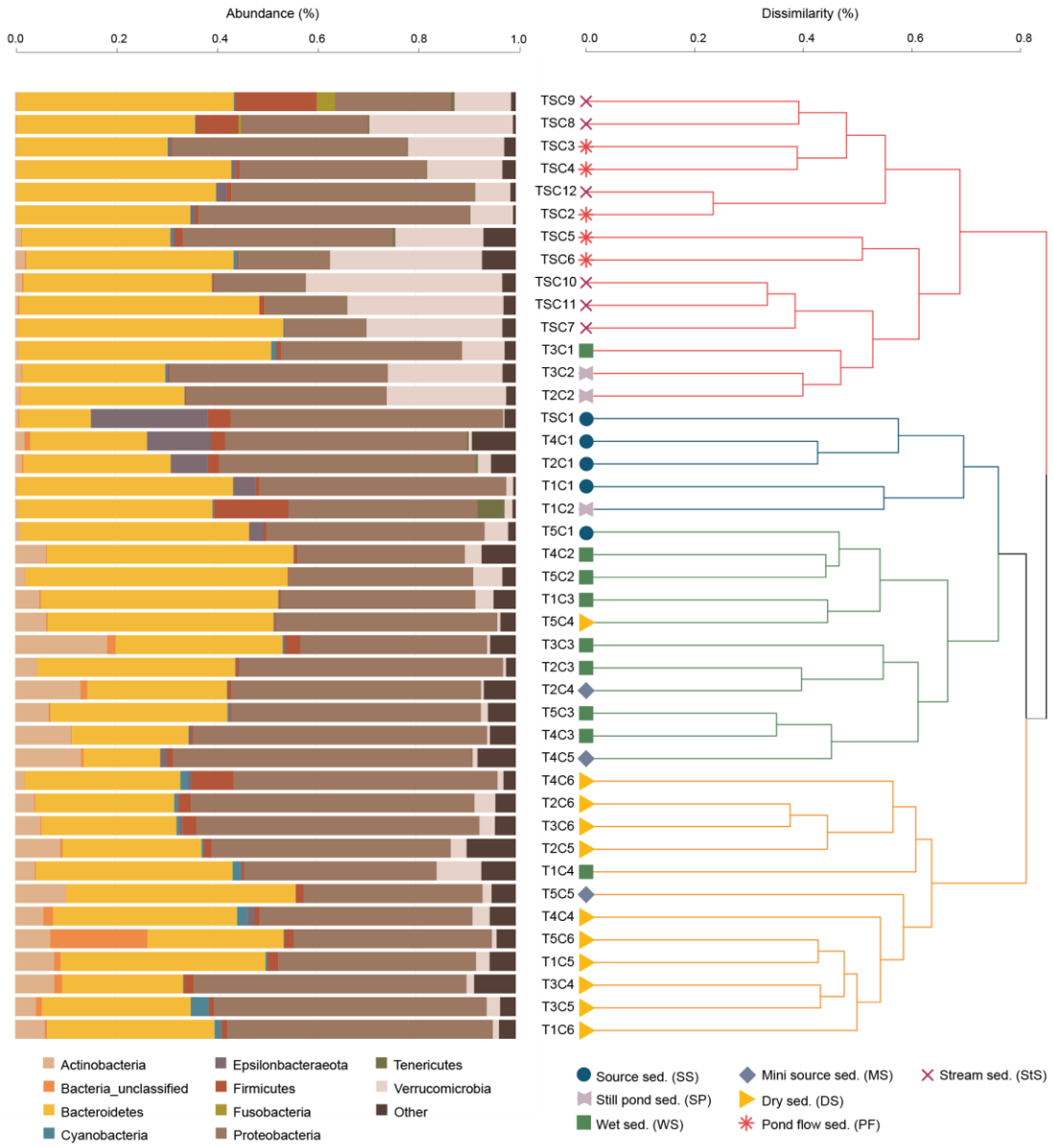

Figure 13: Broad overview over clustering and phylum diversity in 42 samples from Lagoon pingo. The cluster analysis was based on relative abundance of OTUs in sediment samples generated with a universal prokaryote primer pair (515F-Y/926R). The dendrogram was generated using average linkage (UPGMA) with a Bray Curtis distance matrix. The raw dendrogram can be found in the Appendix (Figure A 5). Samples (76%) clustered according to sediment category; pond flow/stream sediment (PF/StS), source sediment (SS), wet sediment (WS) and dry sediment (DS) are shown in red, blue, green and orange, respectively. Bar charts (on the left) display the phyla diversity (>5%) within each sample. Bacteroidetes and Proteobacteria were the two most abundant phyla in most samples.

To further investigate the taxonomic composition of the clusters as microbial habitats, boxes were made to visualize class composition for the respective phyla (Figure 14) with an abundance threshold of 2% (Figure 13). Proteobacteria is shown as both classes and orders

due to special interest in the composition of the most abundant phylum (on average), as well as one of the prominent phyla inhabiting methanotrophic bacteria.

Within each of the phyla Bacteroidetes, Firmicutes, Epsilonbacteraeota and Verrucomicrobia, >90% of the relative abundance was represented by one class, e.g., Bacteroidia, Clostridia, Campylobacteria and Verrucomicrobiae, respectively. This was not the case in cluster DS, where Rhodothermia (<0.05% in all other clusters) was more abundant than Bacteroidia. In every cluster the most abundant Bacteroidia family was Flavobactericeae. In the PF/StS cluster the sequences within Verrucomicrobiae was dominated by the genus *Luteliobacter* (95%), >97% affiliated to the isolate of *Luteolibacter algae* (Yoon et al., 2008), from marine samples. Actinobacteria was only found in cluster WS and DS, where the most pronounced class was the Acidimicrobiia.

In all clusters, Gammaproteobacteria was the most abundant Proteobacterial class, accounting for 73% of the Proteobacterial sequences, followed by Alphaproteobacteria (21% of the sequences). Seven Gammaproteobacterial orders were identified. Betaproteobacteriales was the only order which was represented in all clusters. The Betaproteobacterial bOTU 5 was the most abundant in the universal amplicon library (5.79% of total sequences), sharing >99% identity to hydrogen sulphide oxidizer *Thiobacillus thiparus* (Oyarzún et al., 2003; Villemur et al., 2015). Betaproteobacteriales was the most abundant order within Gammaproteobacteria in WS. Methylococcales was the second most abundant Gammaproteobacterial order in clusters PF/StS, SS and WS, with relative abundance of 7 ± 6.88%, 10 ± 7.5%, 4 ± 5.29%, respectively. This order is known for its type I methanotrophic family Methylococcaceae. In DS, Oceanospirillales was the most dominant order within Gammaproteobacteria, consisting mainly of the genus *Halomonas* (7.5 ± 3.4% of the relative abundance in DS) (Wang et al., 2008). Alteromonadales was found in cluster SS and DS, while Xanthomonadales was only found in cluster WS. Cluster PF/StS was the cluster with the highest relative abundance of Alphaprotobacteria, mainly represented by the Rhodobacteriales. Deltaproteobacteria was only present in cluster SS. The sulphur reducing family Desulfobulbaceae accounted for 59% of the total Deltaproteobacterial sequences and the most prominent genera was *Desulfocapsa* (Korehi et al., 2014). Sulphide oxidizing genera *Sulfurovum* and *Sulfurimonas* (class: Campylobacteria) and *Thiomicrorhabdus* (gammaproteobacterial class Thiomicrospirales) cooccurred with the sulphate reducers in SS.

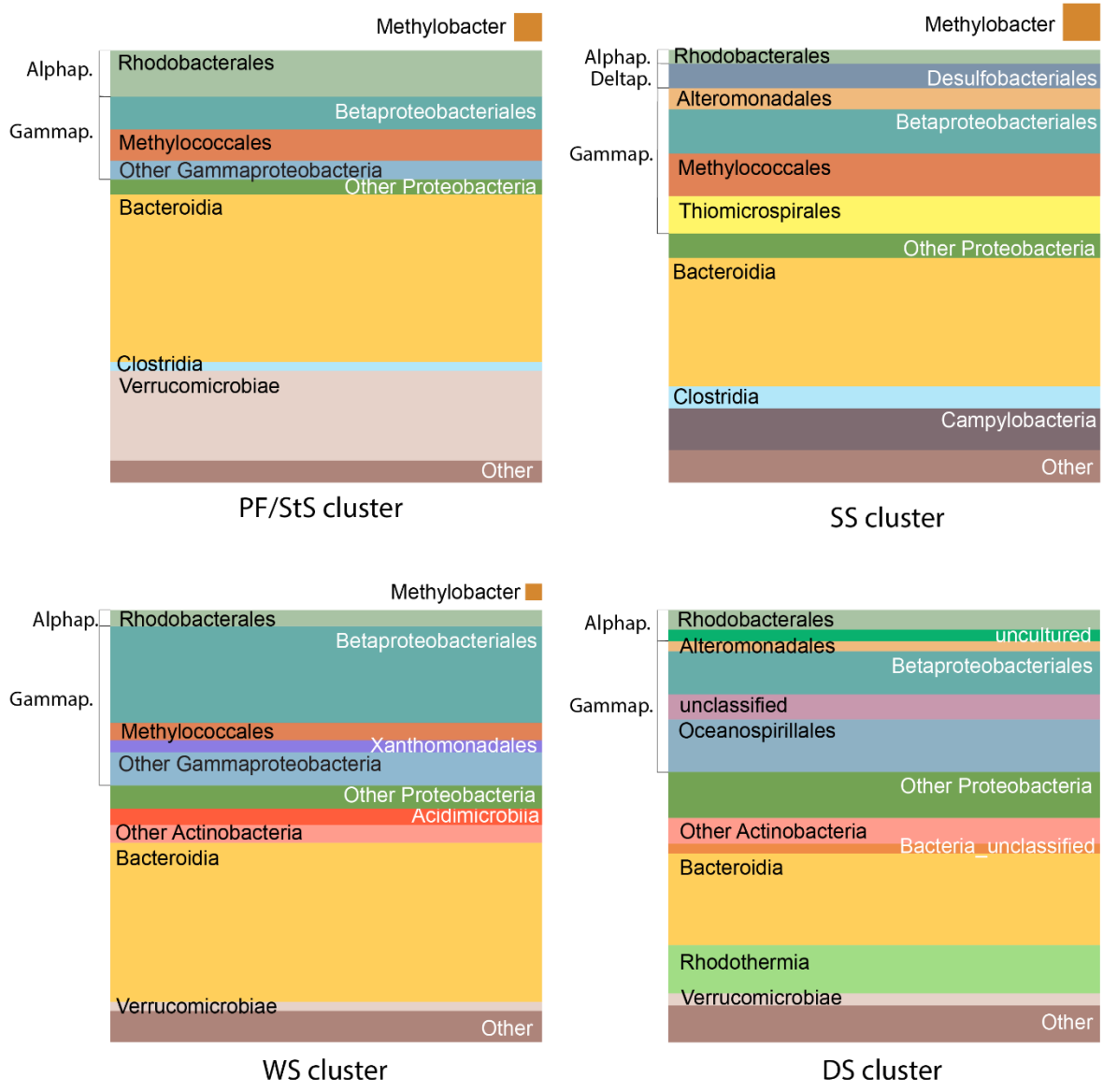

Figure 14: Bacterial class composition of 16S amplicon data displayed as proportions. The sizes of the boxes are based on averages of the relative abundances found in clusters (Figure 13): pond flow/stream sediment (PF/StS), source sediment (SS), wet sediment (WS) and dry sediment (DS). The phylum Proteobacteria is represented as classes (Alpha-, Delta- and Gammaproteobacteria) and orders within the respective classes. The methanotrophic genus Methylobacter is displayed as a separate box. "Other" comprises of all classes <2%.

The DS cluster had the highest alpha diversity of all the sample types, followed by SS, PF/StS and WS in decreasing order. The DS cluster was the most OTU rich group with ~700 OTUs, where 5 – 18% of these were equally abundant, according to the Shannon and Simpson evenness (Table A 1).

4.2.3 Archaeal community structure

To explore the archaeal community composition within sediment samples a cluster analysis was executed and coordinated with bar charts for each individual sample, to elucidate variability within samples. The dendrogram was made based on sequence abundance within

OTUs (Figure A 6). The dendrogram was divided into three main clusters (>80% dissimilarity), highlighting groupings based on sampling location.

The three clusters generated at >80% dissimilarity displayed samples grouping according to sediment category and site location (Figure 15). All sediments from sampling points within the pingo crater clustered together in a large group consisting of 19 samples. The majority of all DS and all StS samples clustered separately with samples that were predominantly from outside the pingo crater, and the stream, respectively. The three clusters are hence referred to as the Edge cluster (yellow), the Stream cluster (red) and the Crater cluster (blue).

Indicated by the dendrogram, community composition varied greatly across and within clusters. The microbial communities within the Stream cluster were the most uniform (>60% similar). Largest variability in community composition was observed within the Edge cluster (10 – 50% similarity).

In total, 66% of the sequences obtained belonged to the phylum was Euryarchaeota. The community composition in the Stream cluster differed from the Edge and Crater clusters by being dominated by Nanoarchaeaeota (87.96 ± 12.14%). The Edge and Crater communities were similar in terms of distribution and relative abundance of Euryarchaeota 76.68 ± 25.14% and 71.34 ± 19.12%, Thaumarchaeota 17.23 ± 17.98% and 18.5 ± 20.42% and Nanoarchaeaeota 5.77 ± 9.71% and 5.44 ± 6.83%, respectively. However, the Crater cluster communities contained a higher number of phyla.

Sub-clusters were observed within the Crater cluster, where samples grouped mainly according to the presence of water, indicated by grey dotted lines (Figure 15). The Crater Flow cluster, comprising of samples situated in flowing water (PF and SS), had a higher relative abundance of Nanoarchaeaeota and Theumarchaeota than the Crater WS cluster (comprising of mainly WS samples).

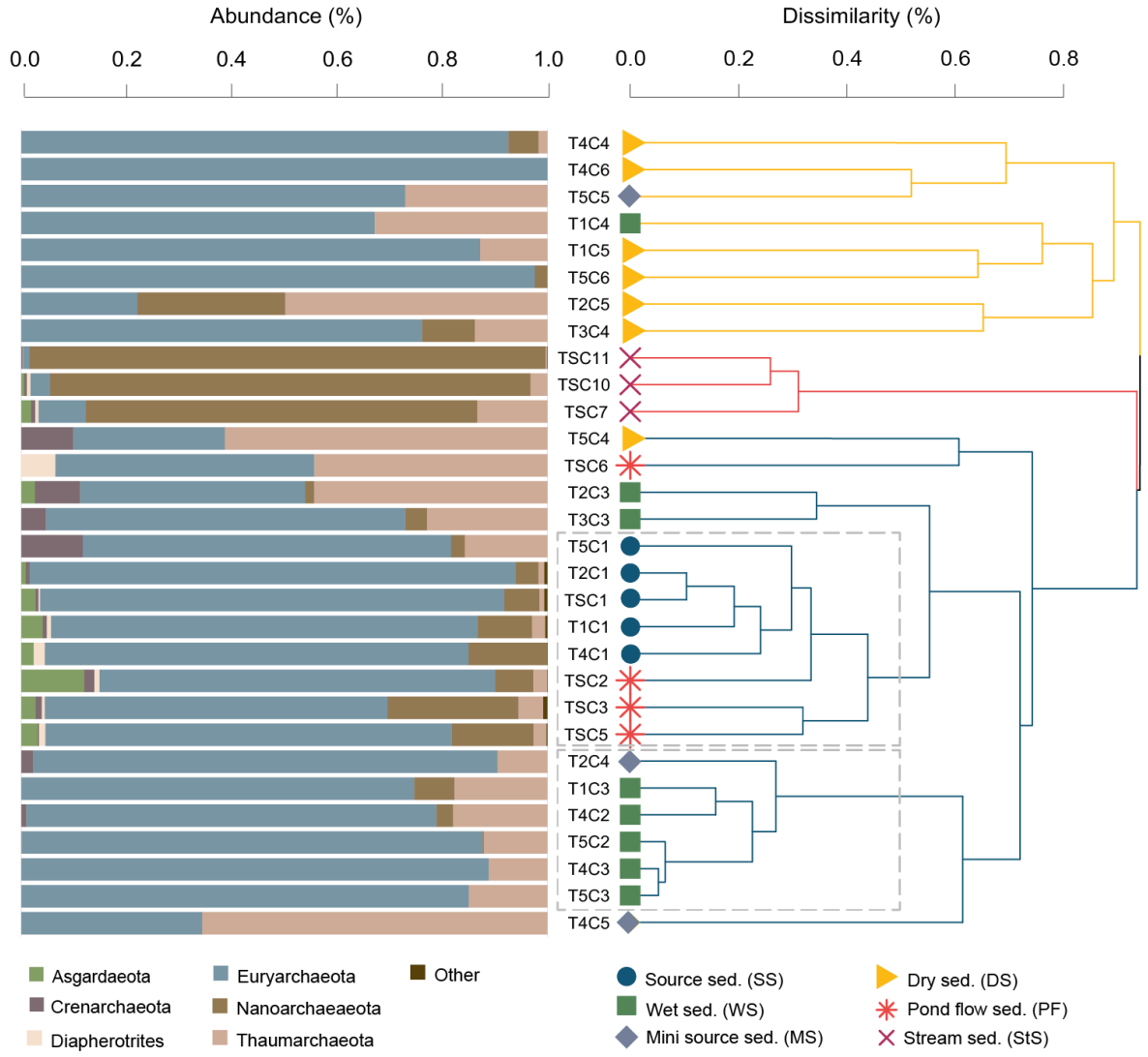

Figure 15: Broad overview showing clustering and phylum diversity in samples from Lagoon pingo. The cluster analysis was based on abundance of OTUs in sediment samples generated using an Archaea specific primer pair (519F/1041R). The dendrogram was generated using average linkage (UPGMA) with a Bray Curtis distance matrix. The raw dendrogram can be found in the Appendix (Figure A 6). The three main clusters are found in colours (yellow, red, and blue). Bar charts (on the left) display the phyla diversity (>1%) within each sample. Sub-clusters within the Crater cluster formed at 50% dissimilarity and are marked by grey dotted lines.

To further investigate the community composition of the archaeal 16S amplicons, and to elucidate the methane cycling agents within the pingo, boxes displaying the proportional relative abundance of the clusters were made (Figure 15).

A substantial variation in relative abundances and composition of classes was seen between clusters that represented different locations (Figure 16). In each cluster, one dominating class was observed. In the Stream cluster, 87.86 ± 12.31% of the relative abundance belonged to Nanoarchaeaeota class Woesearchaea. In the Edge and Crater cluster the Euryarchaeota

classes Halobacteria (58.15 ± 32.85%) and Methanomicrobia (68.34 ± 23.01%) dominated, respectively.

Methane cycling Archaea from the Methanomicrobia class were mainly found in the Crater cluster, where a novel Methanosarcinales represented 41.1 ± 29.78% of the total relative abundance, and the anaerobic methane oxidizers ANME-3 and ANME-2a/b represented 22.59 ± 21.24% and 3.51 ± 6.75%, respectively. The relative abundance of ANME-3 and the novel Methanosarcinales remained low in the Edge and Stream clusters.

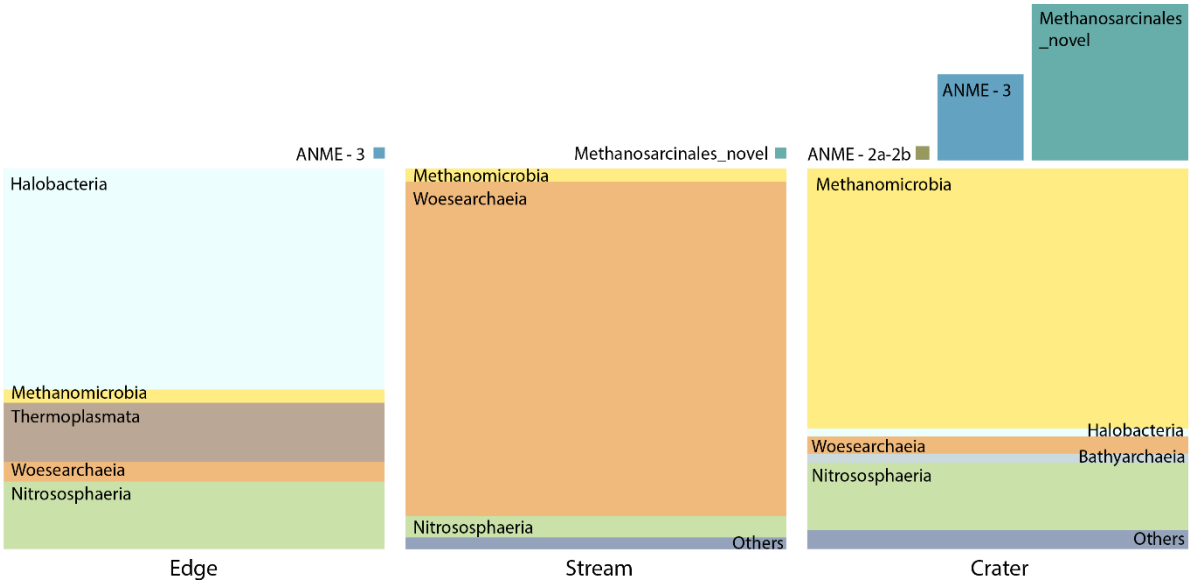

Figure 16: Archaeal class composition of 16S amplicon data displayed as proportions. The sizes of the boxes are based on averages of the relative abundances found in clusters (Figure 15): Edge, Stream and Crater. Genera within the class Methanomicrobia are displayed as separate boxes. "Other" comprises of all classes <2%.

The relative abundance of the Crater sub-clusters is displayed in Figure 17. Methanomicrobia was the dominating class in both clusters, however, the class richness was higher in the sediments underlying moving water (Crater Flow sub-cluster). The proportional relationships between different genera of Methanomicrobia showed two communities, one contributing potentially to methanogenesis and/or AOM though the novel Methanosarcinales (Crater WS) and one defined by AOM likely mediated by ANME-3 and -2 (Crater Flow). The novel genus of Methanosarcinales represented 79.13 ± 8.6% of the Crater WS community, 3 times as great as in sediments situated in the flowing water (Crater Flow). The proportion of ANME-3 in the Crater WS cluster was similar to that found in the Edge cluster. In the Crater Flow sub-cluster, the methane oxidizing community was mainly represented by ANME-3 (39.16 ± 7.77%) and ANME-2a/b (8 ± 8.79%). ANME-1 was present in sequence data, but proportions were ≤1%.

Figure 17: Proportional archaeal class composition of 16S amplicons within sub-clusters found in the Crater cluster (Figure 15) at 50% dissimilarity. Crater Flow consists of samples found in running water (SS and PF). Crater WS consists of the majority of WS samples within the Crater cluster. The sizes of the boxes are based on averages of relative abundance. Genera (>2%) within the class Methanomicrobia are displayed as separate boxes. "Other" comprises of all classes <2%.

The alpha diversity of the archaeal communities was much lower than the bacterial communities (Table A 1). Within the main clusters (Edge, Stream and Crater) the highest number of OTUs was found in the Stream (26 OTUs), followed by the Crater (21 OTUs) and Edge cluster (8 OTUs). However, differences in OTU richness, Shannon- and Simpson indexes and diversity numbers was observed between the Crater sub-clusters, further elucidating these as different ecological niches. The average OTU richness in the Crater Flow (34 OTUs) was four times higher than in the Crater WS (9 OTUs).

4.3 Methane cycling microorganisms

To investigate if methane is an important energy source in the pingo system, OTUs identified as key actors in methane cycling, e.g. methanogenesis and methanotrophy, were selected for further analyses. By investigating the variation in OTU composition and abundance, the functionality of the different ecological niches, as previously defined, could be elucidated. Archaeal and bacterial OTUs are referred to as aOTU and bOTU, respectively.

4.3.1 Phylogenetic analyses of potential key players in methane cycling

After filtration and rarefication of the prokaryote and archaeal OTU tables, these contained 77% and 19% of the total numbers of OTUs, leaving 7152 and 220 OTUs, respectively. All OTUs related to cycling of methane with a total sequence number exceeding the sum of 50, were selected for analyses. The threshold was set to 50 to capture low abundance OTUs but avoid unreliable sequence numbers.

In the prokaryote OTU table, 204 OTUs were placed in the methanotrophic bacterial family Methylococcales. The majority of these OTUs were assigned to unclassified genera of Methylococcaceae, but ~91% of all sequences belonged to 31 OTUs within the genus *Methylobacter*. bOTU 9 and bOTU 360 were the most abundant OTUs within *Methylobacter*, representing 76% and 11% of the sequences, respectively. bOTU 9 showed between 99.27% and 99.03% identity with multiple cloned sequences retrieved from subsurface groundwater cores (Katsuyama et al., 2013) and one cloned sequence from ferrous rich snow (Kojima et al., 2009a), respectively. bOTU 360 had a high degree of identity with bacterial sequences retrieved from freshwater bodies in Alaska (unpublished), Japan (Kojima et al., 2014) and Switzerland (Tomas 2020, in review), with identity of 97.58%, 97.58% and 98.07%, respectively. The closest methanotroph isolate was *Methylobacter tundripaludium* strain SV96 (Wartiainen et al., 2006), which shared 98.55% and 97.10% identity bOTU 9 and 360, respectively. The sequence identity between bOTU 9 and 360 was 96.6%.

OTUs associated with non-Gammaproteobacterial MOB were absent or observed in low quantities. The marine type II methanotroph *Methyloceanibacter spp.* from the Alphaprotobacterial order Rhizobiales was present with a total of 57 sequences (in replicates), and Verrucomicrobia MOB were not present in the dataset.

Within the archaeal class Methanomicrobia there were 27 OTUs. Eight belonged to the anaerobic methane oxidizers ANME-1a, 2a/b and 3. The remaining sequences within Methanomicrobia were clustered under aOTU 1, a novel Methanosarcinales dominating with 60% of the sequences. ANME-1a (aOTU 105), ANME-2a/b (aOTU 28) and ANME-3 (aOTU 2) consisted of 38%. aOTU 1 and 2 were the two most abundant OTUs in the archaeal dataset. Other aOTUs were affiliated with uncultured Methanosarcinales (aOTU 106, 160 and 256).

The novel Methanosarcinales (aOTU 1) showed great degree of relatedness to sequences retrieved from deep-sea hydrothermal vents located in accretion margins off the coast of New

Zealand (Ruff et al., 2013) (98.34%), a mud volcano in Gulf of Cadiz (Maignien and Boon et al, unpublished) (98.34%) off the Atlantic coast of the Iberian peninsula, and a cold seep in the Antarctic (Niemann et al., unpublished) (97.23%). Ruff et al. (2013) uncovered that the site contained a high proportion of ANME-related OTUs, including sequences associated with Methanosarcinaceae, possibly representing methanogenic taxa. All sequences were retrieved from marine sediments, where the sequenced samples from the Haikuragi margin and the Antarctic were from 850->1000m depth. Its closest related species were methanogenic *Methanosalsum natronophilum* strain AME9 (91.13%) and *Methanosalsum zhailinae* (91.13%) from hypersaline soda lakes (Sorokin et al., 2015) and soils (unpublished), respectively. Global alignments using the BLAST search engine showed that aOTU 1 was slightly more related to aOTU 2 (91.9%), than *M. natronophilum* and *M. zhailinae*.

aOTU 105, 28 and 2 were all classified within the three ANME lineages, ANME-1, 2a/b and 3, respectively. The ANME-2a/b and 3 lineages were closer related to each other (91.9% identity), than that of ANME-1 (84.2% and 84.9% identity, respectively). BLAST searches conveyed that the majority of sequences with >97% identity to aOTU 2, 28 and 105 were of deep-sea origin. Sequences found in active methane seeps off the coast of California (Orphan et al., 2001) and New Zealand (Ruff et al., 2013) shared 99.45% and 99.63% sequence identity with aOTU 2 (ANME-3). aOTU 28, assigned to ANME-2a/b, had a 99.45% degree of identity with 16S rRNA sequences retrieved from deep-sea liquid CO_2 reservoirs in the hydrothermal fields in the Yonaguni Knoll (Inagaki et al., 2006). OTU 105 had 99.08% similarity with a sequence classified as ANME-1a found in hydrothermal vents in the Mexico Gulf (Merkel et al., 2013).

4.3.2 Composition and distribution of methane cycling prokaryotes

The bOTU composition and relative abundances were relatively similar in all clusters (Figure 18). bOTU 9 was the dominant OTU in all clusters, followed by bOTU 360. The remaining OTUs had a low relative abundance. bOTUs 348, 451 and 759 were assigned to the methylotroph type I family Methylococcaceae, nine OTUs were assigned *Methylobacter*, while OTU 319 assigned to the marine Alphaproteobacteria *Methyloceanibacter*.

In the clusters based on archaeal amplicon data, the aOTU composition and relative abundances varied more than in the bacterial based clusters. Here, fewer OTUs were found to exceed 50 sequences in total. Overall, aOTU 1 (novel Methanosarcinales) and aOTU 2 (ANME-3) were the two most abundant OTUs. In the Crater WS- and Stream clusters, aOTU

1 was the most abundant, while in the Crater Flow and Edge clusters, aOTU 2 was most abundant. In addition, the methanotrophic ANME-1a (aOTU 105), 2a/b (aOTU 28) and uncultured Methanosarcinales (aOTU 106, 160 and 256) were present.

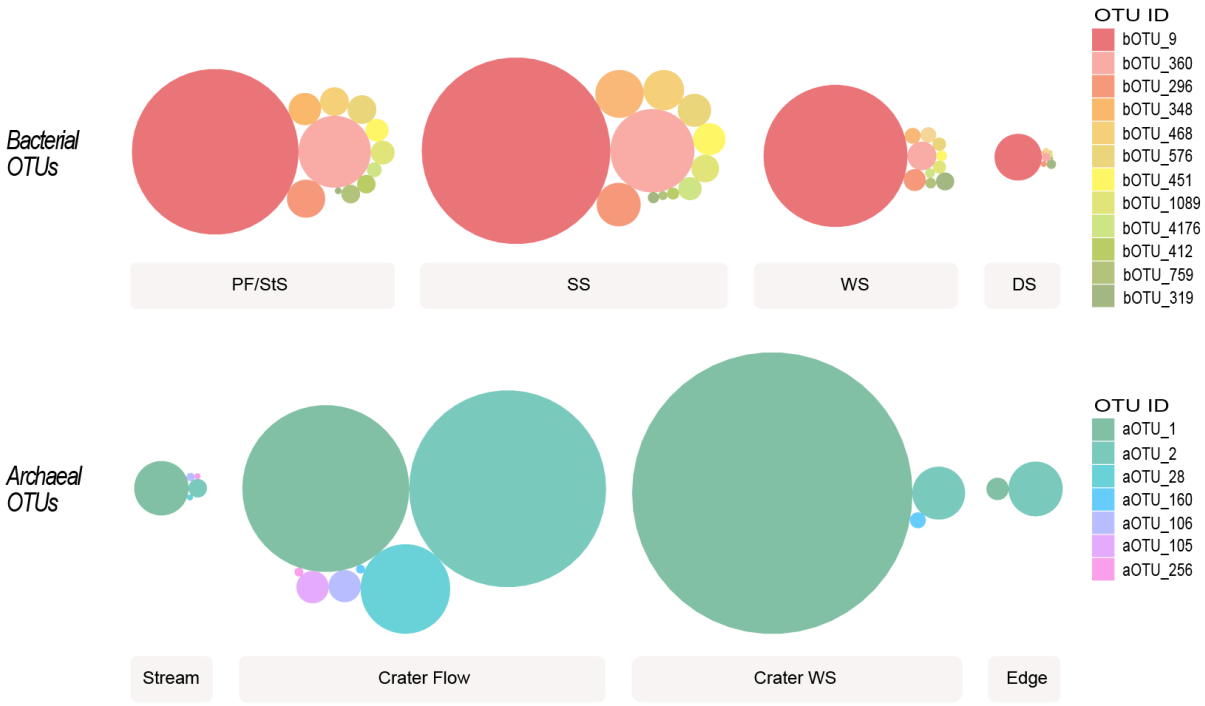

Figure 18: Microbial composition of methanogenic and methanotrophic prokaryotes in and around Lagoon pingo, based on 16S rRNA genes identified from amplicon data. The microbial community is displayed as mean relative abundance of OTUs in ecological niches defined by cluster analyses. The sizes of each circle present the mean relative abundance of the OTUs per cluster. All OTUs that were related to methanogenesis and methanotrophy, that had more than 50 sequences in total were included in the figure. Circles of bacterial and archaeal OTUs are relative to each other, but displayed separately as the ecological niches defined by cluster analyses were different between datasets.

To investigate the local distribution of the selected OTUs and their relationship to the methane flux, oxidation rate and sediment concentration, OTUs were plotted in relative abundances on the schematic map. A minimum of 50 sequences per sample was required to include any OTU (Table A 2; Table A 3). Of the 18 OTUs investigated in Figure 18, five OTUs passed the threshold minimum (Figure 19 and Figure 20).

The presence of the selected OTUs was mainly located in the crater pond. Sequence numbers found in the DS and StS locations rarely surpassed 50 and were therefore not visible on the map. The highest relative abundances of all selected OTUs were found at PF, SP and WS locations (Figure 19 and Figure 20). The *Methylobacter* bOTU 9 and the novel Methanosarcinales aOTU 1 were the most prominent of the selected OTUs with a total relative abundance of ~33% each.

bOTU 9 was ubiquitous to all sediment types; however, the largest abundances were found in locations with both high (PF) and low (SP) methane fluxes (average ~750 and 1.5 nmol m^{-2} s^{-1}) (Figure 19). The methane oxidation rate and methane content remained relatively low (<1 nmol g^{-1} h^{-1} and ~1.5 nmol g^{-1}) in SP location T2C2 and T3C2, where the relative number of bOTU sequences were high (~800 sequences). Relatively low sequence numbers of bOTU 9 were found in WS locations and was near to absent in DS sediments. bOTU 360 had over 50 sequences in sampling points tied to high water content, e.g. SP and PF sediment. The relative abundance of both bOTUs remained <50 sequences in the six last sampling points of the stream, except for TSC12, and TSC10 for bOTU 9. bOTU9 was found in two of the three MS.

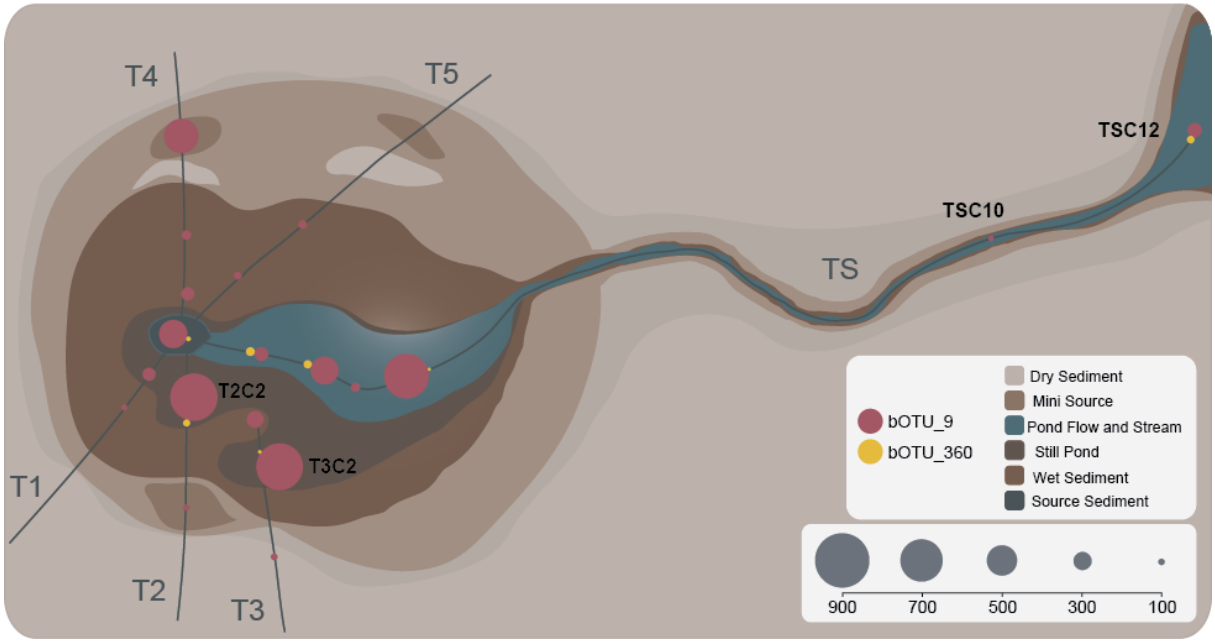

Figure 19: Schematic map of the sampling site with circles displaying the relative abundance of bacterial OTUs (bOTUs) based on ribosomal SSU amplicon data. The OTUs are associated with methane cycling prokaryotes such as aerobic methaotroph Methylobacter (bOTU 9 and 360). The sizes of the circles are relative to the largest circle in the dataset, e.g aOTU 1. All samples with less than 50 sequences were removed from the map as these were too small to visualize. Sequence number in the samples ranged between 0-900 sequences. The sizes of the circles found at the source is based on the average relative abundance of each OTU across all transects. The sampling points that are mentioned in the main text are marked in the schematic.

Relatively high abundances of aOTU 1 (novel Methanosarcinales) were found in all sediment types, apart from DS and StS (Figure 20). The highest abundances of aOTU 1 were found in static WS, where methane fluxes, concentrations and aerobic methane oxidation rates remained low, never exceeding a value of 5 (all units). aOTU 1 and 2 (ANME-3) were present in MS locations, where methane fluxes ranged 375 – 690 nmol m^{-2} s^{-1} and 40 – 375 nmol m^{-2} s^{-1}, respectively. aOTU 1 was present in the same two MS where bOTU 9 was present.

The confirmed anaerobic methane oxidizers were found in locations with registered methane fluxes exceeding 700 nmol m^{-2} s^{-1} (SS and PF), all OTUs had a relative abundance >50 sequences (Figure 19 and Figure 20). ANME-2a/b (aOTU 28) was only observed (>50 sequences) in these locations. Gradients in relative abundance of the OTUs was observed in the PF sediments. The relative abundance of aOTU 1 appeared to faintly decrease with increasing distance to the source and decreasing methane fluxes. A faint opposite trend was observed for the aerobic and anaerobic methane oxidizers, bOTU 9 (Figure 19) and aOTU 28 (Figure 20). In addition to being present in the PF transect, the ANME-3 (aOTU 2) was found in the southern part of the pond, in WS locations where methane fluxes were <3 nmol m^{-2} s^{-1}.

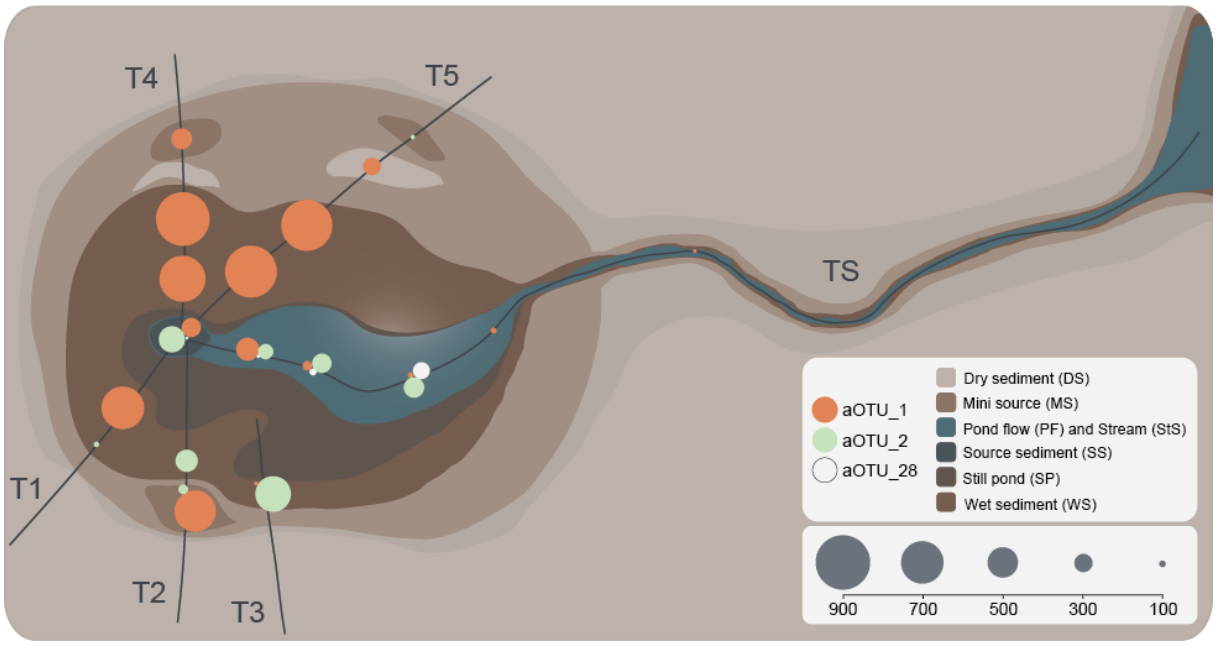

Figure 20: Schematic map of the sampling site with circles displaying the relative abundance of archaeal OTUs (aOTUs) based on ribosomal SSU amplicon data. The OTUs are associated with methane cycling prokaryotes such as the novel Methanosarcinales (OTU 1) and anaerobic methane oxidizers ANME-3 and ANME-2a/b (aOTU 2 and 28). The sizes of the circles are relative to the largest circle in the dataset, e.g aOTU 1. All samples with less than 50 sequences were removed from the map as these were too small to visualize. Sequence number in the samples ranged between 0-900 sequences. The sizes of the circles found at the source is based on the average relative abundance of each OTU across all transects.

4.3.3 Testing relationships between OTUs and environmental parameters

To investigate potential connections and relationships between environmental variables and the relative abundance of known methanotrophic OTUs and the novel aOTU 1, analyses of correlation were executed (for raw data see Table A 4). Relationships between all OTUs introduced in Figure 18 were also investigated.

Correlation analyses were made based on data from all transects. Additional correlation analyses were made based solely on the TS sampling points. This was done to elucidate

distribution and abundance patterns of the selected OTUs within areas where methanotrophic activity was detected (Figure 10).

The analyses based on all transects and on TS-only sampling points yielded approximately the same number of significant relationships between OTU abundances and metadata (Figure 21). In analyses based on all transects, only significant correlations were observed between OTU abundances (aOTU 105, 106, 2, 28 and bOTU 296) and methane flux (rho = 0.61-0.67, $p < 0.01$). The positive correlations seen in the model with all transects, were not observed in the analysis with TS sampling points. Here, only aOTU 1 (novel Methanosarcinales) abundance increased with increasing methane flux (rho = 0.86, p = 0.0065). Significant positive correlation was found between methane concentration and aOTU 1 and 2 (ANME-3) (rho = 0.88 and 0.86, $p < 0.01$). Both OTUs decreased in relative abundance with distance to the source (rho = -0.98 and -0.90, $p < 0.01$). No statistically significant relationships between OTU abundance and pH was found in neither analysis. Methane oxidation rate assays were strictly aerobic, as no anaerobic methane oxidizers were expected on site. The correlation between aOTU 105 (ANME-1a) and methane oxidation rate is thus negligible.

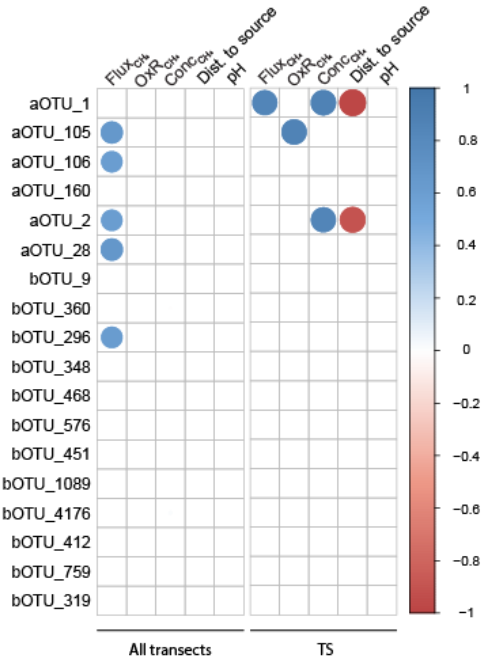

Figure 21: Statistically significant (rho = >-0.6 or >0.6, $p < 0.01$) correlations between OTU abundance and metadata. Left: Analysis based on all available data (all transects). Right: Analysis based on solely TS sampling points.

In both analyses, positive relationships (rho = 0.63-0.98, $p < 0.01$) between bOTU 9, 360, 296, 348, 466, 576, 451, 1089 and 4176 were observed (Figure 22). The negative correlations in OTU abundances were observed in the TS based analysis, where bOTU 412 decreased with

increasing aOTU (1 and 2) and bOTU (9, 360, 296, 348, 466, 576, 451and 1089) abundances (rho = -0.7-(-0.93), $p < 0.01$). In the analysis based on all transects, the relative abundance of ANME-2a/b (aOTU 28) increased simultaneously with ANME-1a and 3 (aOTU 105 and 2) (rho = 0.7 and 0.74, $p < 0.0001$, respectively). A similar trend was observed between ANME-1a (aOTU 105) and an uncultured Methanosarcinales (aOTU 106) (rho = 0.87, $p < 0.01$). Fewer significant correlations between aOTUs and bOTUs were detected (Figure 22). No significant correlations were detected between Alphaproteobacteria genus *Methyloceanibacter* (bOTU 319) and OTU abundance.

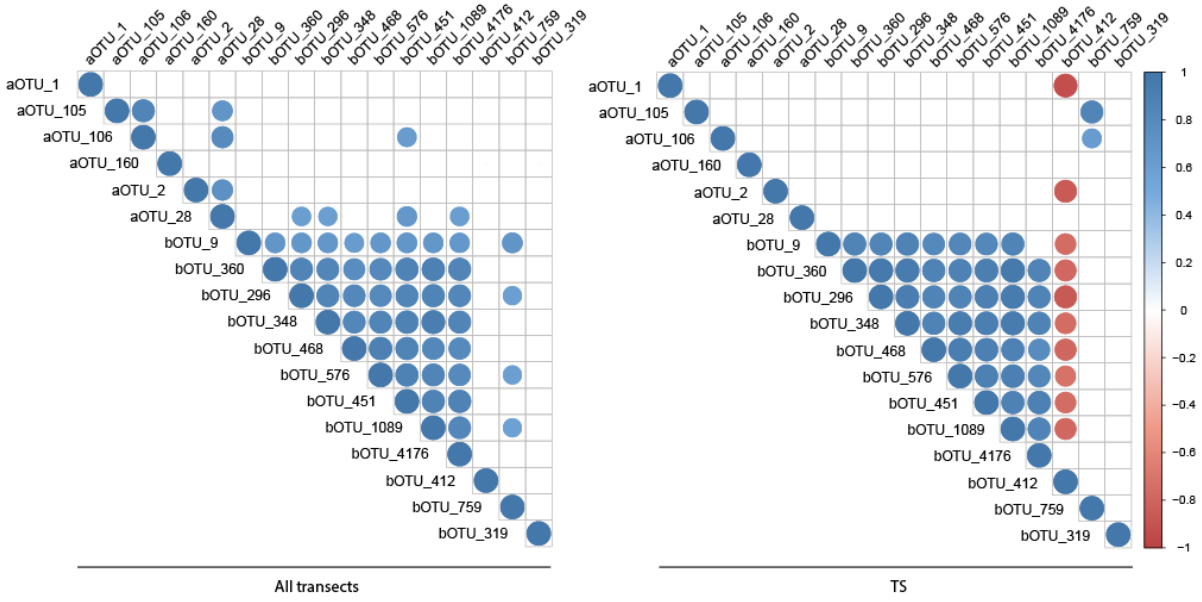

Figure 22: Statistically significant (rho = >-0.6 or >0.6, $p < 0.01$) correlations between OTU abundances. Left: Analysis based on all available data (all transects). Right: Analysis based on solely TS sampling points.

The number of samples varied between the bOTUs and aOTUs, as different rarefication levels had been previously set. The archaeal OTU table had fewer samples (13 samples missing), and a lower average number of sequences per sample, than the prokaryote OTU table. Therefore, the correlations between aOTU abundances and between other variables must be interpreted with caution, as the analyses are based on fewer datapoints, and the variation in sequence number per sample is lower. This also applies for the less abundant bOTUs (296, 348, 468, 576, 451, 1089, 4176, 412, 759 and 319).

5 Discussion

5.1 Lagoon pingo as a dynamic habitat mosaic

Lagoon pingo is a dynamic system that is subject to annual freeze-, thaw-, erosion- and collapse-cycles. In summer, the system is defined by methane-saturated groundwater from subsurface reservoirs. The groundwater surface through a 2 m diameter discharge source that enters a pond at the pingo surface crater. Gradients of moisture and methane availability radiating outwards from the source to the crater edges create distinct, heterogenous habitat patches, promoting the development of a habitat mosaic in the crater. Due to ice-cap melt and water level fluctuations in the pond, the methane supply is not constant during the spring and summer season (Hodson et al., 2019). Consequently, the spatial arrangement of the habitat also varies through this period. Here we present a snapshot of the habitat mosaic and the influence of methane on the microbial community from August 2019. We demonstrate that habitat patches within the mosaic host specialized and unusual microbial communities for a terrestrial system.

5.1.1 Lagoon pingo habitats

Lagoon pingo was characterized by radial repartition of habitats from the main source toward the outside of the crater and a hydrological gradient that follows the stream. The dry sediment (DS) found outside of the crater was not influenced by the source water at the time of sampling and therefore can be considered as a background for the local region with no methane emissions detected (Figure 10) and low water content (Table 2). Within the crater, methane rich sediments lining the outlet of the main spring (SS) were continuously flushed with anoxic, methane-saturated water. Conditions were comparable to those found at marine cold seeps (Hovland and Svensen, 2006; Niemann et al., 2006), but the salinity was approximately 3% of that found in sea water (Hodson et al., 2019). The pond habitat (divided into static water (still pond: SP) and flowing water (pond-flow: PF)) hosted a large community of algal biofilms and was more OTU diverse than the surrounding clay-like wet sediment (WS) (Table A 1). The pond (SP and PF) and the stream (StS) contained the highest DNA biomasses in the system (Figure 11), while dry sediments (DS) and newly established mini sources (MS) supported the lowest DNA biomasses (Figure 11). These data already suggest that the primary source of energy for microbial life in this unusual ecosystem is the water released from the main source discharge. The dry, non-vegetated surface of the mud-like, alkaline sediment at Lagoon pingo is an uncommon feature of the arctic landscape. Most

of the unglaciated landscape of Svalbard is classified as arctic tundra and wetlands (Walker et al., 2005), and dry vegetation-free areas are usually associated with gravel slopes along mountain sides (Johansen et al., 2012). The melt of the ice-cap and subsequent formation of the pond in spring, rather resembles the genesis of thermokrast lakes in arctic regions (Grosse et al., 2013). Like in thermokrast lakes, low oxygen and high methane concentrations is a major characteristic.

5.1.2 Background community

To understand the effect of the methane source on the microbial community, and which microorganisms live independently of this, we inspected the ubiquitous taxonomic groups and those found exclusively outside the crater. Proteobacteria and Bacteroidetes were the most prominent phyla in all habitats investigated, accounting for 30 – 39% and 33 – 48% of the community, respectively. This matches arctic and antarctic marine sediments, as well as lake sediments from the Tibetan Plateau, where the same phyla dominated the microbial communities (Xiong et al., 2012; Carr et al., 2015; Müller et al., 2018). Proteobacteria are also abundant in arctic soils, often co-occurring with high proportions of Actinobacteria (Steven et al., 2008; Tveit et al., 2013; McCann et al., 2016).

Flavobactericeae was the dominating family within Bacteroidia (phyla: Bacteroidetes) in all habitat clusters. Flavobactericeae are omnipresent in marine environments, are often involved in degradation of large polymers (Fernández-Gómez et al., 2013) and has been found to correlate with algal blooms (Pinhassi et al., 2004; Teeling et al., 2012). As this family was ubiquitous to the site, it is possible that the group has similar functions at Lagoon pingo, where photosynthetic biofilms proliferated throughout the sampling period. Proteobacteria was mainly composed of Gammaproteobacteria, which accounted for 19 – 37% of the average sequence number in the sampled habitat clusters (Figure 14). This is in accordance with previous research in arctic and antarctic marine sediments, where Gammaproteobacteria accounted for 15 – 50% of the total 16S sequences (Tian et al., 2009; Teske et al., 2011; Carr et al., 2015; Müller et al., 2018). This contrasts with arctic soil samples where Gammaproteobacteria is seldom the dominant Proteobacteria class (Steven et al., 2008; Chu et al., 2010; Tveit et al., 2013). In the DS located furthest away from the source, *Halomonas* (bacterial class: Oceanospirillales) and the order Halobacteriales (archaeal class: Halobacteria) cooccurred in high percentages (Figure 14; Figure 16). In line with the halophile nature of these taxa (DasSarma and DasSarma, 2017), the dry sediments were

covered in precipitated salts. Halobacteriales present at Lagoon pingo has been found to dominate archaeal communities at salt influenced springs and a high-altitude mud volcano (Elshahed et al., 2004; Perreault et al., 2007; Yang et al., 2012).

5.1.3 Archaea and Bacteria spatial repartition reflects the pingo habitat mosaic

The habitat mosaic of Lagoon pingo was reflected in the archaeal community composition. At each location defined by the cluster analysis: crater, edge and stream (Figure 15), the archaeal class composition was different (Figure 16; Figure 17). Communities within the crater were dominated by methane cycling members of Methanomicrobia (68%) while the stream was dominated by unclassified Wosearchaeota (88%) (Figure 16). Interestingly, ~39% of all sequences within the class Methanomicrobia were affiliated with anaerobic methanotrophic archaea (ANME), frequently found within the SMTZ in marine environments (Knittel and Boetius, 2009; Bhattarai et al., 2019).

Two characteristic habitats within the crater were identified based on the distribution of bacterial taxa. The composition of the SS was unique in the dataset as it was the only habitat where Deltaproteobacteria, the gammaproteobacterial order Thiomicrospirales and the class Campylobacteria were a dominant part of the microbial community. These taxa contain genera involved in the reduction (Desulfobacteriales) and oxidation (Thiomicrospirales and Campylobacteria) of sulphur-containing compounds (Han and Perner, 2015; Kuever et al., 2015; Kojima and Fukui, 2019). This suggests that redox reactions involving sulphur may play a central part in energy transfer in SS, as opposed to other sediment types. Second, the PF/StS habitat was characterized by a high percentage of Verrucomicrobia, mainly comprising of *Luteolibacter algae* (~49% of sequences within Verrucomicrobia) (Yoon et al., 2008). The ecology of the genus remains largely elusive (Zhang et al., 2014), however, degradation activity of the brown algae polysaccharide fucoidan in the isolate *Luteolibacter algae* H-18 has been reported (Ohshiro et al., 2012), suggesting potential degradation processes of photoautotrophs in the pond and stream at Lagoon pingo. In both SS and PF/StS, the aerobic methanotroph *Methylobacter* accounted for 8.6% and 6.5% of the total sequence numbers within the respective habitats, indicating that methane is a central energy and carbon source in this system.

5.2 Pingo methane emissions are mitigated by aerobic and possibly anaerobic microbes

The habitat mosaic formed by the methane seep water selects microbes that has the potential to use methane and subsequently reduce atmospheric methane transfer. We have investigated in detail the key players of these microbial communities to better understand their origin and the role they are playing in the arctic ecosystem.

5.2.1 Prominent methane oxidizing bacteria (MOB) community at Lagoon pingo

The relative size of the methanotrophic community at Lagoon pingo exceeded that of methanotrophic populations found in boreal regions in Canada (Crevecoeur et al., 2019). Crevecoeur et al. (2019) inferred the differences in methanotrophic communities in over 600 lakes, rivers, and soils. They uncovered that the average proportion of methanotrophs in all habitats ranged from 0.07 – 0.22% of the 16S based relative abundance. The relative abundance of MOB in Lagoon pingo exceeded these numbers more than 20-fold.

5.2.1.1 Pingo MOB community dominated by *Methylobacter*

The MOB community at Lagoon pingo was homogeneous, as >99% of MOB sequences were affiliated with the gammaproteobacterial type I MOB genera, *Methylobacter* and unclassified Methylococcaceae (Figure 18). No methanotrophic bacteria from the phylum Verrucomicrobia (Dunfield et al., 2007), nor the candidate phyla NC10 (Ettwig et al., 2010) were detected in this study. Two OTUs (bOTU 9 and 360) closely related (>97% identity) to the arctic *Methylobacter tundripaludum* strain SV97 (Wartiainen et al., 2006) dominated the MOB community at Lagoon pingo. bOTU 9 and 360 accounted for 3.23% and 0.46% of the total sequence count, respectively. *M. tundripaludum* and close relatives are the dominant methanotrophs in many arctic wetland ecosystems in the Canadian high Arctic, Siberia and Svalbard (Liebner et al., 2009; Martineau et al., 2010; Graef et al., 2011; Tveit et al., 2013; Tveit et al., 2014). These studies indicate the importance of *Methylobacter* as a vital component of the methanotrophic filter in Arctic environments. Lagoon pingo is different from the above-mentioned study sites, as these environments were characterized by high organic content and slightly acidic to neutral pH. This poses the question of whether the *Methylobacter* strains identified in Lagoon pingo is different from *M. tundripaludum*, being adapted to vegetation-free, fine grained, alkaline sediments and unusually high methane concentrations.

5.2.1.2 *Methylobacter* distribution

Sequences associated to *Methylobacter* were present in all studied clusters (Figure 18), and it's omnipresence at Lagoon pingo suggests that it is an intrinsic part of the pingo system. Overall, the number of different MOB OTUs and their relative abundances declined with decreasing water content (Figure 18). The compiled relative abundance of the selected MOB OTUs peaked in waterlogged habitats (SS and PF/StS cluster; Figure 18). In drier habitats, where the water content was 33.4% (WS) and 16.6% (DS), the relative abundance of MOB sequences dropped on average by 66% and 96%, respectively. Correspondingly, MOB activity was restricted to waterlogged habitats (Figure 10). Water content is likely an important regulator of methanotrophic activity as water is crucial to cellular integrity and distributes nutrients and dissolved gasses such as CH_4, CO_2 and O_2 to the cells. While this suggest that MOB is largely controlled by water and/or the water content such as dissolved methane, the distribution of the selected MOB OTUs could not be explained by any environmental parameters measured in this study alone (Figure 21). Two thirds of the selected MOB OTUs shared the same patterns in relative abundance at Lagoon pingo (Figure 22), suggesting that these are all in part subject to the same selection pressure, irrespective of water and methane.

The ubiquitous presence of MOB at Lagoon pingo, regardless of the environmental conditions, can be explained in several ways. The sequences inferred herein could be relics of opportunistic MOB communities that thrived under conditions prevalent earlier in the season. Due to the dynamicity of the system, these possibly surfaced from deeper sediment layers or were washed out of the crater during snow and ice melt. Resting mechanisms such as spore formation could be an explanation for *Methylobacter* sequences found in DS, WS and SP habitats. Cellular resting stages have been reported for certain genera of *Methylobacter* (Whittenbury et al., 1970; Bowman et al., 1993), however this was not observed for *M. tundripaladium* SV96 (Wartiainen et al., 2006), the closest relative of bOTU 9 and 360 in pure culture. Spore-like structures were observed in a prospective MOB strain enriched from Lagoon pingo this year (Nagel, 2020), indicating possible stress responses to the extreme physical alterations at Lagoon pingo. However, a confirmation of this must await the isolation of *Methylobacter* strains from Lagoon pingo in pure cultures that allow physiological experiments.

5.2.1.3 *Methylobacter* possibly adapted to low oxygen concentrations

To our surprise, high relative abundances of the presumably aerobic *Methylobacter* was detected in SS, which were continuously flushed with anoxic water (Figure 19). According to phylogenetic inquiries, the cloned sequences with highest degree of relatedness to bOTU 9 and 360 originated from anoxic environments (Katsuyama et al., 2013; Kojima et al., 2014). The cloned sequence with highest identity to bOTU 360 was not specifically addressed in Kojima et al. (2014), but a previous study by Kojima et al. (2009b) explored the MOB community in the same lake system (Lake Mizugaki). In the permanently stratified water column (oxygen concentrations ranging from 0 – 350 µM), strong signals of pelagic *Methylobacter* 16S rRNA were detected at all depths by DGGE. Moreover, bOTU 9 shared a high degree of identity with *Methylobacter* strains retrieved from subsurface (140 m) groundwater, depleted of oxygen (Katsuyama et al., 2013). Several studies have reported finds of *Methylobacter* thriving in anoxic environments, however the energy yielding metabolism of *Methylobacter* under anoxic conditions is not yet known (Biderre-Petit et al., 2011; van Grinsven et al., 2020). Recently, Smith et al. (2018) detected the complete pathway for dissimilatory nitrate reduction in *Methylobacter*. Coupling denitrification with methane oxidation possibly enables *Methylobacter* to thrive in anoxic habitats by using nitrate as the terminal electron acceptor. However, oxidation of methane to methanol by the particulate methane monooxygenase also requires O_2 for the initial oxidative attack on methane, for which no alternative mechanisms have been demonstrated. Genes central in nitrate and nitrite reduction has also been identified in *M. tundripaludum* SV96 (Svenning et al., 2011; Tveit et al., 2013), suggesting that this *Methylobacter* strain can utilize nitrate and nitrite as terminal electron acceptors. However, it is still unknown whether enzymes for cleavage of two nitric oxides to produce N_2 and O_2 exists in *M. tundripaludum* SV96. Recently, van Grinsven et al. (2020) found that the biomass and oxidation rates in anaerobic incubations of *narGHI* (reducing nitrate to nitrite) lacking *Methylobacter* strains' increased by five- and four times, respectively, when adding nitrate and sulfate. van Grinsven et al. (2020) suggests that a syntrophic relationship between *Methylobacter* and nitrate reducing bacteria, feed these *Methylobacter* strains with nitrite. Despite lacking explanation for the oxidative attack on methane and only indications for syntrophic partnerships, it has been unequivocally demonstrated that *Methylobacter* strains are active in anoxic environments. In Lagoon pingo an adaptation to microaerobic and/or anoxic conditions possibly involving nitrate and nitrite utilization may explain the dominance of *Methylobacter* strains suggesting that in addition to aerobic methane oxidation it may be part of an anaerobic methane filter.

5.2.2 Distribution of anaerobic methane oxidizing archaea (ANME)

5.2.2.1 ANME-3 potential key player in AOM activity

In Lagoon pingo, ANME-3 dominated the archaeal library, followed by ANME-2a/b and ANME-1a (Figure 16; Figure 17; Figure 18). The dominance of ANME-3 sequences further elucidate the peculiarity of the pingo as a terrestrial system, as it is reported to have the most narrow distribution of all ANME clades (Knittel and Boetius, 2009), predominantly found in marine mud volcanos (Niemann et al., 2006; Lösekann et al., 2007). To our knowledge ANME-3 has not before been observed in terrestrial mud volcanos, which are temperate analogues to the arctic open system pingos. The relative abundances of these three clades varied across the habitat mosaic, indicating internal selection processes within the site, steering the composition and abundance of ANME. Rossel et al. (2011) reported distinct patterns in intact polar lipids, in environments dominated by ANME-1a, 2a/b and 3, indicating abiotic, external selectors in these environments.

5.2.2.2 Methane

The Crater Flow cluster (Figure 18) was the cluster with the highest diversity of aOTUs related to methane cycling. In fact, 98.8%, 96.5% and 70% of all ANME-1a, 2a/b and 3 sequences, respectively, were found in SS and PF sediments, where the methane fluxes remained relatively high (>700 nmol m^{-2} s^{-1}). Moreover, the abundance of all ANME OTUs correlated positively with methane fluxes when including all transects (Figure 21), suggesting that the availability of methane regulates ANME abundance directly and/or indirectly. It is important to note that methane flux as a measure of methane availability is inherently flawed. Methane flux does not account for methane oxidation, and therefore, does not necessarily reflect the methane available to microorganisms. Methane flux is rather a measure of excess methane. Oxidation rate experiments to detect methanotrophic activity were so far aerobic, not reflecting AOM activity. Thus, in order to identify whether AOM occurs at Lagoon pingo as indicated by the sequencing data, experiments to identify potential AOM rates must be planned for the future.

5.2.2.3 pH

No significant correlations between pH and ANME abundance was observed at Lagoon pingo. This corresponds to earlier studies at the Hydrate Ridge and in the Black Sea, where the pH of microbial mats was not found to be a selective variable for AOM activity (Nauhaus et al., 2005). However, it was observed that ANME-1 has a broader pH optimum (6.8 – 8.1),

than ANME-2 (7 – 7.5). In our study, ANME-3 had the broadest distribution, appearing in relatively high abundances in the SS, PF, WS and MS locations (Figure 20). pH values ranged between 8.5 – 9.7 (data not shown), indicating that the ANME-3 at Lagoon pingo can thrive at least within this pH range.

5.2.2.4 Oxygen availability

The abundance of ANME-2a/b increased with increasing distance to the source in the PF sediments (Figure 20). The opposite was observed for ANME-1a, where the relative abundance number of 16S amplicon sequences decreased with increasing distance to the source (Table A 3). This should be considered indications as sequence numbers were low and data were not appropriate for significance testing. Oxygen concentrations in the groundwater increased from ~0 – 530 µmol L^{-1} between the source and the end of the pond, indicating that the distance to the source could potentially be a measure of dissolved oxygen content, as oxygen would be supplied through photosynthesis and mechanical mixing (by wind) in the pond. Oxygen levels were suggested to regulate ANME distribution at the Hydrate Ridge and the Black Sea (Knittel et al., 2005), as microscopy analyses showed a dominance of ANME-1 cells in microbial biofilm mats in anoxic marine waters. Knittel et al. (2005) saw that in slightly oxygenated waters at the Hydrate Ridge, the total cell count of ANME-1 remained <1% in surface sediment, however, increased to 20 – 30% with depth (>6 cm below sea floor), as oxygen concentrations presumably dropped. The opposite was observed for ANME-2 which accounted for >90% of the total cell biomass in the oxygenated sediments at Hydrate Ridge, but <1% in the anoxic Black Sea biofilm. In our case, ANME-2a/b and 3 were observed in parts of the crater pond, where ANME-1a was absent or accounted for <1% of the relative abundance. Similar observations were made by Pachiadaki et al. (2011) and Chang et al. (2012), where ANME-1 sequence abundance peaked below 10 cm depth at a deep sea and terrestrial mud volcano, respectively. It is possible that the ANME-1a abundance would increase with depth in sediments at Lagoon pingo, however, as we only sampled the upper 1st cm, this remains unclear.

5.2.2.5 Temperature

The predominance of the ANME-2 and 3 lineages over ANME-1 at Lagoon pingo was not surprising, as these exhibit different temperature preferences (Bhattarai et al., 2019). ANME-2 and 3 have been predominantly found at cold seeps where temperatures never exceed 20°C (Nauhaus et al., 2005; Niemann et al., 2006; Heijs et al., 2007; Pachiadaki et al., 2011), opposed to ANME-1 which has been frequently observed at hydrothermal vents and

sediments, exhibiting AOM in temperatures up to 70°C with SRB (Holler et al., 2011) and 90°C without SRB partners (Wankel et al., 2012). In *in vitro* incubations of sediments dominated by ANME-1 and by ANME-2, two contrasting trends were observed by Nauhaus et al. (2005). The AOM activity measured through sulfate reduction (SR), in sediments dominated by ANME-1, increased with elevated temperatures, reaching its maximum at 25°C. In sediments dominated by ANME-2 the optimal temperature for AOM activity was observed between ~6 – 12°C. Temperature was likely a regulating factor in the groundwater pond at Lagoon pingo as well. The temperature of the water never exceeded 2.5°C, suggesting a selective pressure toward cold adapted ANME, possibly explaining the low abundance of ANME-1a compared to ANME-2a/b and 3.

5.2.3 ANME in consortia with sulfate reducing bacteria (SRB)

The distribution of ANME was mainly restricted to the crater pond, where the highest relative abundances were observed in the Crater Flow sub-cluster (Figure 16; Figure 17), comprising of SS and PF samples. Sulfate reducing bacteria (SRB) cooccurred with ANME in the SS samples, represented by the genus *Desulfocapsa* within the family Desulfobulbaceae. Desulfobulbaceae is widely acknowledged as the partnering SRB to ANME-3 (Knittel and Boetius, 2009), which accounted for up to half of the archaeal community in the SS sediments. However, to our knowledge, *Desulfocapsa* has not been observed in consortia with ANME previously, and whether these appear in consortia with ANME-3 at Lagoon pingo remains unknown. A prominent odour of hydrogen sulphide was characteristic for the crater pond and has been previously reported by Orvin (1944) and Hodson et al. (2019). Hydrogen sulphide is a by-product in AOM, suggesting that SRB mediated AOM takes place at Lagoon pingo. Moreover, sulphur oxidizing bacteria, belonging to genera *Thiobacillus*, *Sulfurovum*, *Sulfurimonas* and *Thiomicrorhabdus* were observed in SS sediments (Figure 14), all utilizing sulphide as an energy source (Dahl et al., 2008; Boden et al., 2017) and providing substrate for further AOM activity. However, according to recordings from the summer months in 2017, sulfate concentrations rarely exceeded 1 mM (Hodson et al., 2019), which represents approximately $1/30^{th}$ of the concentration commonly detected at the interface of marine sediments (Orphan et al., 2001; Niemann et al., 2006; Reeburgh, 2007). When the concentrations of sulfate remains below 10 mM, the gibs free energy drops, making AOM-SR less favourable (Tu et al., 2017). Despite possible low sulfate levels at the time of sampling, sequencing results demonstrated a prominent SRB community in SS (5.6% of all sequences at SS), indicating potential AOM-SR activity. However, ANME-1 and 2 SRB partners,

Desulfosarcina/Desulfococcus were not detected. Solitary ANME-1 and 2 have been observed with FISH in AOM active sediments (Orphan et al., 2002; Knittel et al., 2005), suggesting that these clades might also appear as solitary cells at Lagoon pingo, potentially profiting off alternative electron acceptors or reducing sulphurous molecules alone (Milucka et al., 2012; Vigneron et al., 2019). AOM coupled to reduction of iron and manganese have been experimentally demonstrated (Beal et al., 2009) and is the expected energy pathway for ANME in the terrestrial Lei-Gong-Hue mud volcano in Taiwan (Chang et al., 2012; Wang et al., 2014; Tu et al., 2017). AOM coupled with iron or manganese potentially yields 2 to 10 times more energy than sulfate dependent AOM (Beal et al., 2009), and are thus desirable pathways in systems limited by low sulfate availability, such as Lei-Gong-Hue and Lagoon pingo. The collected evidence from Lei-Gong-Hue suggest ANME partnering with *Geobacter* and *Pelobacter* transferring electrons via nanowires and surface cytochromes. However, at Lagoon pingo, these taxa were not abundant (<0.5% of the total 16S sequences) and therefore we do not expect these to be central in AOM at the site. These studies indicate that alternative electron donors than sulfate can drive AOM at Lagoon pingo. AOM coupled with nitrate reduction can be executed by ANME-2d, *Methanopredens* with anammox bacteria (Haroon et al., 2013), however, it was not detected at the site. We suggest that the potential AOM activity, indicated by sequencing results, is possibly mediated partly through ANME-3-SRB partnership, and by ANME-1 and 2 possibly using alternative electron acceptors partnering with unknown bacterial reducers, and/or solitarily.

6 Conclusion

We have presented a snapshot of the microbial community in a highly dynamic and unique arctic terrestrial system, Lagoon pingo. The anoxic, methane saturated seep water shaped the system, creating a radial mosaic of habitat patches. Distinct and unusual microbial communities inhabited these habitat patches, suggesting high levels of specialization and adaptation to an unusual terrestrial system with marine influences.

An abundant MOB community confirmed that methane is one of the main sources for energy in the system. Over 99% of all MOB sequences was affiliated with *Methylobacter* bOTU 9, a close relative of *Methylobacter tundripaludum*, which had a ubiquitous distribution at Lagoon pingo. bOTU 9 was most abundant in sediments underlying the methane rich seep waters, indicating that methane availability and gas transfers in the water regulated the distribution of

Methylobacter. Their high abundance in anoxic sediments at the source further suggested a tolerance to low oxygen concentrations.

ANME-1a, 2a/b and 3 distribution was restricted to the source and pond habitats, explained by the high methane availability and low oxygen content. The dominance of ANME-3 and 2a/b over ANME-1a was likely related to the relatively low temperatures found in the spring water. The presence of ANME on Lagoon Pingo suggests that terminal electron acceptors such as sulfate, oxidized iron or manganese are available through the water flow, making this an intriguing terrestrial equivalent of cold marine methane seeps.

Lagoon pingo contrasts starkly from previously reported ecosystems in the arctic and elsewhere. We confirm that methane is one of the primary energy sources at the seep site and that the atmospheric transfer of methane is mitigated by methane oxidizing bacteria (MOB) and possibly archaea (ANME).

7 Outlook

Upon completing this study, the complex microbial community at Lagoon pingo has been disentangled, yet many questions remain unanswered. To provide a higher resolution understanding of the microbial community functionality, metagenomic/transcriptomic inquiries are required in parallel with enrichment experiments. Such inquiries could also uncover the potential mechanisms that enable *Methylobacter* to remain active under largely anoxic conditions, as well as the functional identity of the novel Methanosarcinales (aOTU 1) which dominated in the wet sediment at Lagoon pingo. Based on methane oxidation rate results herein, it is clear that Lagoon pingo has an active methanotrophic filter, which mitigates atmospheric methane transfer from subsurface reservoirs. Yet, the efficiency of the filter remains unclear. To model and predict the future impact of groundwater-driven methane evasion, more aerobic and anaerobic methane consumption assays, as well as enzymatic reaction experiments are called for.

Bibliography

Alain, K., Holler, T., Musat, F., Elvert, M., Treude, T. and Krüger, M. (2006). Microbiological investigation of methane- and hydrocarbon-discharging mud volcanoes in the Carpathian Mountains, Romania. *Environmental Microbiology, 8*(4), 574-590.

Angel, R., Claus, P. and Conrad, R. (2012). Methanogenic archaea are globally ubiquitous in aerated soils and become active under wet anoxic conditions. *The Isme Journal, 6*(4), 847-862.

Archer, D. (2007). Methane hydrate stability and anthropogenic climate change. *Biogeosciences, 4*(4), 521-544.

Archer, D., Buffett, B. and Brovkin, V. (2009). Ocean methane hydrates as a slow tipping point in the global carbon cycle. *Proceedings of the National Academy of Sciences, 106*(49), 20596-20601.

ASTM D2974-20e1. (2020). Standard test methods for determining the water (moisture) content, ash content, and organic material of peat and other organic soils. *ASTM International, West Conshohocken, PA,*.

Beal, E. J., House, C. H. and Orphan, V. J. (2009). Manganese- and iron-dependent marine methane oxidation. *Science, 325*(5937), 184-187.

Bedward, M., Eppstein, D. and Menzel, P. (2018). packcircles: Circle Packing (Version 0.3.3).

Bhattarai, S., Cassarini, C. and Lens, P. N. L. (2019). Physiology and distribution of archaeal methanotrophs that couple anaerobic oxidation of methane with sulfate reduction. *Microbiology and Molecular Biology Reviews, 83*(3), e00074-00018.

Biddle, J. F., Cardman, Z., Mendlovitz, H., Albert, D. B., Lloyd, K. G., Boetius, A. and Teske, A. (2012). Anaerobic oxidation of methane at different temperature regimes in Guaymas Basin hydrothermal sediments. *The Isme Journal, 6*(5), 1018-1031.

Biderre-Petit, C., Boucher, D., Kuever, J., Alberic, P., Jézéquel, D., Chebance, B., Borrel, G., Fonty, G. and Peyret, P. (2011). Identification of sulfur-cycle prokaryotes in a low-sulfate lake (Lake Pavin) using aprA and 16S rRNA gene markers. *Microbial Ecology, 61*(2), 313-327.

Bodelier, P. L. E., Pérez, G., Veraart, A. J. and Krause, S. M. B. (2019). Methanotroph ecology, environmental distribution and functioning. In E. Y. Lee (Ed.), *Methanotrophs: microbiology fundamentals and biotechnological applications* (pp. 1-38). Cham: Springer International Publishing.

Boden, R., Scott, K. M., Williams, J., Russel, S., Antonen, K., Rae, A. W. and Hutt, L. P. (2017). An evaluation of Thiomicrospira, Hydrogenovibrio and Thioalkalimicrobium: reclassification of four species of Thiomicrospira to each Thiomicrorhabdus gen. nov. and Hydrogenovibrio, and reclassification of all four species of Thioalkalimicrobium to Thiomicrospira. *International Journal of Systematic and Evolutionary Microbiology, 67*(5), 1140-1151.

Boetius, A., Ravenschlag, K., Schubert, C. J., Rickert, D., Widdel, F., Gieseke, A., Amann, R., Jørgensen, B. B., Witte, U. and Pfannkuche, O. (2000). A marine microbial consortium apparently mediating anaerobic oxidation of methane. *Nature, 407*(6804), 623-626.

Bolyen, E., Rideout, J. R., Dillon, M. R., Bokulich, N. A., Abnet, C. C., Al-Ghalith, G. A., Alexander, H., Alm, E. J., Arumugam, M., Asnicar, F., Bai, Y., Bisanz, J. E., Bittinger, K., Brejnrod, A., Brislawn, C. J., Brown, C. T., Callahan, B. J., Caraballo-Rodríguez, A. M., Chase, J., Cope, E. K., Da Silva, R., Diener, C., Dorrestein, P. C., Douglas, G. M., Durall, D. M., Duvallet, C., Edwardson, C. F., Ernst, M., Estaki, M., Fouquier, J., Gauglitz, J. M., Gibbons, S. M., Gibson, D. L., Gonzalez, A., Gorlick, K., Guo, J., Hillmann, B., Holmes, S., Holste, H., Huttenhower, C., Huttley, G. A., Janssen, S., Jarmusch, A. K., Jiang, L., Kaehler, B. D., Kang, K. B., Keefe, C. R., Keim, P., Kelley, S. T., Knights, D., Koester, I., Kosciolek, T., Kreps, J., Langille, M. G. I., Lee, J., Ley, R., Liu, Y.-X., Loftfield, E., Lozupone, C., Maher, M., Marotz, C., Martin, B. D., McDonald, D., McIver, L. J., Melnik, A. V., Metcalf, J. L., Morgan, S. C., Morton, J. T., Naimey, A. T., Navas-Molina, J. A., Nothias, L. F., Orchanian, S. B., Pearson, T., Peoples, S. L., Petras, D., Preuss, M. L., Pruesse, E., Rasmussen, L. B., Rivers, A., Robeson, M. S., Rosenthal, P., Segata, N., Shaffer, M., Shiffer, A., Sinha, R., Song, S. J., Spear, J. R., Swafford, A. D., Thompson, L. R., Torres, P. J., Trinh, P., Tripathi, A., Turnbaugh, P. J., Ul-Hasan, S., van der Hooft, J. J. J., Vargas, F., Vázquez-Baeza, Y., Vogtmann, E., von Hippel, M., Walters, W., Wan, Y., Wang, M., Warren, J., Weber, K. C., Williamson, C. H. D., Willis, A. D., Xu, Z. Z., Zaneveld, J. R., Zhang, Y., Zhu, Q., Knight, R. and Caporaso, J. G. (2019). Reproducible, interactive, scalable and extensible microbiome data science using QIIME 2. *Nature Biotechnology, 37*(8), 852-857.

Borcard, D., Gillet, F. and Legendre, P. (2011). *Numerical ecology with R*: Springer.

Bowman, J. (2006). The methanotrophs — The families Methylococcaceae and Methylocystaceae. In M. Dworkin, S. Falkow, E. Rosenberg, K.-H. Schleifer, & E. Stackebrandt (Eds.), *The Prokaryotes: Volume 5: Proteobacteria: Alpha and Beta Subclasses* (pp. 266-289). New York, NY: Springer New York.

Bowman, J., Sly, L., Nichols, P. and Hayward, A. C. (1993). Revised Taxonomy of the Methanotrophs: Description of Methylobacter gen. nov., Emendation of Methylococcus, Validation of Methylosinus and Methylocystis Species, and a Proposal that the Family Methylococcaceae Includes Only the Group I Methanotrophs. *International Journal of Systematic and Evolutionary Microbiology, 43*(4), 735-753.

Buffett, B. and Archer, D. (2004). Global inventory of methane clathrate: sensitivity to changes in the deep ocean. *Earth and Planetary Science Letters, 227*(3), 185-199.

Bushnell, B., Rood, J. and Singer, E. (2017). BBMerge – Accurate paired shotgun read merging via overlap. *PloS one, 12*(10).

Callahan, B. J., McMurdie, P. J., Rosen, M. J., Han, A. W., Johnson, A. J. A. and Holmes, S. P. (2016). DADA2: High-resolution sample inference from Illumina amplicon data. *Nature Methods, 13*, 581.

Carr, S. A., Orcutt, B. N., Mandernack, K. W. and Spear, J. R. (2015). Abundant Atribacteria in deep marine sediment from the Adélie Basin, Antarctica. *Frontiers in Microbiology, 6*(872).

Chang, Y.-H., Cheng, T.-W., Lai, W.-J., Tsai, W.-Y., Sun, C.-H., Lin, L.-H. and Wang, P.-L. (2012). Microbial methane cycling in a terrestrial mud volcano in eastern Taiwan. *Environmental Microbiology, 14*(4), 895-908.

Cheng, T.-W., Chang, Y.-H., Tang, S.-L., Tseng, C.-H., Chiang, P.-W., Chang, K.-T., Sun, C.-H., Chen, Y.-G., Kuo, H.-C., Wang, C.-H., Chu, P.-H., Song, S.-R., Wang, P.-L. and Lin, L.-H. (2012). Metabolic stratification driven by surface and subsurface interactions in a terrestrial mud volcano. *The Isme Journal, 6*(12), 2280-2290.

Chu, H., Fierer, N., Lauber, C. L., Caporaso, J. G., Knight, R. and Grogan, P. (2010). Soil bacterial diversity in the Arctic is not fundamentally different from that found in other biomes. *Environmental Microbiology, 12*(11), 2998-3006.

Clark, P. U., Dyke, A. S., Shakun, J. D., Carlson, A. E., Clark, J., Wohlfarth, B., Mitrovica, J. X., Hostetler, S. W. and McCabe, A. M. (2009). The last glacial maximum. *Science, 325*(5941), 710-714.

Conrad, R. (2009). The global methane cycle: recent advances in understanding the microbial processes involved. *Environmental Microbiology Reports, 1*(5), 285-292.

Crémière, A., Lepland, A., Chand, S., Sahy, D., Condon, D. J., Noble, S. R., Martma, T., Thorsnes, T., Sauer, S. and Brunstad, H. (2016). Timescales of methane seepage on the Norwegian margin following collapse of the Scandinavian Ice Sheet. *Nature Communications, 7*(1), 11509.

Crevecoeur, S., Ruiz-González, C., Prairie, Y. T. and del Giorgio, P. A. (2019). Large-scale biogeography and environmental regulation of methanotrophic bacteria across boreal inland waters. *Molecular Ecology, 28*(18), 4181-4196.

Dahl, C., Friedrich, C. and Kletzin, A. (2008). Sulfur oxidation in prokaryotes. *eLS*.

Danilova, O. V., Suzina, N. E., Van De Kamp, J., Svenning, M. M., Bodrossy, L. and Dedysh, S. N. (2016). A new cell morphotype among methane oxidizers: a spiral-shaped obligately microaerophilic methanotroph from northern low-oxygen environments. *The Isme Journal, 10*(11), 2734-2743.

DasSarma, S. and DasSarma, P. (2017). Halophiles. *eLS*.

De Anda, V., Chen, L.-X., Dombrowski, N., Hua, Z., Jiang, H.-C., Banfield, J., Li, W.-J. and Barker, B. (submitted 2020). Brockarchaeota, a novel archaeal lineage capable of methylotrophy. *Research Square*.

Dimitrov, L. I. (2002). Mud volcanoes—the most important pathway for degassing deeply buried sediments. *Earth-Science Reviews, 59*(1), 49-76.

Dunfield, P. F., Yuryev, A., Senin, P., Smirnova, A. V., Stott, M. B., Hou, S., Ly, B., Saw, J. H., Zhou, Z., Ren, Y., Wang, J., Mountain, B. W., Crowe, M. A., Weatherby, T. M., Bodelier, P. L. E., Liesack, W., Feng, L., Wang, L. and Alam, M. (2007). Methane oxidation by an extremely acidophilic bacterium of the phylum Verrucomicrobia. *Nature, 450*(7171), 879-882.

Dutta, A., Sar, P., Sarkar, J., Dutta Gupta, S., Gupta, A., Bose, H., Mukherjee, A. and Roy, S. (2019). Archaeal Communities in Deep Terrestrial Subsurface Underneath the Deccan Traps, India. *Frontiers in Microbiology, 10*(1362).

Edgar, R. C. (2010). Search and clustering orders of magnitude faster than BLAST. *Bioinformatics, 26*(19), 2460-2461.

Edgar, R. C. (2016). UNOISE2: improved error-correction for Illumina 16S and ITS amplicon sequencing. *bioRxiv*, 081257.

Elshahed, M. S., Najar, F. Z., Roe, B. A., Oren, A., Dewers, T. A. and Krumholz, L. R. (2004). Survey of archaeal diversity reveals an abundance of halophilic archaea; in a low-salt, sulfide- and sulfur-rich spring. *Applied and Environmental Microbiology, 70*(4), 2230-2039.

Etiope, G. (2012). Methane uncovered. *Nature Geoscience, 5*(6), 373-374.

Etiope, G., Feyzullayev, A. and Baciu, C. L. (2009). Terrestrial methane seeps and mud volcanoes: A global perspective of gas origin. *Marine and Petroleum Geology, 26*(3), 333-344.

Ettwig, K. F., Butler, M. K., Le Paslier, D., Pelletier, E., Mangenot, S., Kuypers, M. M. M., Schreiber, F., Dutilh, B. E., Zedelius, J., de Beer, D., Gloerich, J., Wessels, H. J. C. T., van Alen, T., Luesken, F., Wu, M. L., van de Pas-Schoonen, K. T., Op den Camp, H. J. M., Janssen-Megens, E. M., Francoijs, K.-J., Stunnenberg, H., Weissenbach, J., Jetten, M. S. M. and Strous, M. (2010). Nitrite-driven anaerobic methane oxidation by oxygenic bacteria. *Nature, 464*(7288), 543-548.

Fernández-Gómez, B., Richter, M., Schüler, M., Pinhassi, J., Acinas, S. G., González, J. M. and Pedrós-Alió, C. (2013). Ecology of marine Bacteroidetes: a comparative genomics approach. *The Isme Journal, 7*(5), 1026-1037.

Forwich, M., Baeten, N. J. and Vorren, T. O. (2009). Pockmarks in Spitsbergen fjords. *Norwegian Journal of Geology, 89*(1/2), 66-77.

Fukui, K., Fujii, Y., Mikhailov, N., Ostanin, O. and Iwahana, G. (2007). The lower limit of mountain permafrost in the Russian Altai Mountains. *Permafrost and Periglacial Processes, 18*(2), 129-136.

Førland, E. J., Benestad, R., Hanssen-Bauer, I., Haugen, J. E. and Skaugen, T. E. (2011). Temperature and precipitation development at Svalbard 1900–2100. *Advances in Meteorology, 2011*, 893790.

Galili, T. (2015). dendextend: an R package for visualizing, adjusting and comparing trees of hierarchical clustering. *Bioinformatics, 31*(22), 3718-3720.

Gilbert, G. L., O'Neill, H. B., Nemec, W., Thiel, C., Christiansen, H. H. and Buylaert, J.-P. (2018). Late Quaternary sedimentation and permafrost development in a Svalbard fjord-valley, Norwegian high Arctic. *Sedimentology, 65*(7), 2531-2558.

Gilbert, J. A., Meyer, F., Jansson, J., Gordon, J., Pace, N., Tiedje, J., Ley, R., Fierer, N., Field, D., Kyrpides, N., Glöckner, F.-O., Klenk, H.-P., Wommack, K. E., Glass, E.,

Docherty, K., Gallery, R., Stevens, R. and Knight, R. (2010). The Earth Microbiome Project: Meeting report of the "1st EMP meeting on sample selection and acquisition" at Argonne National Laboratory October 6th 2010. *Standards in Genomic Sciences, 3*(3), 249-253.

Gonzalez-Martínez, A., Chengyuan, S., Rodriguez-Sanchez, A., Pozo, C., Gonzalez-Lopez, J. and Vahala, R. (2018). Application of microbial fuel cell technology for wastewater treatment and electricity generation under Nordic countries climate conditions: Study of performance and microbial communities. *Bioresource Technology, 270*, 1-10.

Goux, X., Calusinska, M., Fossépré, M., Benizri, E. and Delfosse, P. (2016). Start-up phase of an anaerobic full-scale farm reactor – Appearance of mesophilic anaerobic conditions and establishment of the methanogenic microbial community. *Bioresource Technology, 212*, 217-226.

Graef, C., Hestnes, A. G., Svenning, M. M. and Frenzel, P. (2011). The active methanotrophic community in a wetland from the High Arctic. *Environmental Microbiology Reports, 3*(4), 466-472.

Grosse, G. and Jones, B. (2010). Spatial distribution of pingos in Northern Asia. *The Cryosphere Discussions, 5*(1), 13-33.

Grosse, G., Jones, B. M. and Arp, C. D. (2013). Thermokarst lakes, drainage, and drained basins. *Treatise on Geomorphology, 8*, 325-353.

Gupta, V., Smemo, K. A., Yavitt, J. B., Fowle, D., Branfireun, B. and Basiliko, N. (2013). Stable isotopes reveal widespread anaerobic methane oxidation across latitude and peatland type. *Environmental Science & Technology, 47*(15), 8273-8279.

Gurney, S. D. (1998). Aspects of the genesis and geomorphology of pingos: perennial permafrost mounds. *Progress in Physical Geography: Earth and Environment, 22*(3), 307-324.

Hallam, S. J., Putnam, N., Preston, C. M., Detter, J. C., Rokhsar, D., Richardson, P. M. and DeLong, E. F. (2004). Reverse methanogenesis: Testing the hypothesis with environmental genomics. *Science, 305*(5689), 1457.

Han, Y. and Perner, M. (2015). The globally widespread genus Sulfurimonas: versatile energy metabolisms and adaptations to redox clines. *Frontiers in Microbiology, 6*(989).

Hanson, R. S. and Hanson, T. E. (1996). Methanotrophic bacteria. *Microbiological Reviews, 60*(2), 439-471.

Haroon, M. F., Hu, S., Shi, Y., Imelfort, M., Keller, J., Hugenholtz, P., Yuan, Z. and Tyson, G. W. (2013). Anaerobic oxidation of methane coupled to nitrate reduction in a novel archaeal lineage. *Nature, 500*(7464), 567-570.

Heijs, S. K., Haese, R. R., van der Wielen, P. W. J. J., Forney, L. J. and van Elsas, J. D. (2007). Use of 16S rRNA gene based clone libraries to assess microbial communities potentially involved in anaerobic methane oxidation in a Mediterranean cold seep. *Microbial Ecology, 53*(3), 384-398.

Heller, C., Hoppert, M. and Reitner, J. (2008). Immunological localization of coenzyme M reductase in anaerobic methane-oxidizing archaea of ANME 1 and ANME 2 type. *Geomicrobiology Journal, 25*(3-4), 149-156.

Hjelle, A. (1993). *Geology of Svalbard*. Oslo: Polarhåndbok no. 7, Norsk Polarinstitutt.

Hodson, A. J., Nowak, A., Redeker, K. R., Holmlund, E. S., Christiansen, H. H. and Turchyn, A. V. (2019). Seasonal dynamics of methane and carbon dioxide evasion from an open system pingo: Lagoon pingo, Svalbard. *Frontiers in Earth Science, 7*(30).

Hodson, A. J., Nowak, A., Senger, K., Redeker, K., Christiansen, H. H., Jessen, S., Hornum, M. T., Betlem, P., Thornton, S. F., Turchyn, A. V., Olaussen, S. and Marca, A. (2020). Open system pingos as hotspots for sub-permafrost methane emission in Svalbard. *The Cryosphere Discuss., 2020*, 1-21.

Holler, T., Widdel, F., Knittel, K., Amann, R., Kellermann, M. Y., Hinrichs, K.-U., Teske, A., Boetius, A. and Wegener, G. (2011). Thermophilic anaerobic oxidation of methane by marine microbial consortia. *The Isme Journal, 5*(12), 1946-1956.

Hornum, M. T., Hodson, A. J., Jessen, S., Bense, V. and Senger, K. (2020). Numerical modelling of permafrost spring discharge and open-system pingo formation induced by basal permafrost aggradation. *The Cryosphere Discuss., 2020*, 1-36.

Hovland, M. and Svensen, H. (2006). Submarine pingoes: Indicators of shallow gas hydrates in a pockmark at Nyegga, Norwegian Sea. *Marine Geology, 228*(1), 15-23.

Inagaki, F., Kuypers, M. M. M., Tsunogai, U., Ishibashi, J.-i., Nakamura, K.-i., Treude, T., Ohkubo, S., Nakaseama, M., Gena, K., Chiba, H., Hirayama, H., Nunoura, T., Takai, K., Jørgensen, B. B., Horikoshi, K. and Boetius, A. (2006). Microbial community in a sediment-hosted CO2 lake of the southern Okinawa Trough hydrothermal system. *Proceedings of the National Academy of Sciences, 103*(38), 14164-14169.

IPCC. (2014). *Climate change 2014 synthesis report. contribution of working groups I, II, and III to the fifth assessment report of the Intergovernmental Panel on Climate Change*: IPCC.

Joabsson, A. and Christensen, T. R. (2001). Methane emissions from wetlands and their relationship with vascular plants: an Arctic example. *Global Change Biology, 7*(8), 919-932.

Johansen, B. E., Karlsen, S. R. and Tømmervik, H. (2012). Vegetation mapping of Svalbard utilising Landsat TM/ETM+ data. *Polar Record, 48*(1), 47-63.

Jones, B. M., Grosse, G., Hinkel, K. M., Arp, C. D., Walker, S., Beck, R. A. and Galloway, J. P. (2012). Assessment of pingo distribution and morphometry using an IfSAR derived digital surface model, western Arctic Coastal Plain, Northern Alaska. *Geomorphology, 138*(1), 1-14.

Kalyuzhnaya, M. G., Gomez, O. A. and Murrell, J. C. (2019). The methane-oxidizing bacteria (methanotrophs). In T. J. McGenity (Ed.), *Taxonomy, Genomics and Ecophysiology of Hydrocarbon-Degrading Microbes* (pp. 245-278): Springer Nature Switzerland.

Katsuyama, C., Nashimoto, H., Nagaosa, K., Ishibashi, T., Furuta, K., Kinoshita, T., Yoshikawa, H., Aoki, K., Asano, T., Sasaki, Y., Sohrin, R., Komatsu, D. D., Tsunogai, U., Kimura, H., Suwa, Y. and Kato, K. (2013). Occurrence and potential activity of denitrifiers and methanogens in groundwater at 140 m depth in Pliocene diatomaceous mudstone of northern Japan. *FEMS Microbiology Ecology, 86*(3), 532-543.

Kirschke, S., Bousquet, P., Ciais, P., Saunois, M., Canadell, J. G., Dlugokencky, E. J., Bergamaschi, P., Bergmann, D., Blake, D. R., Bruhwiler, L., Cameron-Smith, P., Castaldi, S., Chevallier, F., Feng, L., Fraser, A., Heimann, M., Hodson, E. L., Houweling, S., Josse, B., Fraser, P. J., Krummel, P. B., Lamarque, J.-F., Langenfelds, R. L., Le Quéré, C., Naik, V., O'Doherty, S., Palmer, P. I., Pison, I., Plummer, D., Poulter, B., Prinn, R. G., Rigby, M., Ringeval, B., Santini, M., Schmidt, M., Shindell, D. T., Simpson, I. J., Spahni, R., Steele, L. P., Strode, S. A., Sudo, K., Szopa, S., van der Werf, G. R., Voulgarakis, A., van Weele, M., Weiss, R. F., Williams, J. E. and Zeng, G. (2013). Three decades of global methane sources and sinks. *Nature Geoscience, 6*, 813-823.

Klindworth, A., Pruesse, E., Schweer, T., Peplies, J., Quast, C., Horn, M. and Glöckner, F. O. (2013). Evaluation of general 16S ribosomal RNA gene PCR primers for classical and next-generation sequencing-based diversity studies. *Nucleic acids research, 41*(1), e1.

Knittel, K. and Boetius, A. (2009). Anaerobic oxidation of methane: Progress with an unknown process. *Annual Review of Microbiology, 63*(1), 311-334.

Knittel, K., Lösekann, T., Boetius, A., Kort, R. and Amann, R. (2005). Diversity and distribution of methanotrophic archaea at cold seeps. *Applied and Environmental Microbiology, 71*(1), 467-479.

Kojima, H., Fukuhara, H. and Fukui, M. (2009a). Community structure of microorganisms associated with reddish-brown iron-rich snow. *Systematic and Applied Microbiology, 32*(6), 429-437.

Kojima, H. and Fukui, M. (2019). Thiomicrorhabdus aquaedulcis sp. nov., a sulfur-oxidizing bacterium isolated from lake water. *International Journal of Systematic and Evolutionary Microbiology, 69*(9), 2849-2853.

Kojima, H., Iwata, T. and Fukui, M. (2009b). DNA-based analysis of planktonic methanotrophs in a stratified lake. *Freshwater Biology, 54*(7), 1501-1509.

Kojima, H., Watanabe, T., Iwata, T. and Fukui, M. (2014). Identification of major planktonic sulfur oxidizers in stratified freshwater lake. *PloS one, 9*(4), e93877-e93877.

Kolganova, T. V., Kuznetsov, B. B. and Tourova, T. P. (2002). Designing and testing oligonucleotide primers for amplification and sequencing of archaeal 16S rRNA genes. *Microbiology, 71*(2), 243-246.

Kopf, A. J. (2002). Significance of mud volcanism. *Reviews of Geophysics, 40*(2), 2-1-2-52.

Korehi, H., Blöthe, M. and Schippers, A. (2014). Microbial diversity at the moderate acidic stage in three different sulfidic mine tailings dumps generating acid mine drainage. *Research in Microbiology, 165*(9), 713-718.

Kristiansen, J., Wilken, L. R. and Jürgensen, T. (1995). A bloom of Mallomonas acaroides, a silica-scaled chrysophyte, in the crater pond of a pingo, Northwest Greenland. *Polar Biology, 15*(5), 319-324.

Krüger, M., Meyerdierks, A., Glöckner, F. O., Amann, R., Widdel, F., Kube, M., Reinhardt, R., Kahnt, J., Böcher, R., Thauer, R. K. and Shima, S. (2003). A conspicuous nickel protein in microbial mats that oxidize methane anaerobically. *Nature, 426*, 878-881.

Kuever, J., Rainey, F. A. and Widdel, F. (2015). Desulfobacterales ord. nov. In *Bergey's Manual of Systematics of Archaea and Bacteria* (pp. 1-2).

Kvenvolden, K. A. (1988). Methane hydrates and global climate. *Global Biogeochemical Cycles, 2*(3), 221-229.

Lagerbäck, R. and Rodhe, L. (1985). Pingos in northernmost Sweden. *Geografiska Annaler: Series A, Physical Geography, 67*(3-4), 239-245.

Lambert, S., Tragin, M., Lozano, J.-C., Ghiglione, J.-F., Vaulot, D., Bouget, F.-Y. and Galand, P. E. (2019). Rhythmicity of coastal marine picoeukaryotes, bacteria and archaea despite irregular environmental perturbations. *The Isme Journal, 13*(2), 388-401.

Liebner, S., Rublack, K., Stuehrmann, T. and Wagner, D. (2009). Diversity of aerobic methanotrophic bacteria in a permafrost active layer soil of the Lena Delta, Siberia. *Microbial Ecology, 57*(1), 25-35.

Liestøl, O. (1977). Pingos, springs, and permafrost in Spitsbergen. *Norsk Polarinstitutt Årbok 1977*, 7-29.

Lomborinchen, R. (2000). Frost heaving and related landforms, Mongolia. *Permafrost and Periglacial Processes, 11*(1), 85-90.

Lønne, I. D. A. (2005). Faint traces of high Arctic glaciations: an early Holocene ice-front fluctuation in Bolterdalen, Svalbard. *Boreas, 34*(3), 308-323.

Lösekann, T., Knittel, K., Nadalig, T., Fuchs, B., Niemann, H., Boetius, A. and Amann, R. (2007). Diversity and abundance of aerobic and anaerobic methane oxidizers at the Haakon Mosby mud volcano, Barents Sea. *Applied and Environmental Microbiology, 73*(10), 3348.

Mackay, J. R. (1978). Sub-pingo water lenses, Tuktoyaktuk Peninsula, Northwest Territories. *Canadian Journal of Earth Sciences, 15*(8), 1219-1227.

Mackelprang, R., Waldrop, M. P., DeAngelis, K. M., David, M. M., Chavarria, K. L., Blazewicz, S. J., Rubin, E. M. and Jansson, J. K. (2011). Metagenomic analysis of a permafrost microbial community reveals a rapid response to thaw. *Nature, 480*, 368-371.

Martineau, C., Whyte, L. G. and Greer, C. W. (2010). Stable isotope probing analysis of the diversity and activity of methanotrophic bacteria in soils from the Canadian high Arctic. *Applied and Environmental Microbiology, 76*(17).

McCann, C. M., Wade, M. J., Gray, N. D., Roberts, J. A., Hubert, C. R. J. and Graham, D. W. (2016). Microbial communities in a high Arctic polar desert landscape. *Frontiers in Microbiology, 7*(419).

McDonald, D., Clemente, J. C., Kuczynski, J., Rideout, J. R., Stombaugh, J., Wendel, D., Wilke, A., Huse, S., Hufnagle, J., Meyer, F., Knight, R. and Caporaso, J. G. (2012). The Biological Observation Matrix (BIOM) format or: how I learned to stop worrying and love the ome-ome. *GigaScience, 1*(1), 7.

McGlynn, S. E., Chadwick, G. L., Kempes, C. P. and Orphan, V. J. (2015). Single cell activity reveals direct electron transfer in methanotrophic consortia. *Nature, 526*, 531-535.

Merkel, A. Y., Huber, J. A., Chernyh, N. A., Bonch-Osmolovskaya, E. A. and Lebedinsky, A. V. (2013). Detection of putatively thermophilic anaerobic methanotrophs in diffuse hydrothermal vent fluids. *Applied and Environmental Microbiology, 79*(3), 915-923.

Meyerdierks, A., Kube, M., Kostadinov, I., Teeling, H., Glöckner, F. O., Reinhardt, R. and Amann, R. (2010). Metagenome and mRNA expression analyses of anaerobic methanotrophic archaea of the ANME-1 group. *Environmental Microbiology, 12*(2), 422-439.

Milkov, A. V. (2004). Global estimates of hydrate-bound gas in marine sediments: how much is really out there? *Earth-Science Reviews, 66*(3), 183-197.

Miller, K. E., Lai, C. T., Dahlgren, R. A. and Lipson, D. A. (2019). Anaerobic methane oxidation in high-Arctic Alaskan peatlands as a significant control on net CH4 fluxes. *Soil Systems, 3*(7).

Milucka, J., Ferdelman, T. G., Polerecky, L., Franzke, D., Wegener, G., Schmid, M., Lieberwirth, I., Wagner, M., Widdel, F. and Kuypers, M. M. M. (2012). Zero-valent sulphur is a key intermediate in marine methane oxidation. *Nature, 491*, 541-546.

Müller, A. L., Pelikan, C., de Rezende, J. R., Wasmund, K., Putz, M., Glombitza, C., Kjeldsen, K. U., Jørgensen, B. B. and Loy, A. (2018). Bacterial interactions during sequential degradation of cyanobacterial necromass in a sulfidic arctic marine sediment. *Environmental Microbiology, 20*(8), 2927-2940.

Müller, F. (1959). Beobachtungen uber Pingos. *Meddelelser om Gronland, 153*, 1-127.

Nagel, F. (2020). *Linking methane fluxes and oxidation rates to methane oxidizing bacteria in an Arctic terrestrial methane seep, Svalbard* (Master Thesis), University of Tromsø, Tromsø.

Nauhaus, K., Albrecht, M., Elvert, M., Boetius, A. and Widdel, F. (2007). In vitro cell growth of marine archaeal-bacterial consortia during anaerobic oxidation of methane with sulfate. *Environmental Microbiology, 9*(1), 187-196.

Nauhaus, K., Treude, T., Boetius, A. and Krüger, M. (2005). Environmental regulation of the anaerobic oxidation of methane: a comparison of ANME-I and ANME-II communities. *Environmental Microbiology, 7*(1), 98-106.

Niemann, H., Lösekann, T., de Beer, D., Elvert, M., Nadalig, T., Knittel, K., Amann, R., Sauter, E. J., Schlüter, M., Klages, M., Foucher, J. P. and Boetius, A. (2006). Novel microbial communities of the Haakon Mosby mud volcano and their role as a methane sink. *Nature, 443*, 854-858.

O'Connor, F. M., Boucher, O., Gedney, N., Jones, C. D., Folberth, G. A., Coppell, R., Friedlingstein, P., Collins, W. J., Chappellaz, J., Ridley, J. and Johnson, C. E. (2010). Possible role of wetlands, permafrost, and methane hydrates in the methane cycle under future climate change: A review. *Reviews of Geophysics, 48*(4).

Ohshiro, T., Harada, N., Kobayashi, Y., Miki, Y. and Kawamoto, H. (2012). Microbial fucoidan degradation by Luteolibacter algae H18 with deacetylation. *Bioscience, Biotechnology, and Biochemistry, 76*(3), 620-623.

Oksanen, J., Blanchet, F. G., Friendly, M., Kindt, R., Legendre, P., McGlinn, D., Minchin, P. R., O'Hara, R. B., Simpson, G. L., Solymos, P., Stevens, M. H. H., Szoecs, E. and Wagner, H. (2019). vegan: Community Ecology Package

Orphan, V. J., Hinrichs, K. U., Ussler, W., Paull, C. K., Taylor, L. T., Sylva, S. P., Hayes, J. M. and Delong, E. F. (2001). Comparative analysis of methane-oxidizing archaea and sulfate-reducing bacteria in anoxic marine sediments. *Applied and Environmental Microbiology*, *67*(4), 1922-1934.

Orphan, V. J., House, C. H., Hinrichs, K.-U., McKeegan, K. D. and DeLong, E. F. (2002). Multiple archaeal groups mediate methane oxidation in anoxic cold seep sediments. *Proceedings of the National Academy of Sciences, 99*(11), 7663-7668.

Orphan, V. J., Ussler, W., Naehr, T. H., House, C. H., Hinrichs, K. U. and Paull, C. K. (2004). Geological, geochemical, and microbiological heterogeneity of the seafloor

around methane vents in the Eel River Basin, offshore California. *Chemical Geology, 205*(3), 265-289.

Orvin, A. K. (1944). Litt om kilder på Svalbard. *Norsk Geografisk Tidsskrift - Norwegian Journal of Geography, 10*(1), 16-38.

Oyarzún, P., Arancibia, F., Canales, C. and Aroca, G. E. (2003). Biofiltration of high concentration of hydrogen sulphide using Thiobacillus thioparus. *Process Biochemistry, 39*(2), 165-170.

Pachiadaki, M. G., Kallionaki, A., Dählmann, A., De Lange, G. J. and Kormas, K. A. (2011). Diversity and spatial distribution of prokaryotic communities along a sediment vertical profile of a deep-sea mud volcano. *Microbial Ecology, 62*(3), 655-668.

Panieri, G., Bünz, S., Fornari, D. J., Escartin, J., Serov, P., Jansson, P., Torres, M. E., Johnson, J. E., Hong, W., Sauer, S., Garcia, R. and Gracias, N. (2017). An integrated view of the methane system in the pockmarks at Vestnesa Ridge, 79°N. *Marine Geology, 390*, 282-300.

Parada, A. E., Needham, D. M. and Fuhrman, J. A. (2016). Every base matters: assessing small subunit rRNA primers for marine microbiomes with mock communities, time series and global field samples. *Environmental Microbiology, 18*(5), 1403-1414.

Pausan, M. R., Csorba, C., Singer, G., Till, H., Schöpf, V., Santigli, E., Klug, B., Högenauer, C., Blohs, M. and Moissl-Eichinger, C. (2019). Exploring the archaeome: Detection of archaeal signatures in the human body. *Frontiers in Microbiology, 10*.

Perreault, N. N., Andersen, D. T., Pollard, W. H., Greer, C. W. and Whyte, L. G. (2007). Characterization of the prokaryotic diversity in cold saline perennial springs of the Canadian high Arctic. *Applied and Environmental Microbiology, 73*(5), 1532-1543.

Pinhassi, J., Sala, M. M., Havskum, H., Peters, F., Guadayol, Ò., Malits, A. and Marrasé, C. (2004). Changes in bacterioplankton composition under different phytoplankton regimens. *Applied and Environmental Microbiology, 70*(11), 6753-6766.

Pol, A., Heijmans, K., Harhangi, H. R., Tedesco, D., Jetten, M. S. M. and Op den Camp, H. J. M. (2007). Methanotrophy below pH 1 by a new Verrucomicrobia species. *Nature, 450*, 874-878.

Portnov, A., Vadakkepuliyambatta, S., Mienert, J. and Hubbard, A. (2016). Ice-sheet-driven methane storage and release in the Arctic. *Nature Communications, 7*.

Quince, C., Lanzen, A., Davenport, R. J. and Turnbaugh, P. J. (2011). Removing noise from pyrosequenced amplicons. *BMC Bioinformatics, 12*(1).

R Core Team. (2020). R: A Language and Environment for Statistical Computing (Version 3.6.3). Vienna, Austria: P Foundation for Statistical Computing.

Reay, D. S., Smith, P., Christensen, T. R., James, R. H. and Clark, H. (2018). Methane and global environmental change. *Annual Review of Environment and Resources, 43*(1), 165-192.

Reeburgh, W. S. (2007). Oceanic Methane Biogeochemistry. *Chemical Reviews, 107*(2), 486-513.

Rognes, T., Flouri, T., Nichols, B., Quince, C. and Mahé, F. (2016). VSEARCH: a versatile open source tool for metagenomics. *PeerJ, 4*, e2584-e2584.

Rossel, P. E., Elvert, M., Ramette, A., Boetius, A. and Hinrichs, K.-U. (2011). Factors controlling the distribution of anaerobic methanotrophic communities in marine environments: Evidence from intact polar membrane lipids. *Geochimica et Cosmochimica Acta, 75*(1), 164-184.

Roy, S., Senger, K., Hovland, M., Römer, M. and Braathen, A. (2019). Geological controls on shallow gas distribution and seafloor seepage in an Arctic fjord of Spitsbergen, Norway. *Marine and Petroleum Geology, 107*, 237-254.

RStudio Team. (2016). RStudio: Integrated Development Environment for R (Version 1.1.463). Boston, MA: RStudio, Inc. .

Ruff, S. E., Arnds, J., Knittel, K., Amann, R., Wegener, G., Ramette, A. and Boetius, A. (2013). Microbial communities of deep-sea methane seeps at Hikurangi continental margin (New Zealand). *PloS one, 8*(9), e72627-e72627.

Scheller, S., Goenrich, M., Boecher, R., Thauer, R. K. and Jaun, B. (2010). The key nickel enzyme of methanogenesis catalyses the anaerobic oxidation of methane. *Nature, 465*, 606-608.

Schloss, P. D., Westcott, S. L., Ryabin, T., Hall, J. R., Hartmann, M., Hollister, E. B., Lesniewski, R. A., Oakley, B. B., Parks, D. H., Robinson, C. J., Sahl, J. W., Stres, B., Thallinger, G. G., Van Horn, D. J. and Weber, C. F. (2009). Introducing mothur: Open-source, platform-independent, community-supported software for describing

and comparing microbial communities. *Applied and Environmental Microbiology, 75*(23), 7537-7541.

Schuur, E. A. G., Bockheim, J., Canadell, J. G., Euskirchen, E., Field, C. B., Goryachkin, S. V., Hagemann, S., Kuhry, P., Lafleur, P. M., Lee, H., Mazhitova, G., Nelson, F. E., Rinke, A., Romanovsky, V. E., Shiklomanov, N., Tarnocai, C., Venevsky, S., Vogel, J. G. and Zimov, S. A. (2008). Vulnerability of permafrost carbon to climate change: implications for the global carbon cycle. *BioScience, 58*(8), 701-714.

Smith, G. J., Angle, J. C., Solden, L. M., Borton, M. A., Morin, T. H., Daly, R. A., Johnston, M. D., Stefanik, K. C., Wolfe, R., Gil, B. and Wrighton, K. C. (2018). Members of the genus methylobacter are inferred to account for the majority of aerobic methane oxidation in oxic soils from a freshwater wetland. *mBio, 9*(6), e00815-00818.

Sorokin, D. Y., Abbas, B., Merkel, A. Y., Rijpstra, W. I. C., Damsté, J. S. S., Sukhacheva, M. V. and van Loosdrecht, M. C. M. (2015). Methanosalsum natronophilum sp. nov., and Methanocalculus alkaliphilus sp. nov., haloalkaliphilic methanogens from hypersaline soda lakes. *International Journal of Systematic and Evolutionary Microbiology, 65*(10), 3739-3745.

Spahni, R., Chappellaz, J., Stocker, T. F., Loulergue, L., Hausammann, G., Kawamura, K., Flückiger, J., Schwander, J., Raynaud, D., Masson-Delmotte, V. and Jouzel, J. (2005). Atmospheric methane and nitrous oxide of the late Pleistocene from Antarctic ice cores. *Science, 310*(5752), 1317-1321.

Stams, A. J. M. and Plugge, C. M. (2009). Electron transfer in syntrophic communities of anaerobic bacteria and archaea. *Nature Reviews Microbiology, 7*(8), 568-577.

Steven, B., Pollard, W. H., Greer, C. W. and Whyte, L. G. (2008). Microbial diversity and activity through a permafrost/ground ice core profile from the Canadian high Arctic. *Environmental Microbiology, 10*(12), 3388-3403.

Stolper, D. A., Lawson, M., Davis, C. L., Ferreira, A. A., Neto, E. V. S., Ellis, G. S., Lewan, M. D., Martini, A. M., Tang, Y., Schoell, M., Sessions, A. L. and Eiler, J. M. (2014). Formation temperatures of thermogenic and biogenic methane. *Science, 344*(6191), 1500-1503.

Svendsen, J. I. and Mangerud, J. (1997). Holocene glacial and climatic variations on Spitsbergen, Svalbard. *The Holocene, 7*(1), 45-57.

Svenning, M. M., Hestnes, A. G., Wartiainen, I., Stein, L. Y., Klotz, M. G., Kalyuzhnaya, M. G., Spang, A., Bringel, F., Vuilleumier, S., Lajus, A., Médigue, C., Bruce, D. C.,

Cheng, J.-F., Goodwin, L., Ivanova, N., Han, J., Han, C. S., Hauser, L., Held, B., Land, M. L., Lapidus, A., Lucas, S., Nolan, M., Pitluck, S. and Woyke, T. (2011). Genome sequence of the Arctic methanotroph methylobacter tundripaludum SV96. *Journal of Bacteriology, 193*(22), 6418-6419.

Svensson, H. (1970). Pingos i ytre delen av Adventdalen. *Norsk Polarinstitutt Årbok 1969*, 170-174.

Tarnocai, C., Canadell, J. G., Schuur, E. A. G., Kuhry, P., Mazhitova, G. and Zimov, S. (2009). Soil organic carbon pools in the northern circumpolar permafrost region. *Global Biogeochemical Cycles, 23*(2).

Teeling, H., Fuchs, B. M., Becher, D., Klockow, C., Gardebrecht, A., Bennke, C. M., Kassabgy, M., Huang, S., Mann, A. J., Waldmann, J., Weber, M., Klindworth, A., Otto, A., Lange, J., Bernhardt, J., Reinsch, C., Hecker, M., Peplies, J., Bockelmann, F. D., Callies, U., Gerdts, G., Wichels, A., Wiltshire, K. H., Glöckner, F. O., Schweder, T. and Amann, R. (2012). Substrate-controlled succession of marine bacterioplankton populations pnduced by a phytoplankton bloom. *Science, 336*(6081), 608-611.

Teng, F., Darveekaran Nair, S. S., Zhu, P., Li, S., Huang, S., Li, X., Xu, J. and Yang, F. (2018). Impact of DNA extraction method and targeted 16S-rRNA hypervariable region on oral microbiota profiling. *Scientific Reports, 8*(1).

Teske, A., Durbin, A., Ziervogel, K., Cox, C. and Arnosti, C. (2011). Microbial community composition and function in permanently cold seawater and sediments from an Arctic fjord of Svalbard. *Applied and Environmental Microbiology, 77*(6), 2008-2018.

Teske, A., Hinrichs, K.-U., Edgcomb, V., de Vera Gomez, A., Kysela, D., Sylva, S. P., Sogin, M. L. and Jannasch, H. W. (2002). Microbial diversity of hydrothermal sediments in the Guaymas Basin: evidence for anaerobic methanotrophic communities. *Applied and Environmental Microbiology, 68*(4), 1994-2007.

Thomas, E. K., Castañeda, I. S., McKay, N. P., Briner, J. P., Salacup, J. M., Nguyen, K. Q. and Schweinsberg, A. D. (2018). A wetter Arctic coincident with hemispheric warming 8,000 years ago. *Geophysical Research Letters, 45*(19), 10637-10647.

Tian, F., Yu, Y., Chen, B., Li, H., Yao, Y.-F. and Guo, X.-K. (2009). Bacterial, archaeal and eukaryotic diversity in Arctic sediment as revealed by 16S rRNA and 18S rRNA gene clone libraries analysis. *Polar Biology, 32*(1), 93-103.

Timmers, P. H. A., Suarez-Zuluaga, D. A., van Rossem, M., Diender, M., Stams, A. J. M. and Plugge, C. M. (2016). Anaerobic oxidation of methane associated with sulfate reduction in a natural freshwater gas source. *The Isme Journal, 10*(6), 1400-1412.

Treude, T., Boetius, A., Knittel, K., Wallmann, K. and Jørgensen, B. B. (2003). Anaerobic oxidation of methane above gas hydrates at Hydrate Ridge, NE Pacific Ocean. *Marine Ecology Progress Series, 264*, 1-14.

Tu, T.-H., Wu, L.-W., Lin, Y.-S., Imachi, H., Lin, L.-H. and Wang, P.-L. (2017). Microbial community composition and functional capacity in a terrestrial ferruginous, sulfate-depleted mud volcano. *Frontiers in Microbiology, 8*.

Tveit, A., Schwacke, R., Svenning, M. M. and Urich, T. (2013). Organic carbon transformations in high-Arctic peat soils: key functions and microorganisms. *The Isme Journal, 7*, 299-311.

Tveit, A. T., Urich, T. and Svenning, M. M. (2014). Metatranscriptomic Analysis of Arctic Peat Soil Microbiota. *Applied and Environmental Microbiology, 80*(18), 5761-5772.

Valenzuela, E. I., Prieto-Davó, A., López-Lozano, N. E., Hernández-Eligio, A., Vega-Alvarado, L., Juárez, K., García-González, A. S., López, M. G. and Cervantes, F. J. (2017). Anaerobic methane oxidation driven by microbial reduction of natural organic matter in a tropical wetland. *Applied and Environmental Microbiology, 83*(11), e00645-00617.

van Grinsven, S., Sinninghe Damsté, J. S., Abdala Asbun, A., Engelmann, J. C., Harrison, J. and Villanueva, L. (2020). Methane oxidation in anoxic lake water stimulated by nitrate and sulfate addition. *Environmental Microbiology, 22*(2), 766-782.

Vaughan, D. G., Comiso, J., Allison, I., Carrasco, J., Kaser, G., Kwok, R., Holland, D. and al., n. (2014). Observations: Cryosphere. In T. F. Stocker, D. Qin, G. K. Plattner, M. Tignor, S. K. Allen, J. Boschung, A. Nauels, & al. (Eds.), *Climate change 2013: The physical science basis. Contribution of working group I to the fifth assessment report of the intergovernmental panel on climate change*. Cambridge, United Kingdom and New York, NY, USA: Cambridge University Press.

Vigneron, A., Alsop, E. B., Cruaud, P., Philibert, G., King, B., Baksmaty, L., Lavallee, D., Lomans, B. P., Eloe-Fadrosh, E., Kyrpides, N. C., Head, I. M. and Tsesmetzis, N. (2019). Contrasting pathways for anaerobic methane oxidation in Gulf of Mexico cold seep sediments. *mSystems, 4*(1), e00091-00018.

Vigneron, A., Cruaud, P., Pignet, P., Caprais, J.-C., Cambon-Bonavita, M.-A., Godfroy, A. and Toffin, L. (2013). Archaeal and anaerobic methane oxidizer communities in the Sonora Margin cold seeps, Guaymas Basin (Gulf of California). *The Isme Journal, 7*(8), 1595-1608.

Villemur, R., Juteau, P., Bougie, V., Ménard, J. and Déziel, E. (2015). Development of four-stage moving bed biofilm reactor train with a pre-denitrification configuration for the removal of thiocyanate and cyanate. *Bioresource Technology, 181*, 254-262.

Walker, D. A., Raynolds, M. K., Daniëls, F. J. A., Einarsson, E., Elvebakk, A., Gould, W. A., Katenin, A. E., Kholod, S. S., Markon, C. J., Melnikov, E. S., Moskalenko, N. G., Talbot, S. S., Yurtsev, B. A. and The other members of the, C. T. (2005). The circumpolar Arctic vegetation map. *Journal of Vegetation Science, 16*(3), 267-282.

Wang, B. and French, H. M. (1995). Permafrost on the Tibet Plateau, China. *Quaternary Science Reviews, 14*(3), 255-274.

Wang, P.-L., Chiu, Y.-P., Cheng, T.-W., Chang, Y.-H., Tu, W.-X. and Lin, L.-H. (2014). Spatial variations of community structures and methane cycling across a transect of Lei-Gong-Hou mud volcanoes in eastern Taiwan. *Frontiers in Microbiology, 5*(121).

Wang, Y., Wu, Y.-H., Wang, C.-S., Xu, X.-W., Oren, A., Zhu, X.-F. and Wu, M. (2008). Halomonas salifodinae sp. nov., a halophilic bacterium isolated from a salt mine in China. *International Journal of Systematic and Evolutionary Microbiology, 58*(12), 2855-2858.

Wankel, S. D., Adams, M. M., Johnston, D. T., Hansel, C. M., Joye, S. B. and Girguis, P. R. (2012). Anaerobic methane oxidation in metalliferous hydrothermal sediments: influence on carbon flux and decoupling from sulfate reduction. *Environmental Microbiology, 14*(10), 2726-2740.

Wartiainen, I., Hestnes, A. G., McDonald, I. R. and Svenning, M. M. (2006). Methylobacter tundripaludum sp. nov., a methane-oxidizing bacterium from Arctic wetland soil on the Svalbard islands, Norway (78° N). *International Journal of Systematic and Evolutionary Microbiology, 56*(1), 109-113.

Wegener, G., Krukenberg, V., Riedel, D., Tegetmeyer, H. E. and Boetius, A. (2015). Intercellular wiring enables electron transfer between methanotrophic archaea and bacteria. *Nature, 526*(7574), 587-590.

Wei, T. and Simko, V. (2017). R package "corrplot": Visualizationof a Correlation Matrix.

Weisburg, W. G., Barns, S. M., Pelletier, D. A. and Lane, D. J. (1991). 16S ribosomal DNA amplification for phylogenetic study. *Journal of Bacteriology, 173*(2), 697-703.

Whittenbury, R., Davies, S. L. and Davey, J. F. (1970). Exospores and cysts formed by methane-utilizing bacteria. *Microbiology, 61*(2), 219-226.

Wickham, H. (2016). ggplot2: Elegant Graphics for Data Analysis: Springer-Verlag New York.

Worsley, P. and Gurney, S. D. (1996). Geomorphology and hydrogeological significance of the Holocene pingos in the Karup Valley area, Traill Island, northern east Greenland. *Journal of Quaternary Science, 11*(3), 249-262.

Wrede, C., Brady, S., Rockstroh, S., Dreier, A., Kokoschka, S., Heinzelmann, S. M., Heller, C., Reitner, J., Taviani, M., Daniel, R. and Hoppert, M. (2012). Aerobic and anaerobic methane oxidation in terrestrial mud volcanoes in the Northern Apennines. *Sedimentary Geology, 263-264*, 210-219.

Xiong, J., Liu, Y., Lin, X., Zhang, H., Zeng, J., Hou, J., Yang, Y., Yao, T., Knight, R. and Chu, H. (2012). Geographic distance and pH drive bacterial distribution in alkaline lake sediments across Tibetan Plateau. *Environmental Microbiology, 14*(9), 2457-2466.

Yang, B., Wang, Y. and Qian, P.-Y. (2016). Sensitivity and correlation of hypervariable regions in 16S rRNA genes in phylogenetic analysis. *BMC Bioinformatics, 17*(1), 135.

Yang, H.-M., Lou, K., Sun, J., Zhang, T. and Ma, X.-L. (2012). Prokaryotic diversity of an active mud volcano in the Usu City of Xinjiang, China. *Journal of Basic Microbiology, 52*(1), 79-85.

Yilmaz, P., Parfrey, L. W., Yarza, P., Gerken, J., Pruesse, E., Quast, C., Schweer, T., Peplies, J., Ludwig, W. and Glöckner, F. O. (2013). The SILVA and "All-species Living Tree Project (LTP)" taxonomic frameworks. *Nucleic acids research, 42*(D1), D643-D648.

Yoon, J., Matsuo, Y., Adachi, K., Nozawa, M., Matsuda, S., Kasai, H. and Yokota, A. (2008). Description of Persicirhabdus sediminis gen. nov., sp. nov., Roseibacillus ishigakijimensis gen. nov., sp. nov., Roseibacillus ponti sp. nov., Roseibacillus persicicus sp. nov., Luteolibacter pohnpeiensis gen. nov., sp. nov. and Luteolibacter algae sp. nov., six marine members of the phylum 'Verrucomicrobia', and emended descriptions of the class Verrucomicrobiae, the order Verrucomicrobiales and the family Verrucomicrobiaceae. *International Journal of Systematic and Evolutionary Microbiology, 58*(4), 998-1007.

Yoshikawa, K. (1993). Notes on open-system pingo ice, Adventdalen, Spitsbergen. *Permafrost and Periglacial Processes, 4*(4), 327-334.

Yoshikawa, K. and Harada, K. (1995). Observations on nearshore pingo growth, Adventdalen, Spitsbergen. *Permafrost and Periglacial Processes, 6*(4), 361-372.

Yoshikawa, K. and Nakamura, T. (1996). Pingo growth ages in the delta area, Adventdalen, Spitsbergen. *Polar Record, 32*(183), 347-352.

Zhang, J., Zhang, X., Liu, Y., Xie, S. and Liu, Y. (2014). Bacterioplankton communities in a high-altitude freshwater wetland. *Annals of Microbiology, 64*(3), 1405-1411.

Øvreås, L., Forney, L., Daae, F. L. and Torsvik, V. (1997). Distribution of bacterioplankton in meromictic Lake Saelenvannet, as determined by denaturing gradient gel electrophoresis of PCR-amplified gene fragments coding for 16S rRNA. *Applied and Environmental Microbiology, 63*(9), 3367-3373.

Appendix I: Materials and methods

A: Extraction of TNA from pingo sediments

Preparation of sample sediment prior to grinding

Materials:

Freezer room -20°C:

- Ziplock plastic bags *3
- Hammer and chisel
- Tweezers
- Tablespoon
- Liquid nitrogen
- Big metal tray
- 50 mL tube
- 70% ethanol

Cold room 4°C:

- See protocol for grinding soil samples with grinding jars
- Dry ice

Method:

1. Precool all equipment in -20°C freezer
2. The tweezers, the tablespoon, chisel and the metal tray should be sterilized beforehand (Baking/Autoclaving & drying/UV)
3. Place the sample tube in liquid N_2 along with the new 50 mL tube (for transfer)
4. Place three zip-lock bags inside each other and transfer the heterogenous soil sample into the inner bag and close it. If the sample is stuck inside the tube, the whole tube will be placed inside the bags
5. Place the plastic bags into the metal tray
6. Crush the sample with the hammer and chisel
    - NB: In case all bags break, the hammering should stop, as the hammer is not sterile
7. Empty the bag into the metal tray and mix the pieces quickly
8. Transfer the soil into the new precooled 50 mL tube with tweezers and the tablespoon
9. Keep the crushed sample in liquid N_2
10. Store at -80°C until further processing

Grinding of sediment samples with Grinding Jars (Qiagen)

Materials:

- 2 x grinding jars (Qiagen)
- Small spatula
- Tweezers (small and large)
- 70% Ethanol
- Lysis E tubes
- Weighing scale
- TissueLyser II (Qiagen)

- Liquid N_2 in a plastic container (no glass walls – they break when in contact with the metal grinding jars)
- 50 mL tube for excess sediment bricks (if needed)
- 15 mL tube for cooling down spatula in liquid N_2

Methods:

1) Make sure all the equipment is sterilized (Baking/Autoclaved & dried/ UV)
2) Clean workspace with ethanol
3) Get liquid N_2
4) Weight all lysis tubes
5) Cool grinding jars in liquid N_2
6) Transfer sample soil/sediment (0.5-6 g) into each grinding jar
    a. NB: Transfer a little bit more sample than needed as some of it will freeze to the walls of the grinding jars. Make sure the ball is inside.
7) Cool grinding jar in liquid N_2
8) Place grinding jars in TissueLyser II - using big forceps.
    a. NB: Make sure the grinding jar is properly fastened and balanced before starting the grinding process.
9) Grind at frequency 30 Hz for 30 seconds
10) Cool jars in liq N_2
11) Repeat step 9-10 two more times (3 repetitions in total)
12) Keep jars in N_2 until further use
13) Cool down lysis E tubes in liq N_2 along with the spatula
14) Open the jars and transfer the 0.2 g of the ground sample powder into the lysis E tubes
15) Frequently cool down the grinding jars in liq N_2 to prevent ground sample from thawing

Preparation of equipment and solutions for TNA extraction

Solutions

All solutions are made with DEPC treated water and molecular biology grade chemical compounds, if not ordered directly. All solutions are also DEPC treated if possible and then autoclaved.

TNS

- 500 mM TRIZMA (M.W 121.14) 15.76 g
- 100 mM NaCl (M.W 58.44) 1.17 g
- 10% SDS (M.W 288.38) 20 g
- RNase-free water →200 ml
- Dissolve
- Treat with 0.1% DEPC overnight and autoclave

PEG-6000

37,4g of NaCl and 120g of polyethylene glycol is added to 200ml of DEPC treated water. Then the mix is warmed while stirring to dissolve the compounds, and DEPC water is added up to 400ml. The PEG could also be added while warming and stirring together with water for a smoother dissolving. 0,1% DEPC is then added (0,2ml), the solution is stirred o/n at room temperature and then autoclaved.

70% EtOH

700ml of 100% molecular biology grade ethanol is mixed with 300ml of DEPC treated water for a 1L solution

EB buffer

ordered from Qiagen

Phenol Chloroform Isoamylalcohol (PCI) 25:24:1

Is ordered as molecular biology grade solution

Chloroform Isoamylalcohol (CI) 24:1

Molecular biology grade Chloroform and Isoamylalcohol is mixed in a 24:1 relationship

Linear acrylamide/glycogen

Ordered from Ambion

Make aliquots of all solutions in 50ml gamma grade falcon tubes

For mechanical lysis:

Lysis E tubes from MP biomedicals

Total Nucleic acid extraction of pingo sediment

Cool down the centrifuge to 4°C

Fetch dry ice and keep in a styrofoam box with lid

Use parafilm/tape to cover sample spaces that will not be in use on the adapter head (to prevent dry ice from flying out during bead beating)

Place the lower part of the adapter head in the box with dry ice for cooling

Fetch the lysis E tubes from the -80°C freezer and keep on ice

Thaw samples briefly on ice, and keep on ice for the following steps if not otherwise noted

For each of the lysis matrix E tubes containing 0,20g of soil:

1. Add 500µl of PCI
2. Add 500µl Extraction Buffer (TNS)
3. Add dry ice to the adapter head and bead beat 30sec at 5.0 (program 1)
4. Spin down 10min at 13000g 4°C
5. Transfer supernatant (app. 300µl) to a 2ml tube
6. Repeat step 1-5 **two** times, changing the added volumes of Extraction Buffer and PCI to:
    a. 300 µl (2nd bead beating) and
    b. 200 µl (3rd bead beating step)

    Pool supernatant from 2nd and 3rd bead beating step

7. Extract with 1vol of CI
8. Spin 5min at 13000g and 4°C
9. Transfer supernatant (app. 300µl) to a 2ml tube
10. Extract with 2 vol of PEG-6000 and add glycogen (0.015 mg/ml → 0.003 times the total volume of supernatant and PEG) and let precipitate for 60min
11. Spin 60min at 13000g and 4°C
12. Decant

13. Add 1000µl of ice cold 70% EtOH
14. Spin 10min at 13000g and 4°C
15. Decant
16. Repeat steps 13-15
17. Spin shortly at 13000g and 4°C
18. Remove leftover EtOH carefully with a pipette
19. Dry DNA/RNA for 2-3min at 50°C using a thermomixer
20. Elute pellet in 50µl of EB buffer or DEPC water
21. **Add 0,5µl of RNase inhibitor to every 50µl of total nucleic acids**

B: List of chemicals

Product name	Chemical name	Chemical formula	Manufacturer	Molecular weight
TRIZMA® Base	2-Amino-2-(hydroxymethyl)-1,3-propandiol	$C_4H_{11}NO_3$	Sigma-Aldrich	121.14 g/mol
SDS	Sodium dodecyl sulfate	$CH_3(CH_2)_{11}OSO_3Na$	Sigma-Aldrich	288.38 g/mol
NaCl	Sodium chloride	NaCl	Merck	58.44 g/mol
DEPC	Diethyl pyrocarbonate	$C_6H_{10}O_5$	Sigma-Aldrich	162.14 g/mol
UltraPure™ Phenol:Chloroform:Isoamyl Alcohol	Phenol:chloroform:isoamyl alcohol (25:24:1)	$C_{12}H_{19}Cl_3O_2$	Sigma-Aldrich	301.6 g/mol
Chloroform-Isoamyl alcohol mixture	Cloroform:isoamyl alcohol (24:1)	$C_6H_{13}Cl_3O$	Sigma-Aldrich	207.5 g/mol
Glycogen	-	$(C_6H_{10}O_5)_n$	Invitrogen, Thermo Fisher	666.6 g/mol
Poly(ethylene glycol) 6000	-	$C_{2n}H_{4n+2}O_{n+1}$	Carl Roth	5000 – 6000 g/mol
RiboLock RNase Inhibitor	-	-	Thermo Scientific	49.6 kDa monomer
EtOH	Ethanol 96% vol	C_2H_5OH	VWR	46.07 g/mol
GelRed^R 10,000x in water	-	-	Biotium	-
1 kb DNA Ladder 1 kb Plus DNA Ladder	-	-	GeneRuler, Thermo Fisher	-

C: Script to process sequence data

```
cpu=8
name=PROJECTNAME
#OTU clustering % : 99; 97; 95; 90
OTU=97
#common name after R1/R2
RX=001.fastq
#Database for taxonomy
ref=/Users/dka018/Documents/DataBase.nosync/Mothur/Silva/132/silva.nr_v132.align
tax=/Users/dka018/Documents/DataBase.nosync/Mothur/Silva/132/silva.nr_v132.tax
#taxonomy database name without the extension
taxname=nr_v132
#project_directory
project_home=/Users/dka018/Documents/Projets/CAGE/Amplicon_script.nosync
#uc2otulab path if not set up, otherwise just type uc2otutab.py
pyth=/Applications/python_scriptsuc2otutab.py
#min sequence length
min=250
#max sequence length
max=255
#forward
        #trim left
trimleftf=13
        #trunc length
trunclenf=224
#reverse
        #trim left
trimleftr=13
        #trunc length
trunclenr=155

cd $project_home


############################## Unzip_fastq ################################


gunzip *.gz


mkdir $name.OTUS

mkdir $name.ZOTUS

############################## ZIP&move ###################################

        gzip *.fastq

        cp *.gz $name.OTUS/

########################### IMPORT in qiime2 ##############################

cp *.gz $name.ZOTUS
cd $name.ZOTUS
source activate qiime2

qiime tools import \
  --type 'SampleData[PairedEndSequencesWithQuality]' \
  --input-path ./ \
  --input-format CasavaOneEightSingleLanePerSampleDirFmt \
  --output-path $name.demux-paired-end.qza

rm *.fastq.gz

```

```
63.  qiime demux summarize \
64.    --i-data $name.demux-paired-end.qza \
65.    --o-visualization $name.demux.qzv
66.
67.  ################################ DADA2 ###################################
68.
69.  qiime dada2 denoise-paired \
70.    --i-demultiplexed-seqs $name.demux-paired-end.qza \
71.    --p-trim-left-f $trimleftf \
72.    --p-trim-left-r $trimleftr \
73.    --p-trunc-len-f $trunclenf \
74.    --p-trunc-len-r $trunclenr \
75.    --p-n-threads $cpu \
76.    --p-max-ee 1 \
77.    --o-table $name.ZOTUS.table.qza \
78.    --o-representative-sequences $name.ZOTUS.rep-seqs.qza \
79.    --o-denoising-stats $name.ZOTUS.denoising-stats.qza
80.
81.  ############################## export_files ##################################
82.
83.  qiime tools export \
84.    --input-path $name.ZOTUS.table.qza \
85.    --output-path $name.ZOTUS.table
86.
87.  qiime tools export \
88.    --input-path $name.ZOTUS.rep-seqs.qza \
89.    --output-path $name.ZOTUS.rep-seqs
90.
91.  qiime tools export \
92.    --input-path $name.ZOTUS.denoising-stats.qza \
93.    --output-path $name.ZOTUS.denoising-stats
94.
95.  mkdir $project_home/$name.ZOTUs.results
96.
97.  mv $name.ZOTUS.table/feature-table.biom
       $project_home//$name.ZOTUs.results/$name.ZOTUS.biom
98.  mv $name.ZOTUS.rep-seqs/dna-sequences.fasta
       $project_home//$name.ZOTUs.results/$name.ZOTUS.fa
99.  mv $name.ZOTUS.denoising-stats/stats.tsv
       $project_home//$name.ZOTUs.results/$name.DADA2.stats.tsv
100.
101. ########################### ASSIGN_TAXONOMY ##############################
102.
103. cd $project_home/$name.ZOTUs.results
104.
105. mothur "#classify.seqs(fasta=$name.ZOTUS.fa, reference=$ref, taxonomy=$tax, cutoff=75,
       processors=$cpu)"
106.
107. biom add-metadata --sc-separated taxonomy --observation-header OTUID,taxonomy --
       observation-metadata-fp $name.*.wang.taxonomy -i $name.ZOTUS.biom -o
       $name.ZOTUS.taxonomy.biom
108.
109. biom convert -i $name.ZOTUS.taxonomy.biom -o $name.ZOTUS.taxonomy.txt --to-tsv --header-
       key taxonomy --table-type "OTU table"
110.
111. rm $name.*.wang.taxonomy
112. rm $name.*.wang.tax.summary
113. rm $name.ZOTUS.biom
114. rm mothur*
115.
116. ############################## UNZIP_Rename ##################################
117.
118. cd $project_home/$name.OTUS
119.
120. gunzip *.gz
121.
```

```
122.  ################################## Rename ##################################
123.
124.  for i in *.fastq; do mv $i $(echo $i | sed 's/\_/\./g'); done
125.
126.  ###################### Store the first 3 column, before RX ####################
127.
128.  ls *\.R1\.*\.fastq |cut -d . -f 1,2,3 > list.txt
129.
130.  ######################## MERGE_QUALITY_FILTERING ##########################
131.
132.          while read sample; do
133.                  bbmerge.sh in1=$sample.R1.$RX in2=$sample.R2.$RX out=$sample.merged.fq
134.                  vsearch -fastq_filter $sample.merged.fq -fastaout $sample.filtered.fa -
                      fastq_maxee 1 -threads $cpu
135.          done < list.txt
136.
137.  rm *.fastq
138.
139.  ############################SAMPLES_LABELING#############################
140.
141.          ls *.filtered.fa |cut -d . -f 1,2,3 > $name.list.txt
142.
143.          while read sample; do
144.                  sed 's/\t/;/g' $sample.filtered.fa > $sample.filtered.temp.fa
145.                  sed 's/[[:blank:]]//g' $sample.filtered.temp.fa > $sample.filtered.clean.fa
146.                  sed "-es/^>\(.*\)/>\1;barcodelabel=$sample;/" < $sample.filtered.clean.fa >
                      $sample.filtered.label.fasta
147.
148.          done < $name.list.txt
149.
150.          rm *.filtered.clean.fa
151.          rm *.filtered.temp.fa
152.
153.  ###################### SAMPLES_CONCATENATION ########################
154.
155.          cat *.filtered.label.fasta > $name.filtered.label.fasta
156.
157.          mothur "#summary.seqs(fasta=$name.filtered.label.fasta)"
158.
159.  ################### DEREPLICATION_AND _SIZE_SORTING ####################
160.
161.          vsearch -derep_fulllength $name.filtered.label.fasta -output
              $name.filtered.label.uniques.fasta -sizeout -threads $cpu -minseqlength $min -
              maxseqlength $max
162.          vsearch -sortbysize $name.filtered.label.uniques.fasta -output
              $name.filtered.label.uniques.sort.fasta -minsize 2
163.
164.  ################## OTU_CLUSTERING_AND_CHIMERA_CHECK ####################
165.
166.          usearch -unoise3 $name.filtered.label.uniques.sort.fasta -zotus $name.otus100.fa
167.
168.          vsearch -sortbylength $name.otus100.fa --output $name.otus100.sorted.fa
169.
170.          for id in 99 97 95 90
171.  do
172.    usearch -cluster_smallmem $name.otus100.sorted.fa -id 0.$id -centroids $id.fa

173.    sed 's/Zotu/Otu/g' $id.fa > $name.otus$id.fa
174.    rm $id.fa
175.
176.  done
177.
178.  ########################## ASSIGN_TAXONOMY ############################
179.
180.          mothur "#classify.seqs(fasta=$name.otus$OTU.fa, reference=$ref, taxonomy=$tax,
```

```
        cutoff=75, processors=$cpu)"
181.
182.    ############################ OTU_MAPPING ################################
183.
184.        ide=$(awk "BEGIN print ($OTU)/100")
185.
186.        usearch -otutab $name.filtered.label.fasta -otus $name.otus$OTU.fa -id $ide -otutabout
            $name.otumap -mapout $name.map.txt -threads $cpu
187.
188.    ######################## OTU_TABLE_CONSTRUCTION ##########################
189.
190.        biom convert --table-type="OTU table" -i $name.otumap -o $name.biom --to-json
191.
192.        biom add-metadata --sc-separated taxonomy --observation-header OTUID,taxonomy --
            observation-metadata-fp $name.*.wang.taxonomy -i $name.biom -o
            $name.taxonomy.biom
193.
194.        biom convert -i $name.taxonomy.biom -o $name.taxonomy.txt --to-tsv --header-key
            taxonomy --table-type "OTU table"
195.
196.        mkdir $name.results
197.        mv  $name.taxonomy.txt $name.result/
198.        mv  $name.taxonomy.biom $name.result/
199.        mv  $name.otus$id.fa $name.result/
200.        mkdir $project_home/$name.OTUs.results
201.        mv  $name.taxonomy.txt $project_home/$name.OTUs.results
202.        mv  $name.taxonomy.biom $project_home/$name.OTUs.results
203.        mv  $name.otus$OTU.fa $project_home/$name.OTUs.results
204.
205.    exit
```

Appendix II: Results

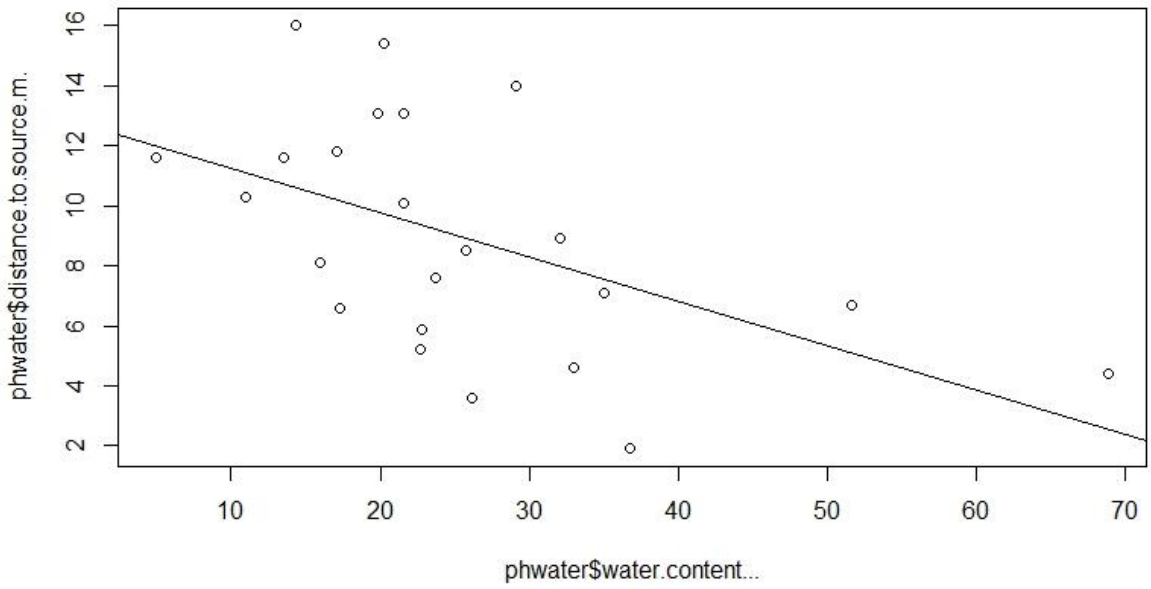

Figure A 1: Linear regression displaying the relationship between water content in the sediment and distance to the source (m) (R2=0.27, F-statistic: 7.7 on 1 and 21 DF, p: 0.011). The regression is based on data from DS, MS and WS locations. The remaining sampling point (PF, SP, SS and StS) were inundated in pond and stream, and exact water content for the sediment is missing. No statistically significant relationship was detected between sediment water content and the distance to the source.

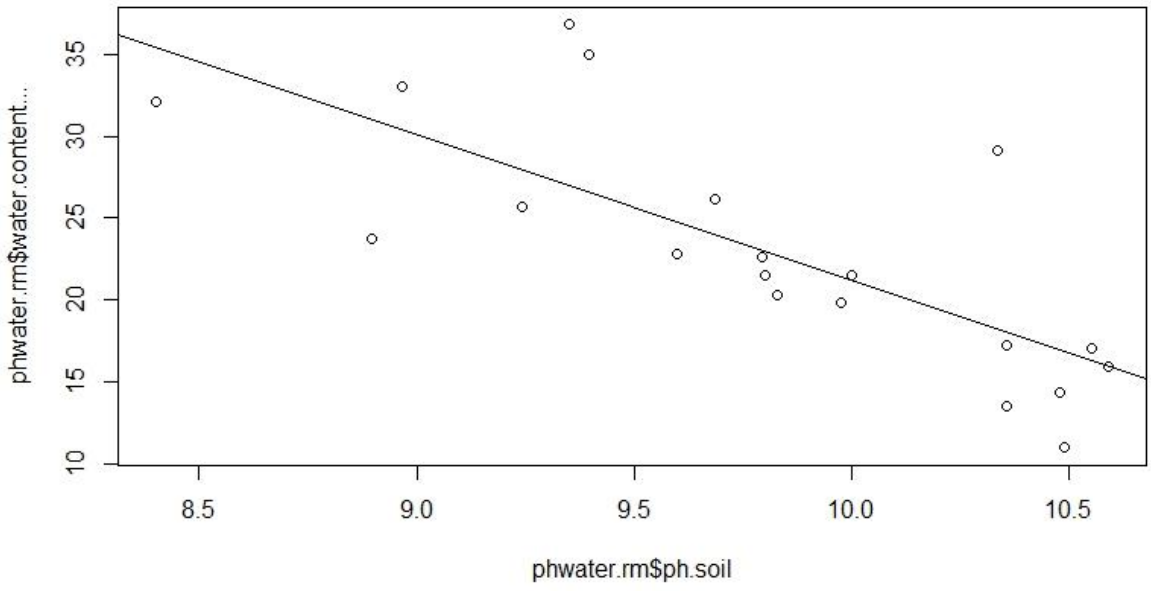

Figure A 2: Linear relationship between pH and water content in DS, MS and WS locations (R^2=0.54, F-statistic: 23.38 on 1 and 18 DF, p: 0.0001). PF, SP, SS and StS were waterlogged and was thus not used for this analysis.

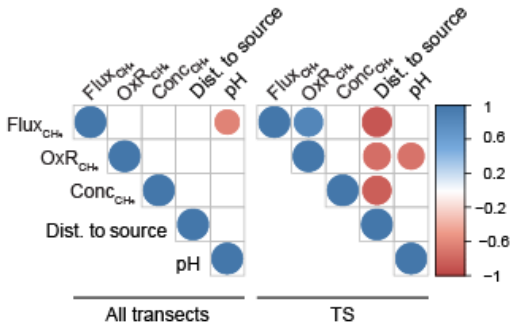

Figure A 3: Statistically significant (rho = >-0.6 or >0.6, p < 0.01) correlations between metadata variables.

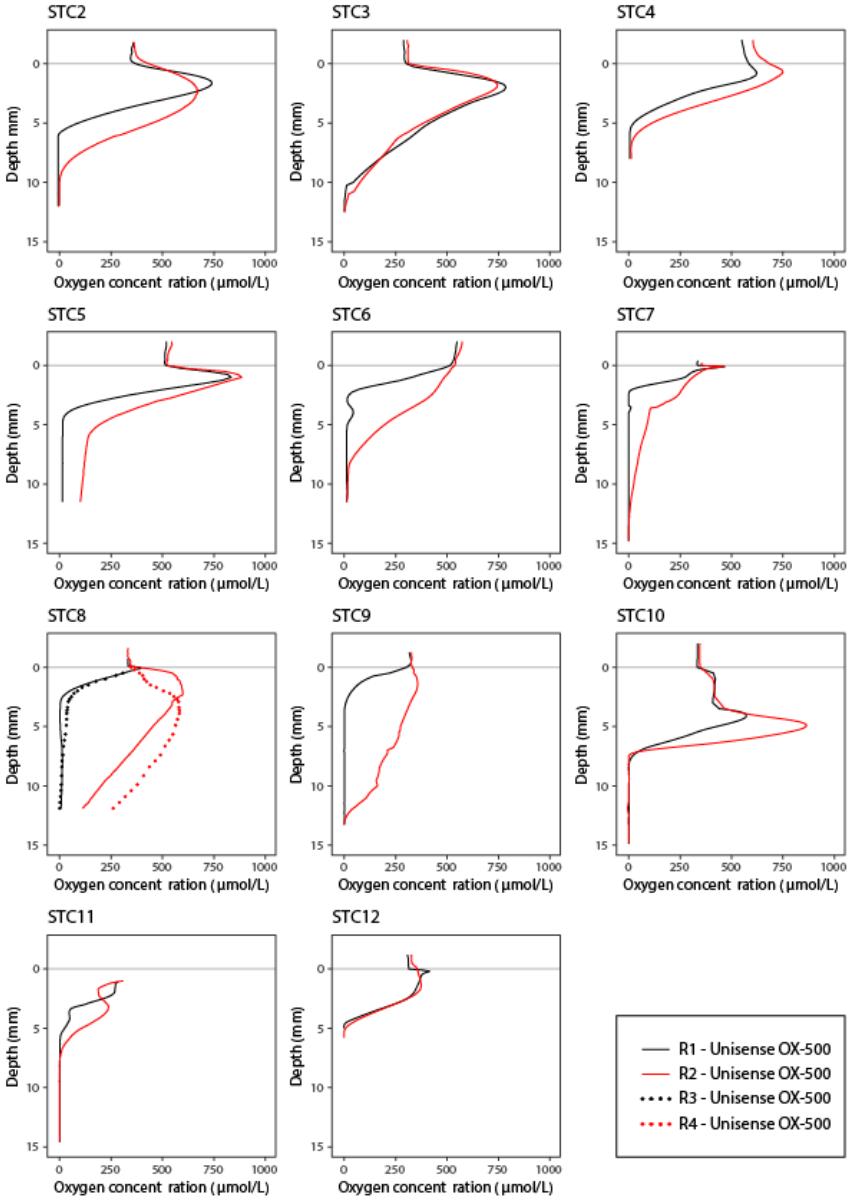

Figure A 4: Vertical oxygen profiles measured in situ in sediment from TS. Depth is measured in mm and oxygen concentration in µmol L^{-1}.

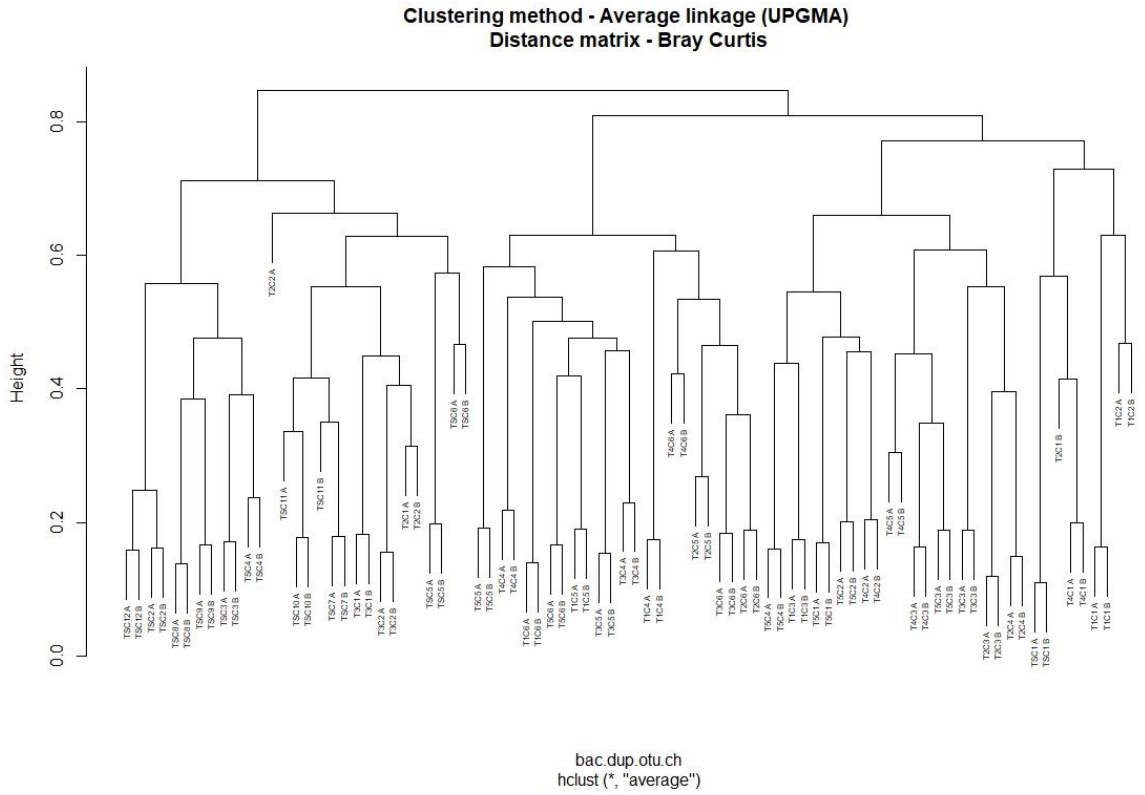

Figure A 5: Dendrogram based on OTUs generated from sequenced DNA using the universal primer pair 515F-Y/926R. Dendrogram contains all subsamples (duplicates). The dendrogram was generated using the function hclust integrated in the vegan package (2.5-6). The distance matrix applied was Bray Curtis and the clustering method was average linkage, also known as unweighted pair-group method.

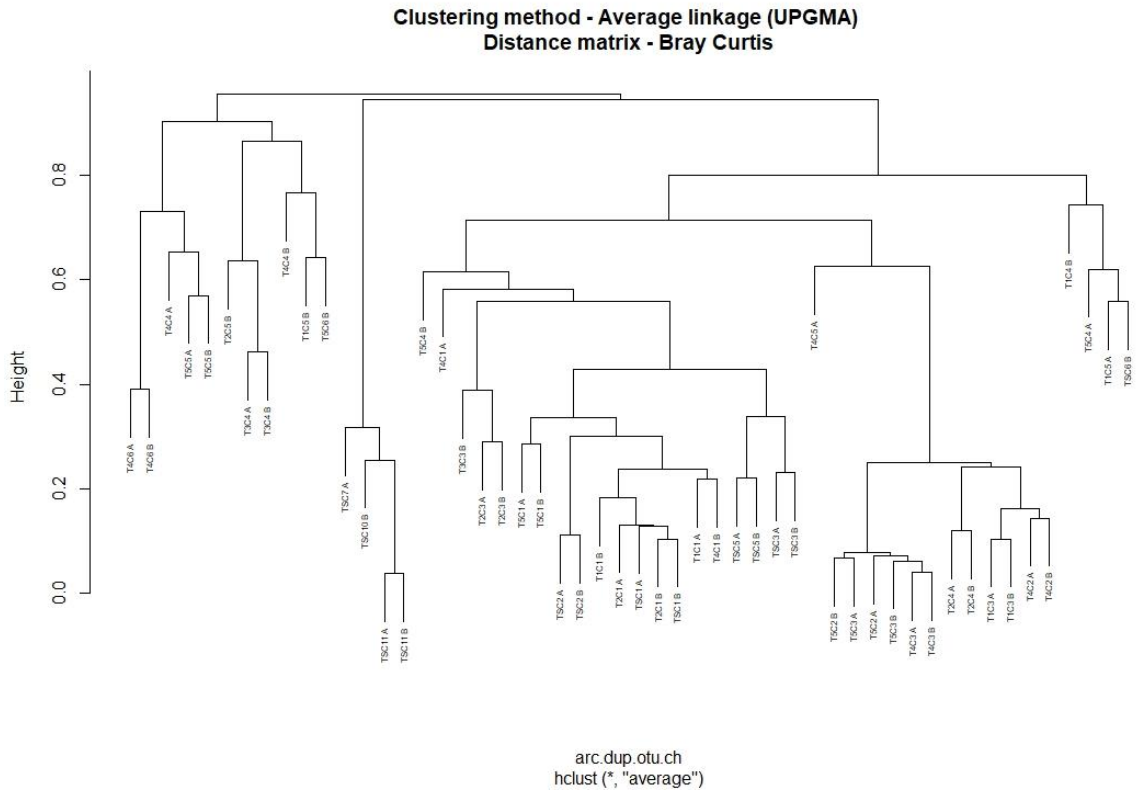

Figure A 6: Dendrogram based on OTUs generated from sequenced DNA using the archaeal primer pair 519F/1041R. Dendrogram including all subsamples (duplicates). The dendrogram was generated using the function hclust integrated in the vegan package (2.5-6). The distance matrix applied was Bray Curtis and the clustering method was average linkage, also known as unweighted pair-group method.

Table A 1: Alpha diversity of ecological niches defined by cluster analyses of bacterial and archaeal communities at Lagoon pingo[a].

Domain	Cluster	OTU richness N0	Shannon diversity index H	Simpson diversity index 1-D	Shannon diversity number N1	Simpson diversity number N2	Shannon evenness E1	Simpson evenness E2
Bac	StS	676.29	4.61	0.036	104.44	30.43	0.153	0.046
Bac	SS	684.50	4.57	0.038	106.07	32.07	0.149	0.045
Bac	WS	658.08	4.50	0.048	95.77	25.88	0.146	0.039
Bac	DS	702.25	4.82	0.029	126.83	37.91	0.181	0.055
Arc	Edge	8.38	1.67	0.25	5.79	4.79	0.72	0.61
Arc	Stream	26.00	1.12	0.61	3.49	1.81	0.13	0.07
Arc	Crater	20.63	1.51	0.39	5.71	3.70	0.39	0.29
Arc	Crater Flow	34.88	1.90	0.26	7.38	4.09	0.26	0.16
Arc	Crater WS	8.83	0.81	0.65	2.33	1.60	0.31	0.23

[a]Shannon diversity number: The exponential of H. Simpson diversity number: The inverse of the Simpson index. Shannon and Simpson evenness: NX/N0.

Table A 2: OTUs identified as methanotrophic bacteria, exceeding the sum of 50 sequences. Number of sequences per OTU is displayed in all samples. The OTUs were identified as Methylobacter or unclassified genera of Methylococcaceae.

	OTU											
	Methylobacter spp.								Methylococcaceae_unclassified			*Methyloceanibacter spp.*
	9	***360***	***296***	***468***	***576***	***1089***	***4176***	***412***	***348***	***451***	***759***	***319***
T1C1	66	9	2	3	1	1	1	0	2	2	0	1
T1C2	216	34	19	13	5	8	2	2	17	7	1	1
T1C3	97	0	1	0	0	0	0	0	0	0	2	1
T1C4	25	0	0	1	1	0	0	0	0	0	0	2
T1C5	13	0	0	0	0	0	0	0	1	0	0	2
T1C6	34	0	0	0	0	0	0	0	0	0	0	0
T2C1	566	26	10	5	3	2	3	3	6	5	3	0
T2C2	785	117	41	26	19	18	4	0	29	8	8	2
T2C3	10	0	1	0	0	0	0	0	0	0	0	0
T2C4	95	0	0	0	0	0	0	0	0	0	0	1
T2C5	23	2	0	0	0	0	0	0	0	0	0	1
T2C6	14	1	0	0	0	0	0	0	0	0	0	1
T3C1	283	20	3	3	4	3	0	3	3	4	4	0
T3C2	775	57	5	8	8	3	3	5	9	4	10	2
T3C3	18	0	0	0	0	0	0	0	1	0	0	0
T3C4	103	1	3	0	0	0	0	0	0	0	0	2
T3C5	10	1	1	1	1	0	0	0	0	0	0	0
T3C6	14	3	0	0	0	1	0	1	0	0	0	0
T4C1	395	43	6	14	3	1	3	2	9	5	0	4
T4C2	219	3	1	0	0	0	0	0	0	0	1	5
T4C3	155	1	0	0	0	0	0	0	0	0	0	4
T4C4	12	1	0	0	0	0	0	0	0	0	0	1
T4C5	568	0	0	0	0	0	0	0	0	0	3	15
T4C6	8	0	0	1	0	0	0	0	0	0	0	0
T5C1	788	60	41	17	13	8	7	0	14	7	4	0
T5C2	121	22	8	9	4	10	2	0	12	4	2	0
T5C3	138	2	0	0	1	0	1	0	0	0	0	3
T5C4	20	2	0	0	1	0	0	0	0	1	0	6
T5C5	3	0	0	0	0	0	0	0	0	0	0	1
T5C6	4	0	0	0	0	0	0	0	0	0	0	0
TSC1	529	241	59	47	43	26	18	0	82	33	0	0
TSC2	232	144	43	33	20	15	2	0	25	9	4	0
TSC3	459	135	43	13	30	12	8	0	34	18	4	0
TSC4	148	24	9	5	3	2	1	3	5	4	1	0
TSC5	740	50	19	8	5	7	1	1	5	8	13	1
TSC6	26	0	2	1	1	0	0	3	0	0	1	1
TSC7	34	12	2	0	1	1	0	4	2	0	2	0
TSC8	32	14	5	0	0	2	1	3	1	0	0	0
TSC9	19	4	1	1	0	0	0	4	0	0	0	0
TSC10	80	22	4	5	7	3	2	16	5	3	1	0
TSC11	11	6	2	0	0	0	1	5	0	1	0	0
TSC12	233	122	23	11	16	12	7	0	27	13	0	0
Sum of sequences per OTU	8121	1179	354	225	190	135	67	55	289	136	64	57

Table A 3: OTUs identified as methane cycling taxa, exceeding the sum of 50 sequences. Number of sequences per OTU is displayed in all samples.

	OTU						
	Methanosarcinales _novel	ANME-3	ANME -2a/b	Uncultured _Methanosarcinales	Uncultured _Methanosarcinales	ANME -1a	Uncultured _Methanosarcinales
	1	***2***	***28***	***160***	***106***	***105***	***256***
T1C1	333	388	37	3	6	24	0
T1C2	-	-	-	-	-	-	-
T1C3	706	4	0	0	0	0	0
T1C4	34	85	0	0	0	0	0
T1C5	0	12	0	0	0	0	0
T1C6	-	-	-	-	-	-	-
T2C1	385	484	30	0	4	7	0
T2C2	-	-	-	-	-	-	-
T2C3	0	371	13	21	0	0	15
T2C4	684	157	0	0	0	0	0
T2C5	0	33	0	0	0	0	0
T2C6	-	-	-	-	-	-	-
T3C1	-	-	-	-	-	-	-
T3C2	-	-	-	-	-	-	-
T3C3	60	590	9	0	0	0	24
T3C4	0	0	0	0	0	0	0
T3C5	-	-	-	-	-	-	-
T3C6	-	-	-	-	-	-	-
T4C1	225	445	85	0	17	32	0
T4C2	762	0	0	15	0	0	0
T4C3	889	0	0	0	0	0	0
T4C4	0	2	0	0	0	0	0
T4C5	344	0	0	0	0	0	0
T4C6	0	0	0	0	0	0	0
T5C1	274	387	38	0	0	0	0
T5C2	860	2	0	0	0	0	0
T5C3	847	4	0	0	0	0	0
T5C4	288	0	0	0	0	0	0
T5C5	0	67	0	0	0	0	0
T5C6	0	5	0	0	0	0	0
TSC1	384	469	6	0	0	0	0
TSC2	382	257	52	0	22	12	0
TSC3	154	324	110	3	25	5	0
TSC4	-	-	-	-	-	-	-
TSC5	87	341	282	0	8	3	6
TSC6	88	33	0	55	0	0	13
TSC7	54	5	0	0	0	1	0
TSC8	-	-	-	-	-	-	-
TSC9	-	-	-	-	-	-	-
TSC10	28	3	0	0	0	0	0
TSC11	6	2	1	0	2	0	0
TSC12	-	-	-	-	-	-	-
Sum of sequences per OTU	7874	4470	663	97	84	84	58

Table A 4: Spearman's rank correlation between OTU abundances and metadata.

ph.soil	-0.6190476	-0.5200299	-0.5073463	0.4364358	-0.6428571	-0.7319251	-0.5384615	-0.6363636	-0.5255936
distance.to.source.m.	-0.97619048	-0.46929532	-0.31709143	-0.09352195	-0.9047619	-0.58554004	-0.55944056	-0.57342657	-0.61730795
Mean_CH4con	0.88095238	0.2663568	0.12683657	0.01558699	0.85714286	0.48795004	0.47552448	0.4125874	0.4620991
Mean_Ox_rate	0.5714286	0.8751723	0.7863867	-0.2182179	0.5952381	0.8295151	0.4755245	0.5594406	0.4938464
Mean_CH4_flux	0.8571429	0.5327136	0.3170914	-0.1870439	0.8333333	0.58554	0.5384615	0.5804196	0.5538134
bOTU_319	0	-0.06711561	-0.06711561	0.41239305	0.25197632	0.12909944	0.12955006	-0.25910011	-0.13069755
bOTU_759	0.18184824	0.865399088	0.63936201	0.079365079	0.36369648	0.596284794	0.468496876	0.267189625	0.254786068
bOTU_412	-0.92710507	-0.59785653	-0.53287213	-0.20763488	-0.85391256	-0.7	-0.7507211	-0.78304881	-0.86246038
bOTU_4176	0.55766794	0.14853865	0.31645191	-0.15079365	0.50917508	0.472058795	0.689657664	0.876439948	0.871519834
bOTU_1089	0.7904333	0.4721139	0.3508955	-0.25873	0.7784571	0.6136009	0.8763743	0.9788536	0.9572208
bOTU_451	0.6946232	0.3508955	0.4721139	-0.1489658	0.730552	0.711777	0.8399906	0.9254134	0.9156563
bOTU_576	0.79043333	0.325375819	0.25519672	-0.0078403	0.73055202	0.466336659	0.846593764	0.892450926	0.879003559
bOTU_468	0.86229091	0.37641516	0.35089549	-0.04704183	0.81438586	0.61360087	0.82690159	0.88344187	0.87344167
bOTU_348	0.7470422	0.4043782	0.3337725	-0.1498714	0.7470422	0.5679445	0.886614	0.9575431	0.930246
bOTU_296	0.7979215	0.4054453	0.4054453	-0.1366178	0.7979215	0.6666799	0.8677586	0.9700554	1
bOTU_360	0.7380952	0.4692953	0.3805097	-0.3273268	0.7380952	0.634335	0.8741259	1	0.9700554
bOTU_9	0.5952381	0.4566117	0.3551424	-0.1870439	0.8809524	0.7563226	1	0.8741259	0.8677586
aOTU_28	0.43915503	0.66284094	0.81880351	-0.07985957	0.68313005	1	0.75632256	0.63433505	0.66667985
aOTU_2	0.83333333	0.36782606	0.2663568	0.09352195	1	0.68313005	0.88095238	0.73809524	0.7979215
aOTU_160	0.23380488	-0.0083034	0.10794424	1	0.09352195	-0.07985957	-0.18704391	-0.32732684	-0.13661782
aOTU_106	0.22830583	0.80405405	1	0.10794424	0.2663568	0.81880351	0.3551424	0.38050972	0.40544532
aOTU_105	0.38050972	1	0.80405405	-0.0083034	0.36782606	0.662840937	0.45661166	0.469295318	0.405445317
aOTU_1	1	0.3805097	0.2283058	0.2338049	0.8333333	0.439155	0.5952381	0.7380952	0.7979215
Kolonne1	aOTU_1	aOTU_105	aOTU_106	aOTU_160	aOTU_2	aOTU_28	bOTU_9	bOTU_360	bOTU_296

-0.5035968	-0.699686	-0.5220662	-0.6015187	-0.5689366	-0.4202601	0.3879324	-0.2745099	0.1295501	-0.6433566
-0.51068968	-0.5972067	-0.56792332	-0.46982527	-0.52653135	-0.30172523	0.58908259	-0.50143806	-0.12955006	-0.88811189
0.31918105	0.59367293	0.43035183	0.33457254	0.42051833	0.14727065	-0.51365128	0.34039226	0.38865017	0.68531469
0.4468535	0.4593898	0.4479892	0.4698253	0.4346534	0.2801734	-0.3017252	0.6368629	-0.1295501	0.8461538
0.5035968	0.4805924	0.4515167	0.416436	0.4876599	0.2658056	-0.4202601	0.4355557	-0.1295501	1
-0.26280173	-0.03273268	-0.09802317	-0.16484512	-0.1963961	-0.36598953	-0.06654355	0.4068381	1	-0.12955006
0.252444702	0.284833755	0.358177516	0.193744128	0.257090208	-0.00940016	-0.22184371	1	0.406838102	0.43555569
-0.75415967	-0.79320927	-0.72294473	-0.7568872	-0.78413365	-0.62177122	1	-0.22184371	-0.06654355	-0.42026014
0.888961153	0.795024393	0.844341461	0.908630282	0.878520105	1	-0.62177122	-0.00940016	-0.36598954	0.265805558
0.9534111	0.8910714	0.9126574	0.8903108	1	0.8785201	-0.7841336	0.2570902	-0.1963961	0.4876599
0.9278039	0.9136927	0.9084747	1	0.8903108	0.9086303	-0.7568872	0.1937441	-0.1648451	0.416436
0.9481353	0.935830364	1	0.908474664	0.912657421	0.844341461	-0.72294473	0.358177516	-0.09802317	0.451516674
0.88172609	1	0.93583036	0.91369271	0.89107143	0.79502439	-0.79320927	0.28483376	-0.03273268	0.48059238
1	0.8817261	0.9481353	0.9278039	0.9534111	0.8889612	-0.7541597	0.2524447	-0.2628017	0.5035968
0.930246	0.8734417	0.8790036	0.9156563	0.9572208	0.8715198	-0.8624604	0.2547861	-0.1306976	0.5538134
0.9575431	0.8834419	0.8924509	0.9254134	0.9788536	0.8764399	-0.7830488	0.2671896	-0.2591001	0.5804196
0.886614	0.8269016	0.8465938	0.8399906	0.8763743	0.6896577	-0.7507211	0.4684969	0.1295501	0.5384615
0.56794452	0.61360087	0.46633666	0.71177701	0.61360087	0.4720588	-0.7	0.59628479	0.12909944	0.58554004
0.74704217	0.81438586	0.73055202	0.73055202	0.77845707	0.50917508	-0.85391256	0.36369648	0.25197632	0.83333333
-0.14987136	-0.04704183	-0.0078403	-0.14896578	-0.25873004	-0.15079365	-0.20763488	0.079365079	0.412393049	-0.187043906
0.33377251	0.35089549	0.25519672	0.47211393	0.35089549	0.31645191	-0.53287213	0.63936201	-0.06711561	0.31709143
0.404378231	0.376415163	0.325375819	0.350895491	0.472113934	0.14853865	-0.59785653	0.865399088	-0.06711561	0.532713604
0.7470422	0.8622909	0.7904333	0.6946232	0.7904333	0.5576679	-0.9271051	0.1818482	0	0.8571429
bOTU_348	bOTU_468	bOTU_576	bOTU_451	bOTU_1089	bOTU_4176	bOTU_412	bOTU_759	bOTU_319	Mean_CH4_flux

-0.7132867	-0.6363636	0.5734266	1
-0.74825175	-0.83916084	1	0.57342657
0.48251748	1	-0.83916084	-0.63636364
1	0.4825175	-0.7482517	-0.7132867
0.8461538	0.6853147	-0.8881119	-0.6433566
-0.12955006	0.38865017	-0.12955006	0.12955006
0.636862941	0.340392262	-0.501438063	-0.27450989
-0.30172523	-0.51365128	0.58908259	0.38793244
0.280173426	0.147270647	-0.301725228	-0.42026014
0.4346534	0.4205183	-0.5265314	-0.5689366
0.4698253	0.3345725	-0.4698253	-0.6015187
0.4479892	0.43035183	-0.567923317	-0.52206616
0.45938977	0.59367293	-0.5972067	-0.69968596
0.4468535	0.319181	-0.5106897	-0.5035968
0.4938464	0.4620991	-0.617308	-0.5255936
0.5594406	0.4125874	-0.5734266	-0.6363636
0.4755245	0.4755245	-0.5594406	-0.5384615
0.82951506	0.48795004	-0.58554004	-0.73192505
0.5952381	0.85714286	-0.9047619	-0.64285714
-0.21821789	0.015586992	-0.093521953	0.43643578
0.78638675	0.12683657	-0.31709143	-0.50734629
0.875172349	0.266356802	-0.469295318	-0.52002995
0.5714286	0.8809524	-0.9761905	-0.6190476
Mean_Ox_rate	Mean_CH4con	distance.to.source.m.	ph.soil